THESIS

Investigating the molecular basis for anesthesia

Author:

Christopher Faulkner

Supervisor:

Professor Nora de Leeuw

Thesis submitted to Cardiff University in partial fulfilment of the requirements for the degree of Doctor of Philosophy

School of Chemistry

December 2021

Acknowledgements

First and foremost, I would like to thank my supervisor Professor Nora H. de Leeuw for her support and guidance throughout my PhD studies. I would also like to thank Dr David Plant and Dr Matthew Habgood from AWE for their guidance and insightful conversations during my PhD.

I would also like to thank the other members of my research group for their help throughout my time working with them. A big thank you also goes to my parents for their love and support throughout this process.

A big thank you also goes to my examiners Professor Jonathan Essex and Dr Alison Paul for evaluating my work, and for the fruitful discussion which has defiently deepened my understanding in this field and improved the scientific messages conveyed in this thesis.

And to anyone who is reading this thesis, thank you for taking an interest in my work and small contribution to the scientific world.

CARDIFF UNIVERSITY

Abstract

School of Chemistry

Doctor of Philosophy

Thesis

by Christopher Faulkner

The molecular mechanisms behind the phenomenon of general anesthesia have remained a mystery despite anesthesia inducing compounds being routinely used in general surgery for decades. Theories of how these molecules cause anesthesia have ranged from the interaction with lipid bilayers to the blocking of ion transport through ion channel proteins, resulting in the disruption of neurotransmission. Both of these theories will be investigated in this work. One area of anesthesia that is often overlooked is the role of the opioid component. Opioids are used primarily as the analgesic component of general anesthesia and the most commonly used opioid in general anesthesia is fentanyl and its analogues. These drugs have been shown to possess anesthetic properties and have been used as induction and maintenance agents for general anesthesia, as well as the main anesthetic component. The aim of this thesis is to investigate the anesthetic properties of fentanyl and its analogues using molecular dynamics simulations and various free energy methods. The interactions between fentanyl and lipid bilayers as well as the *Gloeobacter violaceus* ion channel were investigated and it was found that fentanyl disrupts the structure of the bilayers in a similar way to the general anesthetic propofol and can also modulate the flow of ions through the *Gloeobacter violaceus* ion channel in similar ways to various general anesthetics. This thesis therefore makes a contribution to the fundamental understanding of the anesthetic action of fentanyl and builds on the basis for anesthetic drug discovery.

Contents

List of Figures

Chapter 1

Introduction

1.1 General anesthesia

General anesthesia refers to a medically induced loss of consciousness and sensation, enabling invasive surgical procedures to be performed in the safest possible environment. During general anesthesia, the patient is put into a state of full body paralysis in which they are unresponsive to painful stimulus. The discovery of substances which induce and maintain this effect have revolutionised the field of medicine, and much progress has been made in improving the safety and efficiency of this procedure since the early days of diethyl ether in the 1800s. Although general anesthetics are used extensively in surgical procedures everyday, an in-depth understanding of the mechanisms behind the anesthetic phenomenon has yet to be found. Understanding these mechanisms will allow new drugs to be synthesised which will increase the safety and efficiency of the procedure by acting only at specific sites in which anesthetic action takes place. In this chapter an outline of general anesthesia in a clinical context is given, an outline on the previous attempts to solve this mystery and how they can still help to gain understanding of these elusive mechanisms is given. The background on the systems which will be studied is given in the coming sections.

1.2 General anesthesia in a clinical context

General anesthesia is a complex clinical process which involves the use of multiple pharmaceutical agents. The general anesthesia process has three main steps which must be undertaken for the procedure to be successful. These are: induction, maintenance and emergence. The induction period begins with the administration of a hypnotic drug, a barbiturate, or an etomidate. These drugs sedate the patient and as the dosage is raised over 10 to 15 seconds, the patient becomes unconscious and ventilation is required to support breathing. Opioids are also be administered here to support cardiovascular stability. During the maintenance phase a combination of hypnotics, opioids, muscle relaxants and inhalational agents can be used to ensure the patients vital signs remain stable, and that they remain unconscious and non-responsive. The emergence stage involves gradually stopping the delivery of the anesthetic and adjuvant agents. Most patients will transition smoothly into an awake state, but there are several complications that can arise, such as respiratory/cardiovascular events may occur during this phase.

In recent years, a new method of anesthesia was developed which can limit the potential adverse reactions by utilising hypnotics and opioids in combination. The method is called total intravenous anesthesia (TIVA) and all of the anesthetic agents used are administered by injection, without the use of volatile inhalational agents. This method is generally preferred due to more predictable and rapid recovery, reduced risk of organ toxicity and greater haemodynamic stability.[3,4] The most commonly used drugs for this process are propofol and fentanyl, propofol is used due to it being the only intravenously active hypnotic agent suitable for induction and maintenance of anesthesia. Fentanyl and its analogues are used due to the potent pain killing effect they can produce, and the lower dosages of propofol that are required when used in combination which reduces the chance of side effects.[5–7] Due to TIVA being a favoured method of carrying out general anesthesia and there being a synergistic relationship between propofol and fentanyl, these two drug molecules are studied throughout this work.

1.3 Lipid hypotheses

1.3.1 Outdated

At the turn of the century, Meyer[8] and Overton[9] both observed that the potency of general anesthetics correlates with their solubility in hydrophobic solvent which represents the interior of the cell membrane, this advocates that anesthetics act directly via the plasma membrane. The relationship also states that different anesthetics induce anesthesia at equal concentrations inside the lipid bilayer.[10] This hypothesis formed the basis of research into anesthesia for decades. Miller and Smith built upon this theory in 1973 by introducing the lipid bilayer expansion hypothesis,[11] which took into account the structural differences between anesthetic agents. They postulated that hydrophobic, bulky anesthetic molecules could rapidly diffuse into the cellular membrane interior and accumulate, this accumulation would then cause structural deformations and thickening due to volume displacement within the membrane. This volume expansion of the bilayer structure would then reach a critical point when enough anesthetic molecules had accumulated that it would cause disruption to signalling proteins which are embedded within the cellular membrane. This theory then gave rise to many more physicochemical theories which suggests various disruptions in lipid bilayer properties were responsible for the anesthetic effect, such as phase separation, order parameters and curvature, etc. Several reviews have been written explaining all of these theories.[12,13]

These suggested theories may seem like reasonable explanations to the anesthesia question, but there are several factors which disagree. There are several experimental studies which show that ethanol, which is a general anesthetic, increases the fluidity in erythrocyte, mitochondrial, and synaptosomal membranes.[14–16] However, these effects are small at clinical concentrations and can be replicated by a 1 degree increase in body temperature[17] which clearly does not have an anesthetic affect. The Meyer-Overton hypothesis states that the drugs lipid solubility is directly linked to its anesthetic potency, however, many compounds have been

identified which do not obey this rule. For a compound to be an anesthetic it has to exert amnesic actions, and cause immobilisation,[18,19] however, multiple compounds that were predicted to be anesthetics based upon their lipid solubility only exerted the amnesic action and were hence not classified as anesthetics. Amnesic action refers to the patient experiencing intraoperative amnesia during the surgical procedure which results in no memories of the experience being retained. Immobilisation refers to the patients inability to move. This suggests that multiple interaction sites are responsible for full anesthetic action, not just the lipid bilayer. Anesthetics, like most small drug molecules have enantiomers (R-(+)- and S-(-)-etomidate). In an achiral environment, their physicochemical effects are identical. Although *in vivo*, the R-(+) isomer of etomidate is 10 times more potent than its S-(-) isomer.[20] This suggests that diffusion into the cell membrane would be identical for optical isomers, but there must be an additional stereoselective interaction site in which the anesthetic action is performed.

In summary, the Meyer-Overton hypothesis held strong for decades but various exceptions to the rules were identified. The evidence was pointing to direct disruption of cell signal transduction by direct interaction with transmembrane proteins. However, the lipid membrane is such a huge part of the cellular environment that the idea that it does not have a place in the anesthesia process still seemed unlikely, and hence the modern lipid hypothesis was proposed.

1.3.2 Modern

Cantor proposed a mechanistic and thermodynamic explanation of general anesthesia in 1997, using lattice statistical thermodynamics, which accounts for several of the short comings of the earlier lipid theories.[21] He put forward the idea that when solutes that act at the interface of cell membranes (e.g. anesthetics), the lateral pressure within the membrane increases at the aqueous interface which is then compensated by a decrease in lateral pressure in the center of the hydrophobic phase.

The calculations that were carried out showed that even at low membrane anesthetic concentrations of a few mole percent, the changes in the lateral pressure profile of the membrane could alter the conformational equilibrium of ion channel proteins in such a way that anesthesia was induced. The mechanism by which the inhibition of postsynaptic transmission was achieved relies on the assumptions that when a channel protein is open, the cross-sectional area of the protein is increased near the aqueous interface. The anesthetic which partitions into the membrane causes an increase in the lateral pressure at the interfacial region which then causes the channel protein conformational equilibrium to shift towards the closed state.[21–23]

This theory therefore suggests that anesthetics do not directly act upon membrane proteins, but rather induce lipid membrane perturbation at the interface between the membrane and the protein. This type of mechanism is very different from the usual "lock and key" mechanism of protein-ligand interactions in which the ligand binds directly to the target protein. A slightly different detailed molecular mechanism of how bilayer perturbation can influence the ion-channel was proposed in the same year. Oleamide (fatty acid amide of oleic acid) is an endogenous anaesthetic found in vivo (in the cat's brain) and it is known to potentiate sleep and lower the temperature of the body by closing the gap junction channel connexion.[24]

Recently, super resolution imaging showed direct experimental evidence that volatile anesthetic disrupt the ordered lipid domains as predicted. The study also showed a related mechanism where the anesthetics released the enzyme phospholipase D (PLD) from lipid domains and the enzyme bound to and activated TREK-1 channel by the production of phosphatidic acid.[25]

These results showed experimentally and theoretically, that the lipid membrane is a physiologically relevant target for general anesthetics. Although these proposed mechanisms still do not answer all of the questions, as it is very possible that anesthetics can bind directly to transmembrane proteins which are currently the main drug targets in drug discovery.[26]

1.4 Direct protein binding hypothesis

As an alternative to the various lipid-mediated theories which have been previously proposed, it was postulated that anesthetics can exert their function by directly binding to protein targets. Early work in this area carried out by Franks and Leib showed that various inhalational anesthetics directly inhibited the function of the firefly luciferase enzyme (Figure 1.1) by competitive binding of the substrate.[27,28] This was initially shown to be inhibited by a wide range of inhalational general

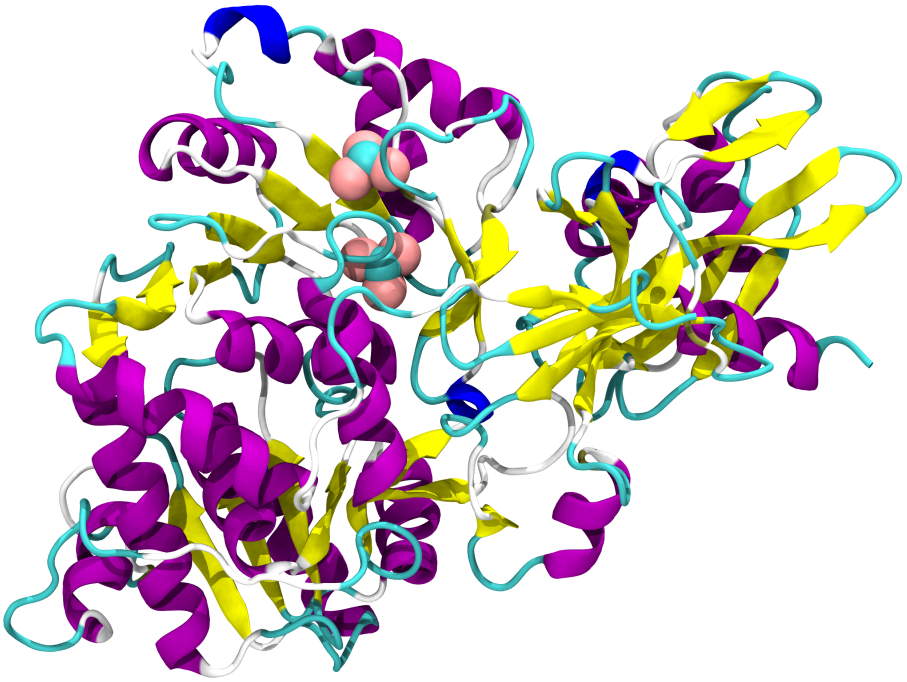

FIGURE 1.1: Structure of the firefly luciferase enzyme with two bound bromoform molecules shown in VDW sphere representation (PDB: 1BA3)

anesthetics with a sensitivity which closely parallels the anesthetic potencies in animals over five orders of magnitude.[27] The crystal structure of firefly luciferase was solved in 1996[29] which allowed atomistic analysis of the structure and binding sites to be carried out. The dimensions and amphiphilic nature of the substrate (luciferin) binding site provides a reasonable explanation of the cutoff observed in homologous series of long chain anesthetic compounds.[30]

The crystal structure of firefly luciferase with a general anesthetic bound was eventually solved in 1998 when bromoform was seen to bind within the luciferin

substrate binding pocket.[28] The binding environment of the bromoform molecule within the luciferin pocket is amphiphilic in nature, with one side of the anesthetic in close contact with apolar residues and the other side in contact with polar residues. The other molecule which is situated in the "external" site resides in a very polar environment with significant solvent exposure.

The studies conducted on anesthetic binding to the firefly luciferase enzyme show that anesthetics can exert their effects by binding to specific protein pockets with very little perturbation to the overall protein structure. Furthermore, anesthetics were also shown to exert their effect on soluble cytoplasmic proteins, such as protein kinase C.[31]

Extensive research efforts were then focused on identifying specific protein targets for general anesthetics. The consensus nowadays is that specific classes of membrane receptors and membrane channels are considered to be the primary targets for general anesthetics.

1.4.1 Membrane protein targets

It is fairly well known that the human genome contains the sequences for between 20000 and 21000 proteins.[32] This knowledge brings up a huge amount of potentially clinically relevant sites for anesthetics. To narrow the possibilities, Hemmings *et al*, suggested the following criteria which has to be met for a site to be viable:[33]

1) Anaesthetics must produce a reversible effect at a functional site with clinically relevant concentrations;

2) A functional site must be situated at a plausible anatomical location to mediate the specific behavioural effects of an anaesthetic;

3) Stereoselectivity of anaesthetic effects in vivo should duplicate the stereoselective effects observed in vitro;

4) A functional site should be insensitive to the effects of nonimmobilizers.

These four rules are met by several ion channel and receptor families, which now make up the leading targets for unveiling the actions of general anesthetics. These molecular targets include: glycine, glutamate, γ-aminobutyric acid A ($GABA_A$), nicotinic acetylcholine, adenosine, and serotonin receptors, as well as ATP-sensitive, background potassium, and voltage-gated channels.[34,35] An in-depth description of the structure and function of these proteins will be given in section 1.5.

1.5 Lipid membranes

Biological membranes are significant components of the cell, they form the boundary between the intracellular domain (inside the cell) and the extracellular domain (outside the cell). They are also present in the cell interior where they separate organelles from the cytosol. They have a large range of functions such as, selective permeability, acting as a barrier to maintain ion concentrations on each side of the cell, and they contain large numbers of proteins which carry out various cellular processes.[36] Among the different types of mammalian cell membranes, the plasma membrane is often the target of selective drugs. The plasma membrane is the most outer cell membrane and is primarily composed of three different classes of lipids: glycerophospholipids, sphingolipids, and sterols.[37] In the case of glycerophospholipids, the head groups show the common structural motif including a glycerol unit (Figure 1.2) bound to the phosphate group. An additional molecular group is also bound to the phosphate which allows the glycerophospholipids to be classified as: phosphatidylcholine (PC), phosphatidyletholamine (PE), phosphatidylserine (PS), phosphatidylglycerol (PG), phosphatidylinositol (PI), and phosphatidic acid (PA). Acyl chains with different length and level of unsaturation are bound to glycerophospholipid head groups. Therefore, the chemical diversity of the lipids in cell membranes is extremely large and varies considerably depending on the specific organisms and even within the same cell, from one membrane type to another.[38] In mammalian plasma membranes, approximately 30 mol% of the phospholipids are PC[39] and concerning the acyl chain composition, acyl chains with 16 and 18

carbon atoms account for 80 mol% of the total phospholipids of which 65 mol% are unsaturated.[40] The plasma membrane is formed in a lipid bilayer structure. This consists of a back to back arrangement of amphiphilic lipid molecules. Figure 1.2 shows the phospholipid 1,2- dioleoyl-sn-glycero-3-phosphocholine (DOPC) which is a lipid that has two carbon 18 unsaturated acyl chains and is used extensively in this work.

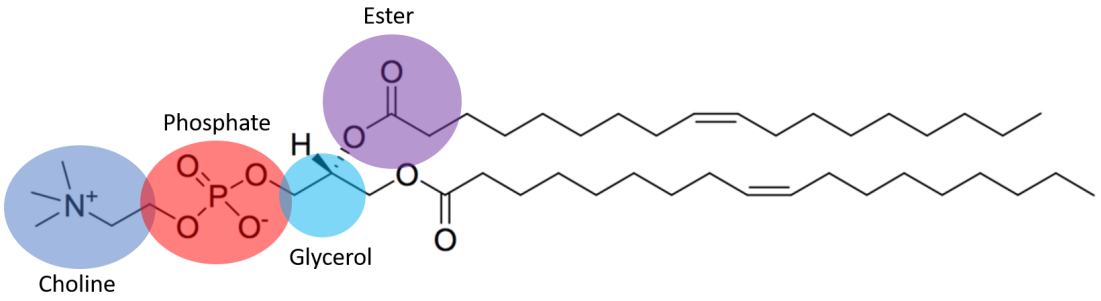

FIGURE 1.2: DOPC phospholipid and its structural components

This type of phospholipid is composed of a positively charged choline head group and a negatively charged glycerophosphoric acid and two unsaturated oleic acid tails. These structural traits help the lipids form the bilayer structure. In an aqueous environment, the lipid molecules will aggregate brining the hydrophobic tail groups together due to the hydrophobic effect which leaves the polar head groups in contact with the aqueous medium. There are a variety of structures in which the lipids can aggregate depending on the types of lipids present, but the bilayer is the most physiologically relevant structure which makes up the main structure of the cell membrane. Multiple non-covalent forces help to maintain the bilayer structure such as; electrostatic repulsion, hydrogen bonding, steric repulsion, Van der Waals attraction, hydrophobic effects and hydration forces.

1.5.1 Membrane transport

The core of a cell membrane is composed of the hydrophobic lipid tails. This hydrophobic region acts as a barrier to passive diffusion of polar molecules from

the cell exterior environment (extracellular fluid) to the interior environment of the cell (cytoplasm). Cells require certain molecules for their survival, so transport mechanisms have evolved. These mechanisms allow the cell to receive the required nutrients to survive and function, and they allow the disposal of waste products. Intracellular ion concentrations are also regulated using these mechanisms. Three different mechanisms are available for membrane transport, namely: passive diffusion, facilitated transport and active transport.[41]

Passive diffusion is the method by which lipid soluble (lipophilic/hydrophobic) molecules which are neutral cross the membrane by solubilising with the lipid molecules which form the hydrophobic barrier. This process is driven by the concentration gradient of the molecule between the extracellular domain and the intracellular domain, allowing the molecules to be transported from the side with the highest concentration to the side with the lowest. This mechanism therefore requires no energy output by the cell. There are three factors which govern passive diffusion, these are:
(1) The lipid solubility of the molecule: This is often expressed as the molecules ability to distribute between a hydrophobic phase and an aqueous phase (oil and water). The higher the solubility in the hydrophobic phase, the easier it will cross the membrane.
(2) The electrical charge of the molecule: Neutral molecules will permeate the membrane easier due to their higher lipophilicity. For weakly charged molecules, the pH of the aqueous environment will have a large influence on the degree of ionisation, and hence their lipid solubility.
(3) The size of the molecule: Small molecules will cross the hydrophobic barrier more rapidly than larger molecules if the previous two criteria are met for both molecules.

Facilitated diffusion shares many similarities with passive diffusion, but the difference is the need for a carrier protein located within the membrane to assist with the transfer across the membrane. The concentration gradient rule applies here the same as it does in passive diffusion. This process is specific in the sense that it applies to molecules that have the ability to bind to the carrier protein. An

example of facilitated diffusion is the absorption of nutrients like glucose across the epithelial membrane of the GI tract. This process is saturable at high concentrations of the transport molecule due to the finite number of carriers which are available for transport and competition for transport can occur between the transport molecules.

Active transport requires a carrier molecule, a membrane protein, and the expenditure of energy by the cell, usually provided by ATP hydrolysis. This allows transport to occur against a concentration gradient. The carrier system is selective for certain properties of molecules, namely their ionisation state. These systems are also saturable and competitive. This mechanism of transport is mostly for elimination of molecules by the liver and the kidneys.

1.5.2 Interactions of drugs with membranes

Pharmaceutical compounds are known to interact with the cell membrane when they are introduced into the body. Understanding how a drug molecule interacts with the membrane can give us knowledge of how that molecule reaches its target and we can thus interpret how that affects its pharmacodynamics and pharmacokinetics. Interactions between drug molecules and the cell membrane is of great interest in pharmaceutical science as these interactions can influence vital properties such as toxicity, absorption, distribution and metabolism. It is therefore of high importance to investigate interactions with the membrane during drug design.

The membrane could also be a direct site for the action of general anesthetics, either by direct interaction with the membrane in which significant structural and mechanical properties of the membrane are disrupted, or by indirect modulation of proteins which reside within the cell membrane.[21,42]

The interactions between drug molecules and membranes could come from the drug interacting with the lipid head groups at the lipid/water interface, or by partitioning into the membrane interior by passive diffusion if the criteria described

in the previous section is met. There are several different ways in which a drug can affect the lipid membrane, for example:

- Cause conformational changes of the lipid tails.
- Increase or decrease the curvature of the lipid membrane.
- Cause phase separation.
- Alter then thickness of the lipid membrane.
- Cause changes in the membranes electrostatic potential.
- Change the phase transition temperatures
- Alter the compressibility modulus of the membrane.

The membrane itself can also impact the activity of the drug molecule:

- Affect the drugs diffusion pathway to a binding site within a receptor protein.
- Accumulation of the drug within the membrane (toxicity).
- Cause changes in the conformation of the drug molecule which could potentially alter the binding of the drug to a receptor.

For lipophilic drugs, like those studied in the coming chapters, the permeation into membranes is a crucial part of their action. The membrane can provide a pathway to receptor binding so understanding drug permeation is very important in pharmaceutical science. To understand this process, experimental permeability assays are used extensively in pharmaceutical research. There are two main types which are often used, the Caco-2 cell monolayer assay and the parallel artificial membrane permeability assay.

Caco-2 cell assays are used to measure the permeation rate of a drug through a monolayer of human carcinoma cells using various forms of spectroscopy.[43] This

method has been shown to provide good agreement with *in vivo* results, however, due to this method using an assay of live cells, inconsistencies can be seen due to the potential differences in the state of the cells in each assay. This process can also often be slow due to the meticulous preparation required to create a suitable and stable monolayer.

Parallel artificial membrane permeability assay (PAMPA) is another technique which has been developed to study drug-membrane permeation. PAMPA overcomes the drawbacks of Caco-2 assays by allowing faster experiments and removing the chance of active transport by only measuring passive permeation. The basic setup is similar to the Caco-2 method as it involves an artificial lipid membrane located between two plates, one with the drug and another with the receiving solution. The same spectroscopic measurements can be used to obtain the permeability coefficient of the drug.

1.5.3 Computational investigations into anesthetic-membrane interactions

The development of computational techniques such as molecular dynamics simulations have allowed researchers to study the interactions between anesthetic drugs and lipid bilayers at atomic resolutions. Unbiased all-atom MD simulations have been shown to accurately characterise the effects that anesthetics have on the strucutral and mechanical properties of lipid membranes, course-grained simulations have also been useful[44] although this technique is usually reserved for studying large scale transitions[45] in membrane systems as opposed to drug-membrane interactions. One of the first studies that looked directly at anesthetic interactions with lipid bilayers was carried out in 1995 by Huang *et al.*[46] where they inserted a trichloroethylene molecule into a small 24 DOPC bilayer. They were able to show that the anesthetic caused three major perturbations of the bilayer structure. An increase in the ratio of the effective areas of hydrocarbon tails was observed which suggested that the lipids near the anesthetic formed a hexagonal phase. There was also a slight increase in the frequency of chain dihedral angles found in the gauche

conformation, and a slight increase in the lateral mean square- displacement of the lipid molecules. Enhanced sampling free energy methods are commonly used to calculate free energy profiles of membrane crossing for anesthetic molecules, first demonstrated by Pohorille *et al.*[47]

Calculations from Pohorille *et al.*[47,48] showed that anesthetic molecules preferred to interact at the head group-water interface. MD simulations of halothane showed that this was the case[49] and they identified a number of strucutral perturbations, such as an increase in area per lipid, the orientation of the head group dipole, and a decrease in the order of the acyl chains which was predicted experimentally.[50] These studies suggest that anesthetics occupy this interface site and non-anesthetics occupy the center of the bilayer[51] irrespective of the degree of saturation of the acyl chains. Similar results have also been seen for xenon which is able to diffuse between lipid tails and head groups, inducing more lateral expansion and lipid tail disorder compared to neon, argon and krypton which remain at the center of the bilayer.[52] Similar results have also been shown for other anesthetics, such as ethanol[53] and enflurane.[54]

Several studies have also tried to understand the effects of pressure in bilayer systems containing anesthetics in order to rationalise the known pressure reversal of anesthesia, that is, the inverse correlation between pressure and anesthetic potency.[55] The pressure reversal of anesthesia suggests that the application of 100 bar pressure can reverse general anesthesia, this was demonstrated on animals placed in hyperbaric pressure chambers. It was also shown that pressure reversal of anesthesia was also reversible, as anesthesia resumed upon the removal of additional pressure.[56] This was thought to occur due to anesthetics partitioning into membranes causing an increase in membrane thickness and the application of pressure returned the membrane to its normal thickness. This was later disproved as the application of hydrostatic pressure thickens fluid membranes, rather than thinning them.[57] The phenomena of pressure reversal is also difficult to explain in terms of anesthetic binding to receptors. For example, the pressures required to affect enzyme-substrate binding are at least an order of magnitude greater than those required for reversal of anesthesia.[58,59] MD simulations carried out by Chau

et al.[60] used very high concentrations of halothane at elevated pressures in DMPC bilayers. They showed that under high pressures, the halothane molecules showed an elevated incidence of aggregation which they suggested would impact halothane binding to membrane protein sites. In contrast to these observations, aggregation of isoflurane molecules in lipid bilayers was not observed at high pressures which suggest that halothane may be an isolated example.[61]

The advancement of computational methods such as molecular dynamics simulations have allowed the in-depth study of the interactions between anesthetics and lipid membranes. The study of these interactions allow the comparisons between different anesthetic molecules to made which can give information about differences in action observed experimentally. The inclusion of other components, such as membrane proteins will allow studies to be conducted into indirect modulation of proteins which is a possible component of the general anesthesia mystery.

1.6 Ion channel proteins

Ion channel proteins are integral membrane proteins which allow the diffusion of ions down their electrochemical gradient between the extracellular medium and the cell cytoplasm in the interior of the cell. The conduction of ions can be controlled by the actions of various external stimuli, such as ligand binding, changes in transmembrane voltage, heat, or mechanical actions on the protein, and is responsible for regulating electrical signals across the cell membrane. Pentameric ligand-gated ion channels (pLGICs) which are studied extensively in this work are responsible for the rapid conversion of chemical signals to electrical impulses throughout the nervous system, this process is vital for neurotransmission (Figure 1.3).

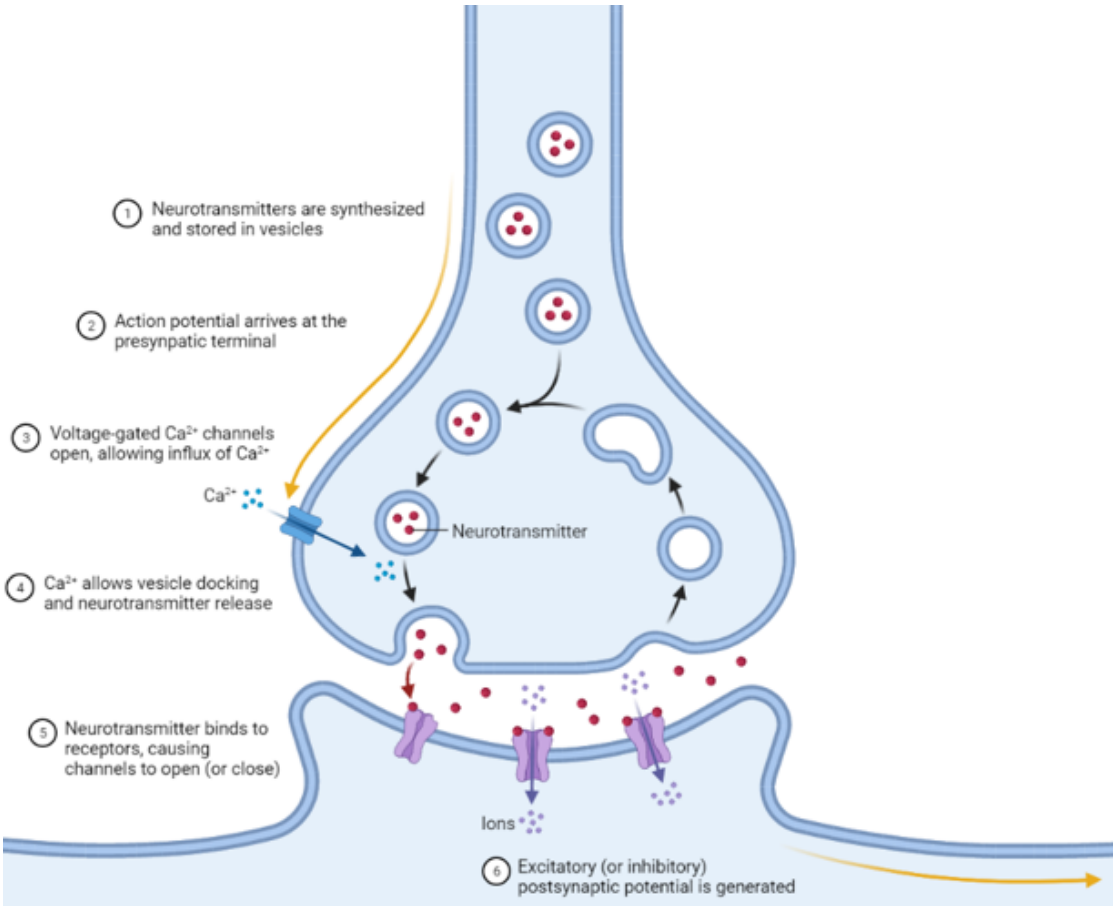

FIGURE 1.3: Graphical representation of synaptic transmission between a pre and post synaptic neuron. pLGICs are shown in purple

These types of ion channel proteins are from the cys-loop receptor family and they have been identified as putative targets for general anesthetics with the response either being inhibition or potentiation depending on the type of channel.[62]

1.6.1 Structure of pLGICs

The overall structure of pLGICs contains five homologous subunits which form a pentameric arrangement (Figure 1.4 A). Each individual subunit contains C- and N- terminal extracellular and cytoplasmic and transmembrane domains.[63,64] The orthosteric agonist binding site is located in the extracellular domain around the β9-β10 loop (loop C), alongside the cys-loop which is a key characteristic of

these receptors, this 13-residue loop is flanked by cysteine residues which form a disulfide bond (Figure 1.4 B).

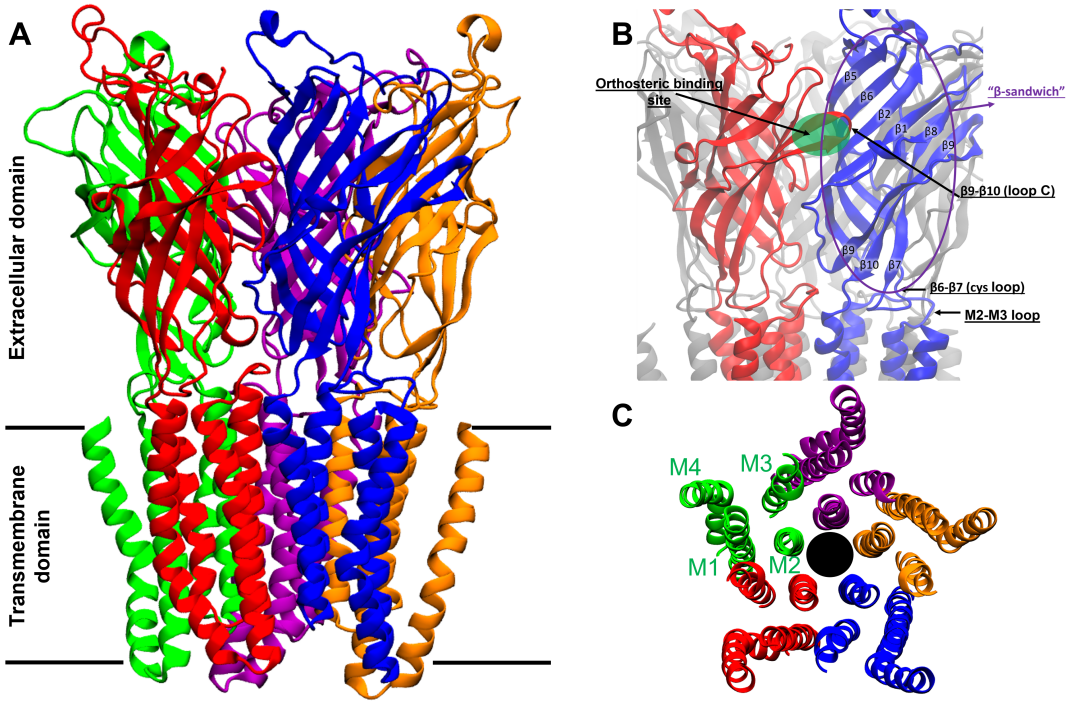

FIGURE 1.4: (A) Graphical representation of the GLIC protein highlighting the position it takes within the cell membrane, each colour represents an individual subunit (S1-S5). (B) Graphical representation of the extracellular domain with two subunits highlighted (blue and red). Structurally significant components of the extracellular domain are labelled. (C) Transmembrane domain alpha helices with each colour representing an individual subunit. Each individual helix in a subunit is labelled. Black sphere represents the channel pore

The symmetry of the transmembrane domain forms the ion conducting pore which is formed by the four transmembrane helices (M1-M4). The M2 helix of each subunit forms the pore itself (Figure 1.4 C) and a cytoplasmic domain of variable length intersects helices M3 and M4.[35]

Prokaryotic homologues of pLGICs have been discovered and high resolution crystal structures were able to be resolved. Two crystal structures which represent the closed and open states of a pLGIC, those from *Erwinia chrysanthemi* (ELIC)[65] and the *Gloeobacter violaceus* (GLIC).[64] The GLIC channel which is represented in Figure 1.4 is used thoroughly in this work. The structures of these proteins consist

of a homologous transmembrane domain (M1-M4) and a large extracellular domain which consists of 8 beta sheets which form the "β-sandwich" domain. It has been shown that GLIC is highly susceptible to general anesthetics.[66] These structures are therefore an ideal target to study the mechanisms of anesthetic actions at pLGICs. It should be noted that other receptors in the cys-loop family have been studied during anesthetic research, such as the glycine receptor,[67] nicotinic acetylcholine receptor (nAChR),[68] $GABA_A$ receptor,[69] and the GluCl channel.[70] These studies have often focused on computational studies using homology models.

1.6.2 Computational investigations into anesthetic-pLGIC interactions

After the discovery of the open state GLIC crystal structures, work began to try and identify possible sites where anesthetic agents may exert their effect. Molecular dynamics simulations provide a good method which allows the binding of anesthetics, and the affect this binding has on the protein to be investigated. A study conducted by Brannigan *et al.*[71] utilised "flooding" molecular dynamics simulations in which a large concentration of drug molecules are added to the system in order to search for as many binding sites as possible. They aimed to ascertain where the general anesthetic isoflurane bound to the GLIC structure and if there were any indications that it could alter the functional state of the channel. Multiple binding sites were identified in both the extracellular domain and the transmembrane domain. The site that was determined to have the most functional relevance was a binding site within the ion conducting pore where isoflurane was observed to bind as a dimer. The presence of isoflurane within the pore suggests that isoflurane could exert its anesthetic effect by physically blocking the passage of ions from the extracellular region to the intracellular region, instead of causing a conformational change within the protein that causes the channel to adopt a closed conformation. Binding of isoflurane was also found in an intrasubunit site in which the authors speculate that residence within this site determine agonist

susceptibility in a position behind the M2 helices parallel to the hydrophobic gate region which could influence the state of the receptor.[71]

A crystal structure (PDB 3P50) was solved which showed propofol binding within a transmembrane "anesthetic binding site" which is located in an intrasubunit crevice (Figure 1.5).[72]

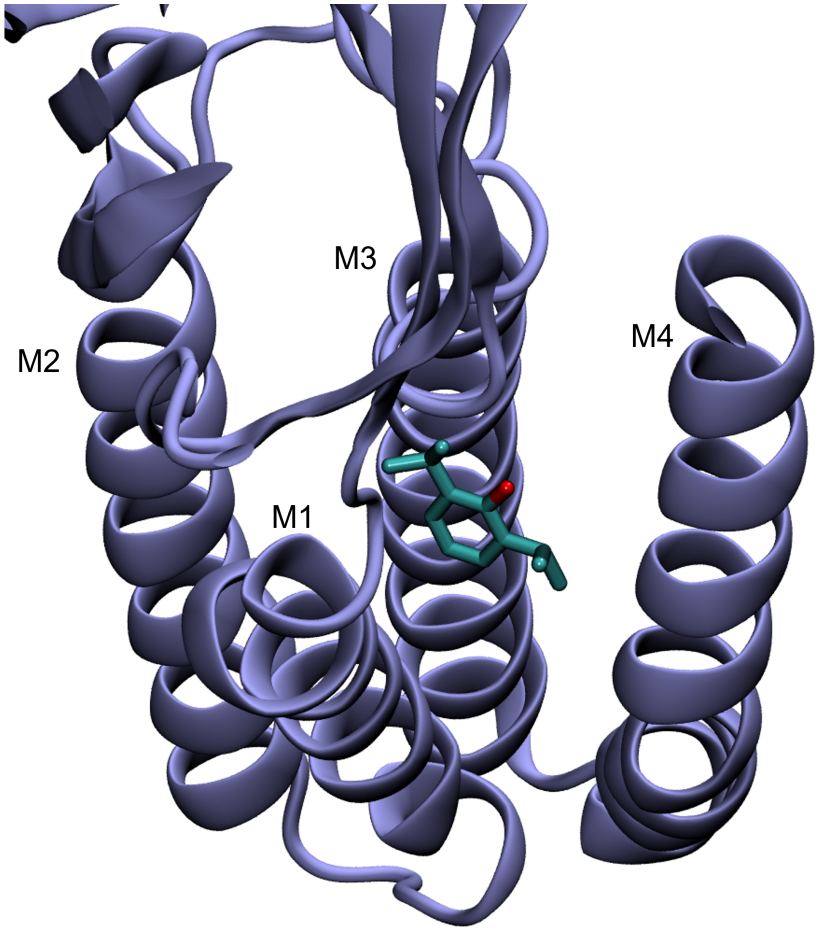

FIGURE 1.5: Propofol binding site within a subunit

The authors performed MD simulations of propofol within this site and concluded that the drug molecule became less mobile in this site over the duration of the simulations. There are several problems with the simulations that were carried out, as these simulations were only 30 ns in length which is insufficient to draw any conclusions about the drug molecule stability within the site. The simulations were conducted directly from the crystal structure with the drug molecule bound in the site, so no pathway of binding was determined and the drug molecule could have

moved from this binding site to another. There was also no analysis conducted on the protein dynamics with the drug molecule bound compared to a pure protein structure which would have helped determine if/how the drug molecule altered the active state of the protein.

Willenbring *et al.*[73] carried out docking calculations and MD simulations of isoflurane interacting at GLIC. They found that prolonged binding caused intersubunit salt bridges in the extracellular domain to break which caused an inward tilt of the M2 helices which provides a mechanism by which isoflurane contributes to channel closure. Similar mechanisms that involve the breaking of salt bridges have also been observed for halothane which was shown to bind near the M2-M3 loop which caused increased mobilisation of the cys-loop and perturbation of the D32-R192 salt bridge.[74,75] These components of the ion channel are also thought to be crucial for channel gating, as when they are removed, the open state is rapidly destabilised.[76]

To further investigate the previously mentioned pore binding of isoflurane, LeBard *et al.*[77] performed free energy perturbation (FEP) calculations on monomers and dimers of isoflurane and propofol to calculate their binding affinities within the channel pore. They found that the binding affinities of isoflurane as a dimer, and propofol as a dimer both resembled the micromolar affinity determined experimentally and were consistent with a pore-block mechanism.

The analgesic/anesthetic drug ketamine has been shown to bind in the extracellular domain of the GLIC structure (Figure 1.6). The crystal structure of (R)-ketamine binding within an extracellular intersubunit site has been solved.[78] The binding of (R)-ketamine in this site caused significant strucutral changes in the protein structure which has been shown by MD simulations.[79] Ketamine binding was shown to increase the flexibilities of loop C, M2-M3 linker and loop F. The binding also caused the formation of a hydrophobic gate in the channel pore in which hydrophobic residues tilt or rotate towards the pore center which blocks the passage of water molecules causing rapid dehydration of the pore. Multiple

intersubunit and intrasubunit salt bridges were observed to break upon ketamine binding.[79]

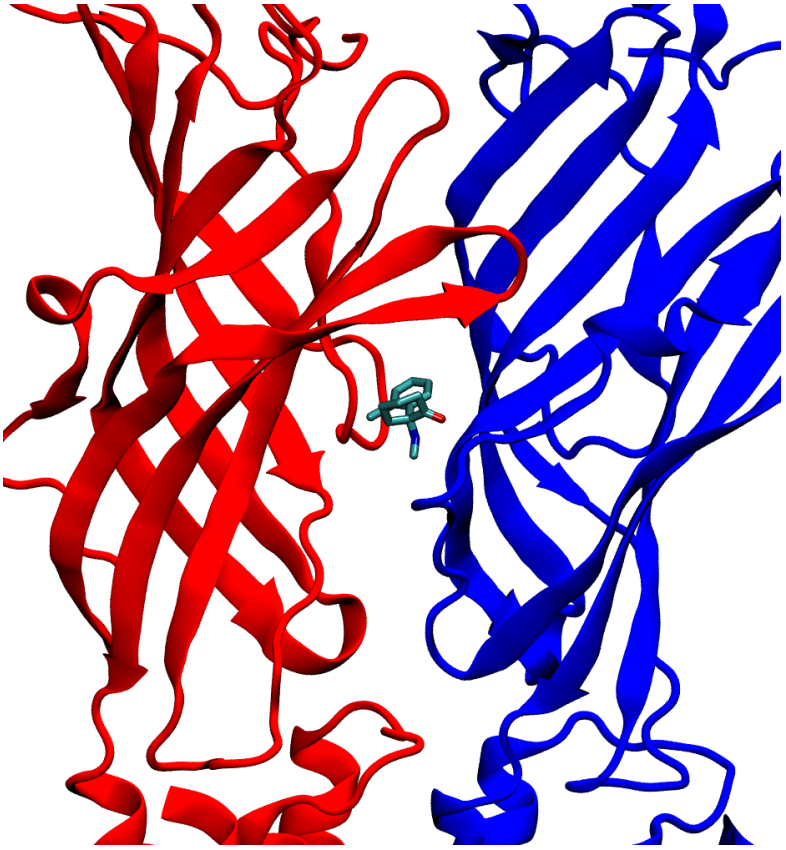

FIGURE 1.6: Ketamine intersubunit binding site

This summary of studies show the variation in the anesthetic binding sites which have been found for the GLIC channel using experimental and computational methods. It is therefore a good target to look for new binding sites for different anesthetics which can then be compared to the data already available to see differences in binding, and the effect on the protein structure and its activation state.

1.7 The quantum theory of anesthesia and its relation to consciousness

As explained in previous sections, anesthesia remains one of the most important pharmacological discoveries of the modern medical age which has resulted in safer and more efficient surgical practices. Yet despite over a century of research, both clinical and academic, the mechanisms which underlie the reversible loss of memory and consciousness is still a mystery. Also still not known are the molecular mechanisms by which the brain produces memory and consciousness, and the mechanisms behind these two great unknowns are very likely to be related in some way. Understanding the mechanisms behind general anesthesia could not only resolve existential and philosophical issues regarding consciousness, but also aid in the design and development of new anesthetic drugs which are currently discovered serendipitously, rather than by rational design.

Modern research which has been carried out across the fields of pharmacology, neuroscience and medicine have not yet shown any targets or mechanisms by which anesthetics cause loss of memory and consciousness. But the mechanisms of anesthesia still currently offer the best way in which we can gain an understanding of consciousness and the encoding of memories. It is well known that several non-conscious brain activities continue, and no new memories are retained when a person is put under general anesthesia. Sensory-evoked potentials continue during anesthesia which shows that the anesthetics are selective for consciousness. Understanding anesthesia might require an understanding of consciousness, and *vice versa.*[80]

During the 1980s a theory was put forward which suggested that anesthetic agents act in a unitary quantum phase in hydrophobic pockets distributed throughout cytoskeletal microtubule subunit proteins, as well as in channel proteins.[81–83] The basics of this idea was that the anesthetic agent acted on some quantum electronic activity in the neuronal hydrophobic regions, rather than the traditional binding to membrane protein receptors. Under conditions in which no anesthetic has

entered the system, London force dipoles in the hydrophobic regions of the protein target coupled and oscillated coherently, and this coupling was theorised to be necessary for consciousness. When anesthetic was present within the system, the anesthetic molecule was thought to bind within these hydrophobic regions by their own London force coupling which would disperse the endogenous dipoles formed in the native protein and hence disrupt the coupling necessary for consciousness.[84] This theory has been investigated recently by by Luca Turin *et al.*[85] who utilised electron spin resonance measurements and quantum chemical calculations to study the anesthetic effects on electron spin in drosophila (fruit flies). They were able to show that there is a link between the unconsciousness in flies and the electron currents detectable by a change in the electron spin quantum observable in the presence of anesthetic agents.[85]

To try and work out where these quantum effects might take place, a theory of consciousness was presented in which quantum computations within microtubules were investigated.[86] Molecular modelling has suggested that electron resonance transfer among aromatic amino acid tryptophan rings in tubulin subunits of microtubules, and from one tubulin dimer to another through microtubules in a quantum electronic process necessary for consciousness.[84] Craddock *et al.* further showed that gaseous anesthetics can bind within these same regions, and could act there to prevent consciousness. This has been called the 'quantum mobility theory' of anesthetic action.[87]

1.7.1 Interactions between anesthetics and microtubules

The main functions of microtubules are to generate the shape of the cell and create movement by their assembly and coordinated activities with other components of the cell cytoplasm, such as microtubule-associated proteins (MAPs).

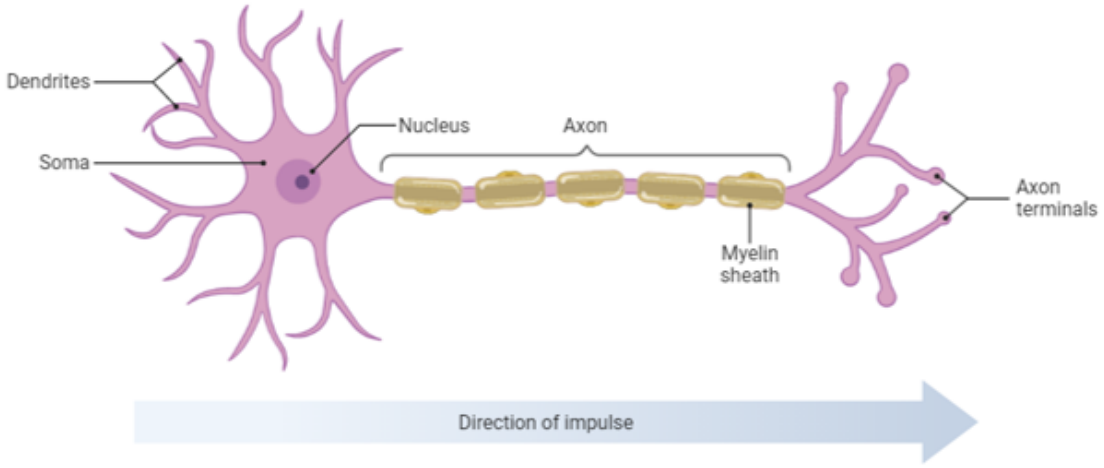

FIGURE 1.7: The basic structure of a neuron with key components labelled

In neurons (Figure 1.7), microtubules are critical for the cell morphology; establishing and maintaining the structure of axons and dendrites. In the neuron axon, microtubules are of the same polarity and are long and continuous, whereas the microtubules in the dendrites are shorter with mixed orientations. These microtubules and their associated proteins (MAPs) are crucial for a wide range of neuronal processes.[88,89]

Microtubules are cylindrical polymers composed of tubulin which is a hetero-dimer. Each dimer of tubulin is composed of an α and β monomer (Figure 1.8 A). These dimers will self-assemble to form microtubules in a guanosine triphosphate (GTP) dependent process. These microtubules are hollow cylinders of 13 linear chains which are called protofilaments (Figure 1.8 B). Monomers are held together by intra-dimer electrostatic interactions while protofilaments are formed by longitudinal interactions between monomers (Figure 1.8 C).

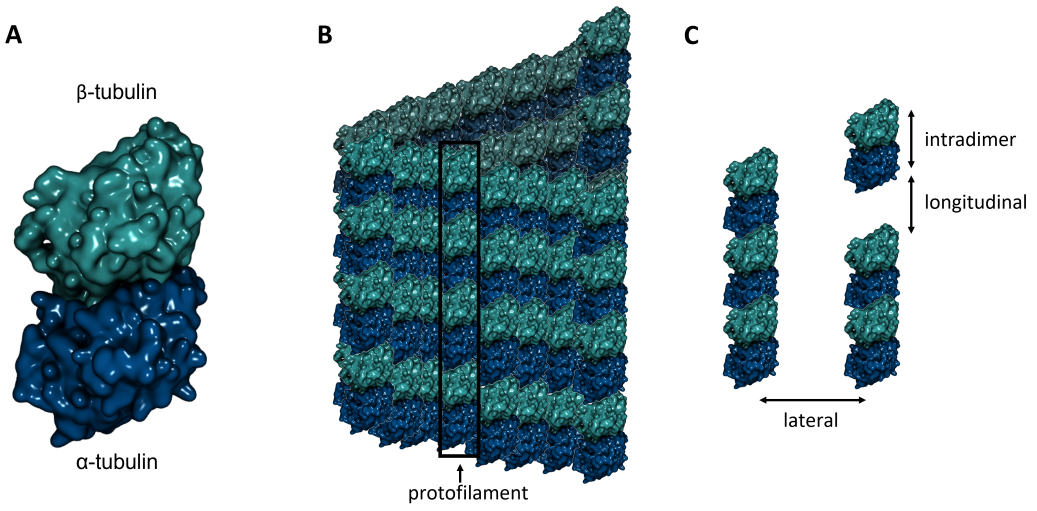

FIGURE 1.8: (A) Tubulin dimer. (B) Microtubule with protofilament highlighted. (C) Interactions between tubulin in microtubule formation

Binding affinities of various anesthetic agents have been shown to be around a thousand-fold weaker in tubulin compared to that of membrane proteins.[90] However there are over 10,000 times more binding sites for anesthetics in tubulin compared to membrane protein binding sites which would result in significant occupation of tubulin sites by anesthetics at clinical concentrations.[91,92] Anesthetics have been shown to interact at longitudinal interfaces and affect the hydrogen bond strengths and disrupt normal microtubule function. Anesthetic binding sites were shown to contain residues which were involved in hydrogen bonding at various interfaces of the microtubule. Anesthetic binding affects the hydrogen bonding networks between dimers at multiple interfaces, these interactions are crucial for coordinated movement of tubulin proteins and the overall stability of the microtubule.[93]

1.7.2 Quantum effects in microtubules

Quantum effects are very likely to play a key role in the biological function of various systems. Electron superpositions have been shown to influence nuclear movement which suggests that quantum superposition of various protein conformations

occurs before one is chosen.[94] Recently, Matsuno has shown magnetic quantum coherence in actin which is a main component of the cytoskeleton in all cells.[95] Other examples of quantum effects such as quantum resonance effects and quantum coherence have been shown in various biological systems which suggest that quantum mechanisms are important throughout biochemistry and biology.[96–98]

Anesthetics interact with hydrophobic regions of proteins by forming London forces inside the pockets and this may stop the mobility of the electrons required for quantum dipoles, superposition, biological function and consciousness. Tuszynski *et al.* investigated the possibility of anesthetic-sensitive dipole functions inside tubulin, which is the protein that forms microtubules.[80] They mapped the network of aromatic residues within tubulin which maps the π-resonance clouds which are located close to each other. Each tubulin dimer has a network of aromatic residues which span the entire structure (Figure 1.9).

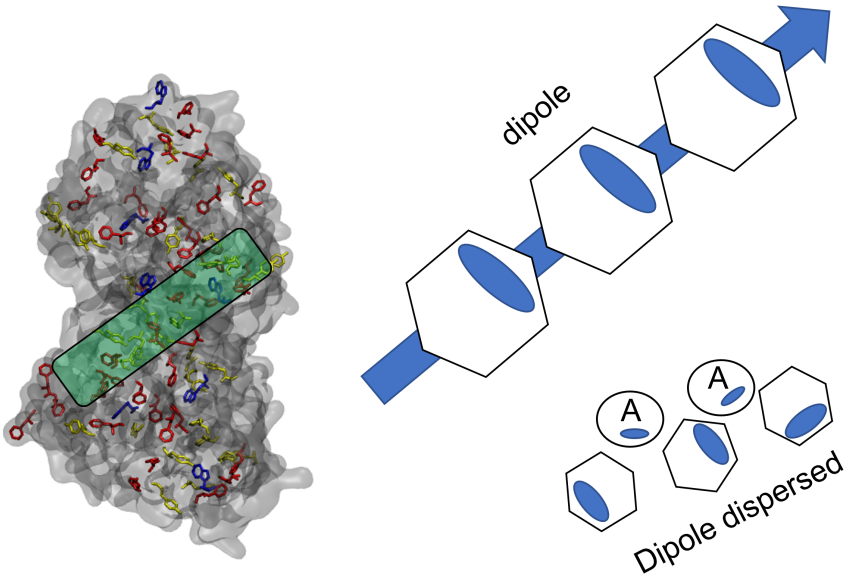

FIGURE 1.9: (Left) Tubulin dimer with phenylalanine residues (red), tyrosine residues (yellow) and tryptophan residues (blue), hypothetical quantum channel of aromatic rings (green) are shown. (Right) Aromatic rings showing dipoles necessary for quantum mobility, and anesthetics dispersing dipoles

They suggest that anesthetics act in these quantum channels inside microtubules and interrupt quantum dipoles, energy transfer and electron mobility which results

in loss of consciousness. Their calculations showed that π-stack terahertz dipole oscillations can be dispersed by general anesthetics which account for the loss of consciousness during general anesthesia.

Whilst these theories are attractive and might possibly have a role to play in the general anesthetic process, there remains a distinct lack of empirical data to back up the theories that have been proposed. When Hameroff[82] proposed an account of anesthetic action as evidence for a quantum mechanical theory of consciousness there was not really a purely biochemical theory of anesthesia available. In recent times however, as described in previous sections, the hypothesis of direct and indirect modulation of ion channel proteins which disrupt neurotransmission has exploded. Substantial empirical support including crystal structures of anesthetic molecules bound to ion channels which appear to be in the closed state, and electrophysiology experiments which show modulation of the channel function in the presence of anesthetics have added so much value to the ion channel hypothesis.

These findings highlight another possibilities for the mechanisms behind general anesthesia as opposed to direct binding to membrane proteins which inhibits electrical signal conduction between neurons, although these process could very well act together. Experimental validation of the quantum theory of anesthesia will require investigations to be carried out at the level of individual neurons which in the near future could be possible. Large scale computational investigations into the dynamics of microtubules and MAPs in a relevant cellular environment are also not possible currently due to the vast size and timescales that would be required, and it is also not possible to include the quantum effects of the channels within microtubules in a system of this size. With advances in computational hardware and software, these calculations might one day be possible.

1.8 Summary

Many molecules have been discovered which can induce and maintain general anesthesia, which has allowed surgical procedures to be carried out under safer and more efficient conditions. Combinations of these anesthetic agents have revealed new methods of carrying out general anesthesia, such as the combination of propofol and fentanyl which allows for a process called total intravenous anesthesia (TIVA) which allows for rapid recovery, greater haemodynamic stability and reduced risk of organ toxicity. Even though these methods have been used routinely for decades, the underlying mechanisms behind the phenomenon of anesthesia remain relatively unknown. Computational simulation methods can allow the investigation of these mechanisms at atomic level detail.

- Based on the legacy of the Meyer-Overton hypothesis which recognised that the lipid solubility of anesthetic molecules correlated with their potency. Although exceptions to this theory have been found, the lipid membrane remains an important area for anesthetic research, and drug design in general. Interactions between these drug molecules and the lipid membrane can be studied with classical simulation methods such as molecular dynamics.

- Experimental studies have shown that general anesthetics can modulate the function of membrane protein ion channels which convert chemical signals to electrical impulses throughout the nervous system. Figure 1.10 shows the binding sites which have been identified for anesthetic molecules on pentameric ligand-gated ion channels. These binding sites have all been shown to induce channel close which inhibits the conduction of ions, despite the difference in each binding site location. Molecular dynamics simulations allow the study of anesthetic binding to these proteins which can then reveal how the binding affects the function of the protein.

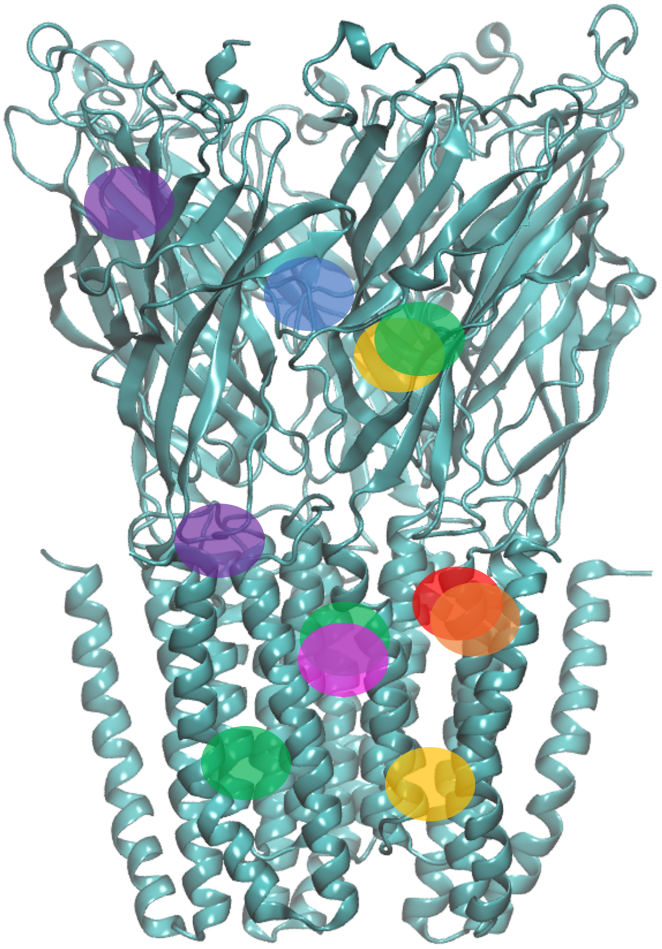

FIGURE 1.10: Ligand-gated ion channel binding sites for ketamine (blue), propofol (red), halothane (purple), bromoform (yellow), desflurane (orange), isoflurane (pink) and xenon (green)

- The interactions of anesthetic drugs with lipid membranes and ion channel proteins using molecular dynamics simulations is the main focus of this work. Firstly, the background on the theory of MD simulations and how they can be applied to these systems is required.

Chapter 2

Theory and modelling

2.1 Introduction to simulation

Computational modelling has become a powerful tool in many areas of scientific research. The advancement of computer hardware and development of efficient algorithms have allowed theoretical modelling to be applied to a wide range of scientific problems. These models allow scientists to investigate properties of their system which are unable to be probed experimentally, or at small timescales where experiments can not accurately measure. In chemistry, there are many models based on different levels of theory which can be employed, see Figure 2.1. The most computationally expensive of the methods available are those based on quantum mechanics. The two most common quantum chemical methods are correlated methods such as Coupled-Cluster (CC) and Møller-Plesset (MP), and Density Functional Theory (DFT). These types of calculations are limited to the study of small systems on the order of tens of atoms, so are used for modelling electronic properties of small molecules and chemical reactivity, often with no explicit solvent, for example. This renders these methods unsuitable for the study of large biological systems.

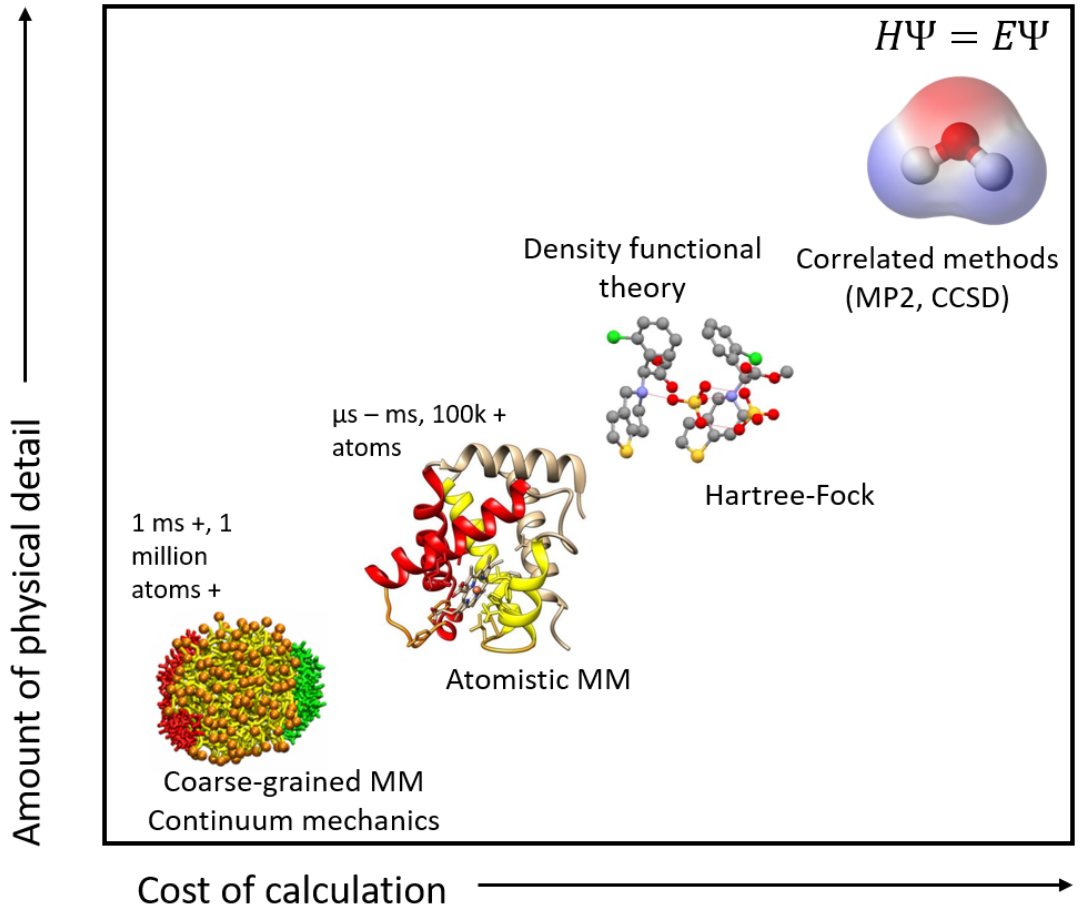

FIGURE 2.1: Various computational methods which are at the disposal of the computational chemist

To overcome the system size problem encountered by quantum methods, models based on molecular mechanics (MM), namely molecular dynamics (MD) are used for the study of biologically relevant systems. These methodologies currently allow the study of systems in the order of 100,000 + atoms over multiple μs. Although, there are computers which have been developed specifically for the application of molecular dynamics simulations, namely MDGRAPE[99] and ANTON[100] which allow simulations of huge systems (millions of atoms) up to millisecond timescales. In the coming sections I will briefly review the theory of quantum chemical calculations which are used to develop the more approximate classical models, which will also be reviewed in greater detail.

2.2 Quantum chemistry

Theoretical calculations have been used for a long time now to predict unknown phenomenon in chemistry and to aid in the design of experiments and interpretation of the results. Quantum mechanics was formulated in the early 20th century which allowed matter at the atomic scale to be described with the Schrödinger equation. This theoretical approach gave the first description of how a physical system changes over time at a quantum level of detail. In the modern day, quantum chemical methods are used extensively in the parametrisation of classical molecular dynamics forcefields which will be discussed later.

The time-independent variation of the Schrödinger equation can be written as:

$$E\Psi(R,r) = \hat{H}\Psi(R,r) \tag{2.1}$$

The solution to this equation gives the wave function (Ψ) of the systems. The wave function contains all of the measurable information for a physical system and depends on the nuclear and electronic coordinates R and r respectively. $\hat{\mathrm{H}}$ represents the Hamiltonian operator for the system which contains the kinetic and potential energy terms. This Hamiltonian on a molecular level takes the form:

$$\hat{H} = \hat{T}_{nuc} + \hat{T}_{el} + \hat{U}_{nuc-nuc} + \hat{U}_{el-el} + \hat{U}_{el-nuc} \tag{2.2}$$

The $\hat{\mathrm{T}}_{el}$ and $\hat{\mathrm{T}}_{nuc}$ operators are the kinetic operators for electrons and nuclei respectively, $\hat{\mathrm{U}}_{nuc-nuc}$ represents the nuclei-nuclei potential energy operator, the electron-nuclei and electron-electron potential energy operators are $\hat{\mathrm{U}}_{el-nuc}$ and $\hat{\mathrm{U}}_{el-el}$ respectively.

Solving these equations for the hydrogen atom is trivial, but solving for any system which is of any scientific interest is non-trivial as a many-body problem is present. Therefore when we are using algorithms to calculate quantum chemical properties, approximations are used to solve the equations.

The first approximation that is considered is the Born-Oppenheimer approximation. This well known approximation postulates that due to the mass of the electron being so small in comparison to the mass of the nucleus, the nucleus can be assumed stationary on an electronic timescale. Using this, we can solve the electronic part of the Schrödinger using nuclear positions. Hence, the equation has the form:

$$E_{el}\Psi(R,r) = \hat{H}_{el}\Psi(R,r) \tag{2.3}$$

Where the electronic Hamiltonian ($\hat{\mathrm{H}}_{el}$) is represented as:

$$\hat{H}_{el} = \hat{T}_{el} + \hat{U}_{el-el} + \hat{U}_{el-nuc} \tag{2.4}$$

By solving these equations, the potential energy surface (PES) which results is used for determining nuclear motion.

This theoretical methodology is still extremely complex so the Hartree-Fock (HF) method is often applied to give an approximate solution to the electronic Schrödinger equation of a physical system. This methodology uses a one-electron approximation that states that the motion of a single electron is independent of all other electrons. This approximation is expressed as:

$$\Psi(r_1, r_2, ..., r_N) = \psi_1(r_1)\psi_2(r_2)....\psi_N(r_N) \tag{2.5}$$

We can then represent the system electronic wave function as a sum of the single electron wave functions, hence all electron-electron interactions are "averaged" which drastically reduces computational cost, but also significantly reduces the accuracy of the calculation.

The Hartree-Fock equations rely on their own solutions so they have to be solved iteratively using something called the variational principle to calculate the ground-state energy and the wave function. This principle states that an approximate of the true wave function will give a higher energy than the systems true energy. Thus the more accurate the approximate wave function, the closer the resulting energy will be to the true energy. This is obtained when the energy of the system

is at its minimum. Small iterative changes to the approximate wave function are made until a minimum energy is achieved.

HF methods will use a basis set expansion in which each molecular orbital ψ(r) is expanded in terms of the basis functions ϕ(r) which are atomic orbitals. Each molecular orbital becomes a liner combination of atomic orbitals:

$$\psi_i(r) = \sum_{v=1}^{n_{basis}} c_{vi}\phi_v(r) \tag{2.6}$$

The HF equations can then be expressed as:

$$\bar{F}_i \sum_{v=1}^{n_{basis}} c_{vi}\phi_v = \epsilon_i \sum_{v=1}^{n_{basis}} c_{vi}\phi_v \tag{2.7}$$

Multiplying by a specific basis function and integrating yields the Roothaan-Hall equations for a closed system[101] which is written as a matrix equation:

$$FC = SC\epsilon \tag{2.8}$$

Where F is the Fock matrix, C is the molecular orbital expansion coefficients matrix, S is the overlap matrix of basis functions and ϵ is the diagonal matrix of orbital energies.[102] The molecular orbitals may be obtained by solving the Roothaan-Hall equation using the variational principle.

To fully represent a molecular orbital we would need to expand with a complete basis set. This would however contain an infinite number of basis functions which is not practical by any means so a molecular orbital can only be approximated by the above methodology. The accuracy of the molecular orbitals will increase as the number of basis functions increases, but the cost of the HF calculations scales as the fourth power of the number of basis functions.[103] The choice of basis functions ϕ(r) is important so they have a behaviour which agrees with the properties of the system and allows fast conversion as more functions are added.

The main downside to HF methods is the neglect of electron correlation effects. Post-Hartree-Fock methods such as Coupled-Cluster (CC) and Møller-Plesset (MP)

have been developed which explicitly take into account electron correlation but at an increased computational cost.

The evolution of high performance and GPU computing over the past decade have given rise to huge advances in the amount of calculations that can be performed in a reasonable amount of time, but quantum chemical calculations remain unsuitable for very large, biological systems. QM calculations have been used for small proteins but for systems in the order of 100,000 + atoms, the timescales required are far too large for practical use. Despite this, quantum chemical calculations are of high importance in deriving parameters for MD simulation.

2.3 Molecular mechanics

Theoretically it is possible to calculate the development of a large molecular system over time using quantum chemical methods, but in reality you would need an enormous amount of computing power and time to calculate even a nanosecond of data for a small protein. In order to study large biomolecular systems computationally, classical molecular mechanics (MM) is applied. MM methods ignore all electronic motion and can therefore study large systems over nanosecond to millisecond timescales. Instead of applying a quantum level of theory to the calculation, MM methods apply the Born-Oppenheimer approximation to calculate the systems energy based only on nuclear positions.

2.3.1 Forcefields

The main component of any MM method is the force field. The forcefield consists of a number of terms which represent bonded and non-bonded interactions (Figure 2.2). Solving these terms will give the potential energy of the system. There is an ever increasing list of software packages which can perform classical MD and most packages have forcefields which have slight differences based on what they are designed to study. In this work, the Assisted Model Building with Energy

Refinement (AMBER)[104] MD forcefields are used extensively, so the AMBER functional form will be described.

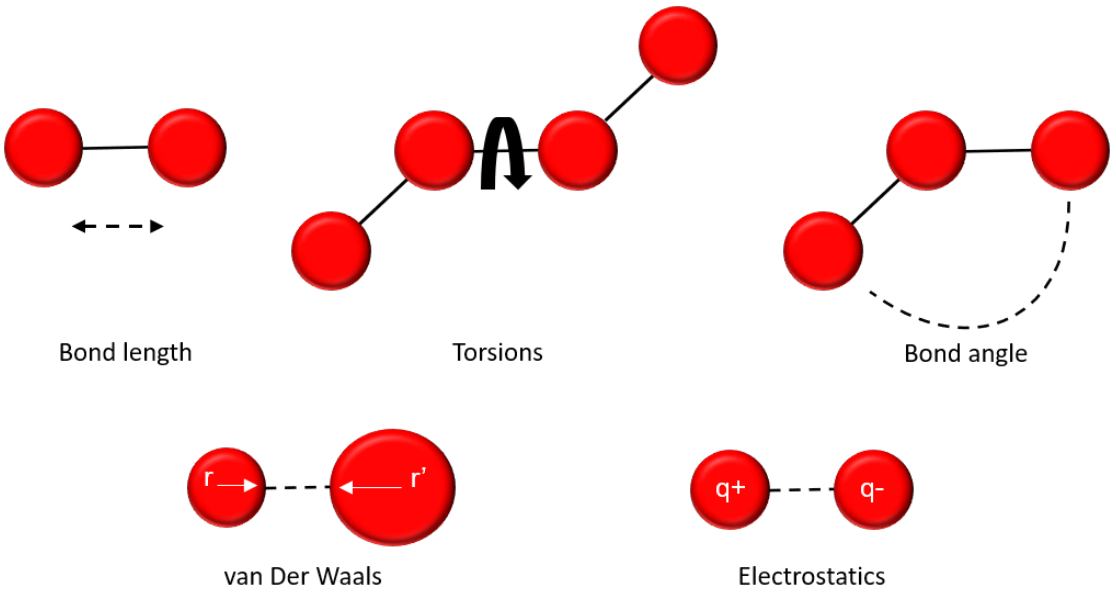

FIGURE 2.2: The basic bonded (top) and non-bonded (bottom) interactions that are evaluated by a molecular mechanics force field to determine the potential energy of a system

Atoms during MD simulations are represented as charged spheres with no explicit electrons. Electrons are represented implicitly by point charges which are centred on each atom. The interactions shown in Figure 2.2 are described by mathematical terms and empirical parameters which can come from experiment or QM calculations. The AMBER forcefields have the form:

$$V(r^N) = \sum_{bonds} k_b(l - l_0)^2 + \sum_{angles} k_a(\theta - \theta_0)^2 + \sum_{torsions} \sum_{n} \frac{1}{2} V_n[1 + cos(n\omega - \gamma)] + \sum_{j=1}^{N-1} \sum_{i=j+1}^{N} \left\{ 4\epsilon_{ij} \left[\left(\frac{\sigma_{ij}}{r_{ij}} \right)^{12} - \left(\frac{\sigma_{ij}}{r_{ij}} \right)^{6} \right] + \frac{q_i q_j}{4\pi\epsilon_0 r_{ij}} \right\} \tag{2.9}$$

Term 1, summing over bonds, describes bond stretching using Hooke's law where k_b is the force constant. Here, the force constant is used to determine the amount of energy used in stretching the bond from the equilibrium bond length l_0. Term 2, summing over angles, again used Hooke's law but to describe angle bending. k_a is the force constant which determines the amount of energy used in bending

the angle away from its equilibrium vales θ_0. The third term is used to describe rotational motion around a dihedral or torsion angle. This is described by a cosine series expansion with periodicity n, torsion angle ω, offset γ and barrier height V_n.

The first three terms constitute the bonded interactions within the system, terms four and five describe the non bonded interactions. The fourth term describes the van der Waals (vdWs) interactions by a 12-6 Lennard-Jones (LJ) potential. This potential describes both inter-particle Pauli repulsion due to overlaps of the electron cloud, and long range attraction due to induced-dipole effects as adjacent particles' electron clouds adapt to one another. The repulsive 12th power term is empirical and the attractive 6th power is derived from the London formula for the interaction energy of uncharged molecules.[105] ϵ_{ij} represents the potential energy minimum and σ_{ij} is the distance at which the inter-particle potential is zero. Term 5 describes the the electrostatic interactions which occur between charged or polar particles, these are described by Coulomb's law. ϵ_0 represents the electrical permittivity of free space, q is the partial charge on each atom and r_{ij} is the distance between each of the particles.

2.3.2 Molecular dynamics simulation

As eluded to earlier, the potential energy landscape about a particle determines the force that the particle experiences, which is equal to mass times acceleration:

$$\boldsymbol{F} = m\frac{d^2\boldsymbol{r}}{dt^2} \tag{2.10}$$

$\mathbf{F}$ represents the force, m is the mass of the particle and $\frac{d^2\boldsymbol{r}}{dt^2}$ is the acceleration (2nd derivative with respect to time). The force on any atom in the system is calculated from the negative gradient of the potential energy:

$$\boldsymbol{F} = -\nabla U(\boldsymbol{r}) \tag{2.11}$$

To obtain a relationship between velocity, acceleration and position, we can combine the above equations:

$$\boldsymbol{a} = \frac{d^2\boldsymbol{r}}{dt^2} = \frac{d\boldsymbol{v}}{dt} \quad \text{where velocity} \quad \boldsymbol{V} = \frac{d\boldsymbol{r}}{dt} \tag{2.12}$$

Now that we can describe the particles position, velocity and acceleration, we have to determine how the system propagates over time. This can be achieved by integrating Newton's equations of motion. Doing this analytically is not feasible, so there are multiple schemes can can be used to do this numerically. Numerical integration methods can be used which allow for repeated integration of the forces over small time intervals to produce a trajectory. The most commonly used algorithms are the velocity Verlet or leapfrog algorithms. The velocity Verlet method is considered more complete, as it is able to calculate the velocities and positions at the same time step. This algorithm is summarised in the following equations.

$$\boldsymbol{r}(t + \delta(t)) = \boldsymbol{r}(t) + \boldsymbol{v}(t)\delta t + \frac{1}{2}\boldsymbol{\alpha}(t)\delta t^2, \tag{2.13}$$

$$\boldsymbol{v}\left(t + \frac{\delta t}{2}\right) = \boldsymbol{v}(t) + \frac{1}{2}\boldsymbol{\alpha}(t)\delta t, \tag{2.14}$$

$$\boldsymbol{\alpha}(t + \delta t) = -\frac{1}{m}\nabla U(\boldsymbol{r}(t + \delta t)), \tag{2.15}$$

$$\boldsymbol{v}(t + \delta t) = \boldsymbol{v}\left(t + \frac{\delta t}{2}\right) + \frac{1}{2}\boldsymbol{\alpha}(t + \delta t)\delta t. \tag{2.16}$$

Where, $\boldsymbol{r}$ is the position of the particle, $\boldsymbol{v}$ is the velocity of the particle, $\boldsymbol{\alpha}$ is the acceleration of the particle. Newton's laws state that the energy should be conserved, therefore the trajectories are sampled under the microcanonical ensemble in which the number of particles, volume and energy are conserved. To sample at constant pressures and temperatures which is desired during biomolecular simulation, a barostat and thermostat is required which is discussed in the coming sections.

The time steps purpose is to define the time in between each step of the MD simulation. The value of the time step is chosen so that it is significantly shorter than the highest frequency vibration that is possible in the system, this is to stop

atoms coming too close together or overlapping between MD steps as this would cause massive spikes in energy in the system due to repulsion between the atoms leading to a failed simulation. In an ideal situation we would employ a very short time step for atomistic MD simulation in the region of 0.5 fs per step, but this would severely limit the amount of sampling that could be achieved during the simulation. Typical MD simulations of biological systems will use a 2 fs time step and that is what we have used throughout this thesis. We should note that the bond stretching of a covalent bond to hydrogen is on the order of 10 fs which would, in theory, limit the time step of the system to around 1 fs, these motions are often constrained using a constraint algorithm, such as the SHAKE algorithm[106] which is used in this thesis. The use of these algorithms allow the use of a larger, more computationally efficient time step.

2.3.3 Solvation

When conducting simulations of biological systems, solvation must be taken into account. Solvation in MD simulations can be added in two ways; an implicit model can be used in which there are no explicit solvent molecules included in the system, the solvent is instead modelled by a homogeneously polarizable medium. Using these solvent models will significantly reduce the computation time of the simulation, but there is no explicit detail about how the solvent is interacting with the system. In all of the MD simulations carried out in this thesis, explicit solvation has been used. To model the water in our systems, TIP3P waters were used, this model is a very popular model in MD simulations which has been parametrised to reproduce several properties of water, such as, expansion coefficients and density.[107] This model is made up of a three-point, rigid water model with two hydrogen atoms bound to a single oxygen atom. An artificial "bond" is present between each hydrogen atom which maintains the rigidity of the water molecule. Each atom possesses a partial charge, but only the oxygen atom has Lennard-Jones parameters with a VdW radius which surrounds the hydrogen

atoms also. The rigid nature of this model allows it to be used with constraint algorithms such as SHAKE.

2.3.4 Periodic boundary conditions

In order to avoid edge effects, its is crucial to model an infinite system rather than a finite system. In MD simulations this is done by implementing periodic boundary conditions (PBC), where our simulation box "sees" copies of itself on each side (Figure 2.3). When this setup is employed, a particle which leaves the simulation box at one side is reinserted into the opposite side with an intact velocity vector, therefore, our system has no spatial limitations. The main thing to consider when using PBC is that the system has be large enough so that it avoids propagation of any internal correlations, or any correlations which can be amplified artificially, and result in trajectories which are erroneous. If this consideration is met, a system using PBC is very likely an excellent model of liquid bulk phase behaviour.

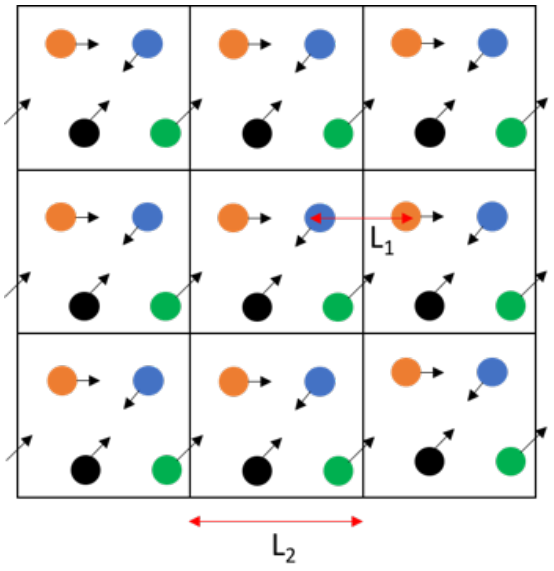

FIGURE 2.3: Four particles in a box with PBC. The system is effectively replicated infinitely to avoid edge effects. The box size L2 must be greater than twice the longest interaction cutoff between contained particles, L1 , so that a particle never interacts with itself

2.3.5 Temperature and pressure control

During the simulation of biomolecules, it is often important to conduct the simulations in the isothermal-isobaric (NPT) ensemble, in which the pressure and temperature are maintained at a set value throughout the simulation. There are many different methods available to control these variables, but throughout this thesis the Langevin thermostat is used to control the temperature, and the Berendsen barostat is used to control the pressure.

2.3.5.1 Langevin thermostat

When we consider how large particles move through a continuum of smaller particles, the Langevin equation

$$\ddot{x} = \nabla\phi - \gamma\dot{x} + \sigma\xi \tag{2.17}$$

or

$$\frac{d\mathbf{q}_i}{dt} = \frac{\mathbf{p}_i}{m_i}, \frac{d\mathbf{p}_i}{dt} = -\frac{\delta\phi(\mathbf{q})}{\delta\mathbf{q}_i} - \gamma\mathbf{p}_i + \sigma\xi_i \tag{2.18}$$

is taken into account. The smaller particles create a damping force to the momenta, -$\gamma\mathbf{p}_i$, as the large particles move through the smaller ones. The smaller thermal particles also move with kinetic energy and give random kicks to the large particles. σ,γ are connected by a fluctuation-dissipation relation

$$\sigma^2 = 2\gamma m_i kT \tag{2.19}$$

which is required to recover the canonical ensemble distribution. The Langevin equation is applied to MD simulations by assuming that the atoms in the system are embedded in a sea of smaller fictional particles. The solvent influences the dynamics of the solute via random collisions and by imposing a frictional drag force on the motion of the solute in the solvent.

At each time step, ΔT, the Langevin thermostat changes the equation of motion so that the change of momenta is

$$\Delta \mathbf{p}_i = \left(\frac{\delta \phi(\mathbf{q})}{\delta \mathbf{q}_i} - \gamma \mathbf{p}_i + \delta p \right) \Delta t \tag{2.20}$$

where $\gamma \mathbf{p}_i$ damp the momenta and δp is a Gaussian distributed random number with probability

$$\rho(\delta p) = \frac{1}{\sqrt{2\pi\sigma}} exp\left(-\frac{|\delta p|^2}{2\sigma^2} \right). \tag{2.21}$$

And standard deviation $\sigma^2 = 2\gamma \mathrm{m}_i \mathrm{kT}$. The random fluctuating force represents the thermal kicks from the smaller particles. The damping factor and the random force combine to give the correct canonical ensemble. Typical advantage for Langevin thermostat is that we need fewer computations per time step since we eliminate many atoms and include them implicitly by stochastic terms.

2.3.5.2 Berendsen barostat

With the Berendsen barostat, the system is made to obey the equation of motion at the beginning of each time step

$$\frac{dP(t)}{dt} = \frac{P_{md} - P(t)}{\tau_P} \tag{2.22}$$

where P(t) is the instantaneous pressure, P_{md} is the desired pressure, and τ_P is the barostat relaxation time constant. The leads to variations in the simulation box size, where at each step the box volume is scaled by a factor η, and the coordinates and box vectors by $\eta^{1/3}$:

$$\eta(t) = 1 - \frac{\Delta t}{\tau_P} \gamma (P_{md} - P(t)) \tag{2.23}$$

where γ is the isothermal compressibility of the system. Throughout this thesis, anisotropic coupling is used in which different scaling factors are used for different dimensions as the systems studied are non-isotropic. γ is usually a specified constant which takes to be the isothermal compressibility of water. Exact values are

not critical to the algorithm as it relies on the ratio γ/τ_P. τ_P is a specified time constant for pressure fluctuations. For the strength of the coupling between the system and the pressure bath, the larger τ_P, the weaker the coupling.

2.4 MD simulation of lipid bilayers and membrane proteins

2.4.1 Lipid membranes

Lipid membranes have been a system of interest for theoretical investigation due to their challenging structure and biological significance. A lot of research has been performed which has focused on developing suitable methodologies for studying the structural and dynamic properties of lipid bilayers by MD simulation.

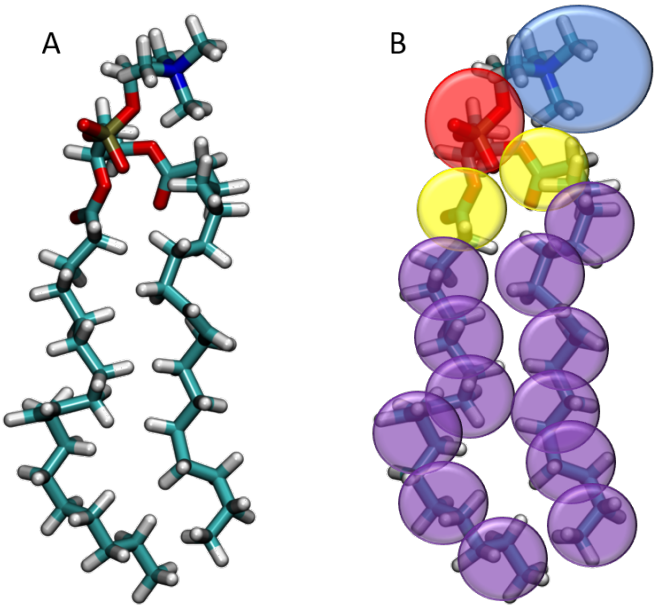

FIGURE 2.4: (A) Atomistic representation of DOPC in AA-MD simulation. (B) Coarse-grained representation of DOPC in CG-MD simulation

When simulating lipid bilayers, there are three possible representations which are routinely used. The first option is the all-atom representation (AA), the method

explicitly describes each atom in the system so the most information can be obtained which is more computationally expensive. The second option is the united-atom representation (UA) where the atoms that make up methyl and methylene groups are represented as one interaction site. This method is less computationally expensive than AA. The third and least computationally expensive option is the coarse-grained representation (CG) where multiple atoms are represented by a single interaction site or "bead" (Figure 2.4). The simpler the representation used for the simulation, the longer the timescales are that can be explored, but with the penalty of less atomic level detail. In this work I am interested in studying the explicit interactions between drug molecules and lipid bilayers and ion channel proteins which require atomic level detail. If the aim was to investigate large scale membrane motions, CG methods would be more suitable as the timescales required would be much greater.

As the Amber16/18 simulation programs for all of the MD simulations in this thesis, we can use the well parametrised protein forcefield, ff14SB[108] for treatment of proteins, the lipid14[109] lipid forcefield to describe the lipids and the GAFF2[110] forcefield to describe small drug molecules, all at atomic level detail with simulation speeds of 200 + ns/day for lipid bilayer systems, and 60 + ns/day for membrane ion-channel simulations using the CUDA implementation of the code on GPU cards.

2.4.1.1 Special considerations for bilayer simulations

Nowadays there are plenty of suitable parameters which can be used for simulations of lipid bilayers, but there are several considerations which have to be taken into account to avoid erroneous trajectories.

Timescale and system size

Timescales have long been one of the main issues in biomolecular simulation. Early studies which investigated lipid bilayers ran simulations of up to 10 ns in length on systems containing as little as 24 lipid molecules. Using systems of this size

and running such short simulations would make it very unlikely that good comparisons to experimental data could be made as these systems would not reach equilibrium. In order to accurately reproduce experimental properties, bilayer simulations should be carried out in the order of 100 ns to allow the conformation of the head groups to reach equilibrium. The size of the system should also be appropriate to achieve a suitable equilibrium and have enough lipids so accurate predictions of bulk properties can be made. All atom simulations of bilayer typically consist of 64 lipids per leaflet totalling 128 lipids in the bilayer, this size has been shown to be sufficient for reproducing structural properties. However, if complex membrane motions such as bending and fluctuations are of interest, bilayers will have to be much larger in order to observe these large scale structural changes, coarse-grained models are often used for these studies. Throughout this thesis our systems will consist of 128 lipids for membrane simulations and the timescales will be in the order of hundreds of nanoseconds.

Temperature and pressure

In the Amber code, the Berendsen and Langevin thermostats have been tested thoroughly for temperature control in lipid bilayer simulations.[111] The Langevin thermostat which is used extensively in this thesis was shown to give bilayer properties which were in good correlation with experimental observations, the Berendsen thermostat was shown to not conserve the canonical ensemble.[112] The main barostat in the Amber code is the Berendsen barostat which has been shown to accurately reproduce bilayer equilibrium properties including properties which depend on volume fluctuations, including isothermal area compressibility modulus.[113]

Treatment of long-range forces

Various studies have been conducted using multiple different methodologies to compare the treatment of electrostatics in lipid bilayer simulations. These methods are either a simple cut-off (i.e. electrostatic interactions beyond the cut-off are ignored) or the particle mesh Ewald (PME) method is used to treat electrostatics beyond the defined cut-off distance.[113,114] Anézo *et al.* employed a simple cut-off method, which they found caused bilayers to contract when they implemented

longer cut-off values, which caused reductions in the mobility of the lipid head groups and they were packed closer together. This also altered several of the key strucutral properties of the membrane.[113] The increase in energetically favourable interactions within the area defined by the cut-off which allowed the contraction to occur, this caused a reduction on the outward pressure of the membrane. This effect becomes more pronounced as the defined cut-off distance is increased. Much greater stability was achieved when the PME method was used which beyond the cut-off maps atomic partial charges onto a 'PME grid', which typically has sides of 1 Å. The charge distribution is then determined by a Fast Fourier Transform (FFT) of the Poisson equation in reciprocal space. This allows for the full evaluation of electrostatic interaction energies in a system. The PME method is the most computationally efficient method for dealing with electrostatics in bilayer systems is the main choice in bilayer simulation studies.[114]

Based on this evidence it is appropriate to conclude that this method is suitable for use in bilayer simulations to treat long-range electrostatics. The analytical dispersion correction which is used to account for long-range van der Waals forces which is the only option available in many simulation packages is theoretically not really suitable for heterogeneous systems such as membranes, more rigorous treatment with PME has shown only negligible differences so analytical dispersion correction is used due to lower computational cost.

2.4.1.2 Membrane protein simulation

Simulations of complex biological systems, such as membrane proteins, require very careful setup procedures to ensure that the system being simulated is as close to the target system as possible. In order to capture protein structural change over time or by ligand binding, a starting structure is required. Many structures obtained by experimental methods such as x-ray crystallography, cryogenic electron microscopy or nuclear magnetic resonance spectroscopy will have an issue which will have to be dealt with when setting up the simulation. Examples of these issues are defining

the protonation states of titratable residues, modelling disulfide bonds or missing loop regions.

These proteins must also be placed into a suitable environment. The aqueous solvent is made up of water molecules and a suitable number of ions to achieve the target physiological concentration. The most vital component is the membrane bilayer in which the protein will reside. In our studies of the *Gloeobacter violaceus* ion channel (GLIC), we used a homogeneous DOPC (1,2-dioleoyl-sn-glycero-3-phosphocholine) bilayer, which arguably does not mimic a real mammalian cell membrane. The choice of lipid molecule may be vital as the function many proteins have been shown to be affected by specific lipid molecules.

Molecular dynamics simulations are usually carried out within a box with fixed dimensions. Periodic boundary conditions ensure that as an atom travels outwith the boundary defined by the box, it will appear on the other side. To optimise the performance of the simulation, the system should be constructed so that it contains the lowest number of atoms required, yet still be large enough to avoid artefacts which can be caused by the PBCs. It is necessary that the size of the system will increase with the size of the protein that is being studied. Our simulations of the GLIC protein contained around 230,000 atoms, whereas larger ion channels and transporters could require over 1,000,000 atoms.

Assuming that the system is setup correctly, the simulation will follow its natural course over the defined time. However, if the event in which you wish to study is slow and requires an unrealistic amount of time to observe, as many process of membrane proteins do, the limitations of MD apply particularly to these systems. Therefore, enhanced sampling methods might be required to sample the molecular dynamics of these systems.

2.4.1.3 Limitations of MD simulation

Molecular dynamics simulations have so far been shown throughout many research areas to be very useful, especially for studying complex biological systems, but they

are by no means perfect and there are some limitations which should always be kept in mind. The forcefield used for the simulation must be accurate for the type of system that is being studied, if a poor choice is made then the output of the simulation will be worthless. Classical forcefields generally are not fully accurate as they do not incorporate quantum effects into the calculation, and with a few exceptions like the AMOEBA forcefield[115], the polarizability of molecules. There is currently no forcefield available that can provide parameters for every type of molecule, so for example, a ligand molecule will need its own custom parameters, and generating them can be a challenging process, so care must be taken when selecting a forcefield for the system of interest as a poor choice can render the simulations a waste of time.

When performing MD simulations of biological systems, the timesteps are often in the range of 2 to 4 femtoseconds which will require 1 x 10^9 timesteps to reach the microsecond timescale, at which many biological processes of interest take place. Many developments in the areas of software and hardware, like the development of Graphical Processing Units (GPUs) and the software which allows them to be used to accelerate MD simulations allowing longer timescales to be reached in shorter real world time. However, the problem of limited sampling still remains for many complex systems. Even with further dramatic increases in computing power, the size and complexity of the systems will also increase, hence the timescale problem will likely always be an issue.

As computing power increases and longer, more complex simulations can be performed, the amount of information that is produced will also grow considerably. This will lead to challenges in the post-processing methods for analysing the huge amount of data to obtain the relevant information. Large systems with atom counts reaching the millions are highly dimensional, which leads to the quadratic growth of pairwise interactions which take place at every timestep. This makes extracting useful information from the trajectory a very challenging task.

Chapter 3

Simulation of propofol and fentanyl-membrane systems

An important stage of the mechanism of action of any drug molecule is the diffusion through the cellular membrane. The favoured positions of these molecules within the target membranes also affect their transport and metabolism. The most important membrane encountered by drug molecules is the plasma membrane into which pharmaceuticals penetrate and interact with to reach the target cells. The major components within these membranes are the phosphatidylcholine (PC) lipids, which are hence most commonly used in the modelling of drug-membrane interactions. Knowledge of the interactions between drug molecules and lipids is essential to understanding their mechanism of action and efficiency.

In this work I study the drug-membrane interactions of two major components of the general anesthesia process, namely propofol and fentanyl. Firstly, the interactions of these two drugs with two different phospholipid bilayers was studied, namely dioleoylphosphatidylcholine (DOPC) and dipalmitoylphosphatidylcholine (DPPC), to investigate the role that different levels of saturation and chain length have on the drug-membrane interactions. Both drug molecules were found to penetrate both bilayers and reside below the lipid head group region but with different

positions being adopted. Various structural changes were observed in each membrane which becomes more evident with higher concentrations of drug molecules partitioned into the membrane.

3.1 Drug molecules

Since its introduction, propofol has been extensively used in general surgery as a general anesthetic to induce and maintain anesthesia. Propofol is routinely used alongside opioid analgesics such as fentanyl. The use of these opioid analgesics has been shown to potentiate the effects of propofol,[116] thereby reducing the amount of drug required to induce anesthesia, which in turn reduces the negative side effects of propofol anesthesia, e.g., a large drop in blood pressure and apnoea.[117,118] Propofol is proposed to interact and bind to the γ-aminobutyric acid (GABA) receptors,[119] consisting of ligand-gated ion channels ($GABA_A$) and G protein-coupled receptors ($GABA_B$), which control the flow of ions from the synaptic cleft into the intracellular domain.[120] Studies have also suggested that propofol acts at G protein-coupled receptors by inhibiting the function of M1 muscarinic acetylcholine receptors.[121] These studies suggest many possible binding sites for propofol, but a complete mechanism for the action of anesthesia still remains unknown.

Fentanyl is used in surgery as the analgesic component to general anesthesia but it can also be used as the main anesthetic component.[122] Various studies have shown that when used in combination with propofol, it provides a safer and more satisfactory anesthesia experience.[123,5,124] Fentanyl is known to act at various opioid sites throughout the body but predominately at the μ-opioid receptor, although it also binds to δ and κ-opioid receptors.[125] Although the binding sites for opioid drugs are relatively well known, it still remains unclear why fentanyl is able to potentiate propofol and act as an anesthetic. I have shown that fentanyl also modulates the *Gloeobacter violaceus* ion channel which is a known site for anesthetic interaction.[2]

Propofol, as shown in Figure 3.1 A, consists of a benzene ring core with two isopropyl groups at the 2 and 6 positions and one hydroxyl group in-between. The hydroxyl group is reasonably well guarded by the steric bulk of the isopropyl groups, so hydrogen-bonding will only be available in certain orientations. The structure of fentanyl, shown in Figure 3.1 B, differs significantly from propofol. Fentanyl has an almost linear, flexible backbone consisting of two aromatic and one aliphatic 6-membered rings and an acetyl group bonded to the terminal nitrogen.

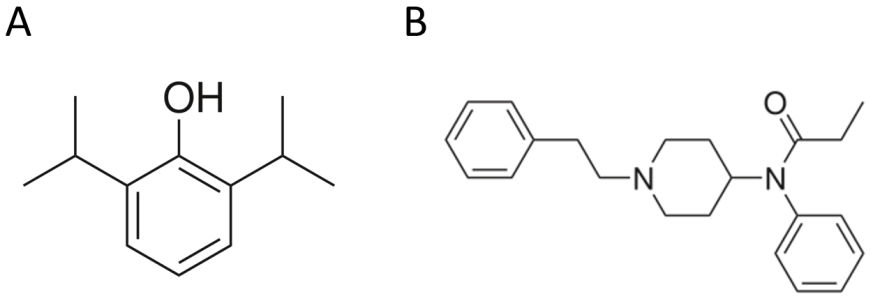

FIGURE 3.1: Chemical structures of propofol (A) and fentanyl (B)

3.2 Single drug-bilayer simulations

In order to observe the natural diffusion of each drug molecule into the lipid bilayers and the membrane mobility inside the bilayers, four 128-DOPC and four 128-DPPC systems were constructed where each molecule was placed individually inside either the bilayer hydrophobic phase or the water phase. Pure bilayer were also simulated to obtain structural parameters for comparison with the drug-membrane systems. Bilayer structures were generated using the CHARMM-GUI server.[126]

Simulation of these systems allowed the examination of the diffusion process of each drug into each bilayer and how the drug altered the membrane structural and mechanical properties by calculating: favoured position of each drug, the area per lipid, the isothermal compressibility modulus, lipid lateral diffusion, lipid tale order parameters, hydrogen-bonds and radial distribution functions.

3.2.1 Simulation set up

Molecular dynamics simulations were carried out using the GPU version of the Amber16 simulation package[127,128] with the lipid14,[109] ff14SB[108] and GAFF2[110] forcefields. The TIP3P water model[107] was used to describe the water molecules. 0.15 M KCl salt concentration was added to the water layer. The full system was minimised for 10000 steps, of which the first 5000 steps used the steepest descent method and the remaining steps used the conjugate gradient method. The system was then heated from 0 K to 100 K using Langevin dynamics for 5 ps at a constant volume with restraints on the lipid (force constant 10 kcal/mol Å^2). After this, the volume was allowed to change freely and the temperature increased to a lipid dependant value (303 K for DOPC and 323 K for DPPC) with a Langevin collision frequency of $\gamma = 1.0$ ps^{-1}, and anisotropic regulation (1 atm) with a time constant of 2 ps for 100 ps. The same restraint was maintained on the lipids. Production simulations were carried out in the isothermal isobaric (NPT) ensemble which maintains a constant number of particles, pressure and temperature. System temperature was maintained using the Langevin thermostat[129] with a collision frequency of $\gamma = 1.0$ ps^{-1}. The pressure was maintained at 1 atm using the anisotropic Berendsen method[130] with a pressure relaxation time of 1.0 ps. Three-dimensional periodic boundary conditions with the usual minimum image convention were used. The SHAKE algorithm[131] was used to constrain covalent bonds to hydrogen, allowing the use of a 2 fs time step. Electrostatic interactions were treated with the PME method using a cutoff of 10 Å. The pure bilayer simulations were run for a total of 125 ns with the first 25 ns discarded from analysis. Simulations containing the drug molecules were also run for the same time. All production simulations were run in triplicate and the results are presented as block averages over the three repeats ± standard deviation. For each replicate simulation, the positions of the drug molecules were randomised and each simulation was started with random particle velocities. Analysis was performed using CPPTRAJ[132] and VMD.[133]

3.2.2 Single drug-bilayer simulation results

3.2.2.1 Area per lipid

The area per lipid is considered to be one of the most important properties to describe the behaviour of the bilayer and whether or not it is in the correct, biologically relevant L_α phase. This area can be calculated easily from MD trajectories. The calculation involves dividing the xy cross-sectional area of the orthorhombic periodic cell (i.e., the lateral area of the bilayer) by the number of lipids.[134] The areas per lipid calculated for each pure bilayer simulation are shown in Table 3.1. The results obtained were within 3-4 % of the experimental values from the literature, which suggests that the pure bilayers are in the correct phase and have equilibrated sufficiently to be used for the drug-membrane simulations. The results for bilayers containing propofol are also shown in Table 3.1. Here, we see an increase in area per lipid when propofol is simulated in the center of each bilayer (0.25 Å in DOPC and 0.27 Å in DPPC) due to the drug molecule interacting in the upper chain region around the carbonyl groups at the head group chain interface. When propofol was simulated in the water phase, natural diffusion into both lipid bilayers was observed, leading to a larger increase in area due to disruption in the head group regions. This expansion of area per lipid can be rationalised in terms of lone pair repulsion as propofol diffuses through the head group region. A similar pattern is observed when fentanyl is in the center of the bilayer as a further increase in area was observed, especially for DPPC. My simulations of DPPC indicate that fentanyl does not lie as closely to the head group region as propofol does, but rather lies parallel and slightly below the carbonyl groups. Spontaneous diffusion was observed in the DOPC system for fentanyl which caused a small 0.1 Å increase in the area per lipid. This observation can be explained by fentanyl diffusing in a linear conformation, which causes less disruption, whereas propofol is much more dynamic in its diffusion process, adopting more conformations. The calculated volume per lipid followed the same trend as the area per lipid as they are directly proportional.

Lipid	Drug	A_L (Å^2)	V_L (Å^3)	K_A (mNm^{-1})	D_{HH} (Å)	D_{xy} (10^{-8}cm^{2}s^{-1})
DOPC experimental	none	67.4, 72.5[135]	1303[136]	265, 318[136]	35.3, 37.1[135]	11.5, 17[137]
DOPC calculated	none	70.1 ± 0.2	1274.2 ± 1.1	285.2 ± 19.7	37 ± 0.2	6.30
DPPC experimental	none	63.1, 64.3[138]	1232[136]	231[139]	38, 38.3[135]	12.5, 15.2[140]
DPPC calculated	none	62.9 ± 0.3	1175 ± 0.2	231.9 ± 22.7	37.8 ± 0.2	8.8
DOPC	Propofol center	70.3 ± 0.3	1275 ± 1.5	419.5 ± 15.6	36.25 ± 1.1	12.75
	Propofol water	70.94 ± 0.2	1279.7 ± 1.0	333 ± 30.1	36.75 ± 0.5	11.25
	Fentanyl center	70.33 ± 0.2	1261.7 ± 1.3	227.6 ± 16.0	36.5 ± 1.0	7.9
	Fentanyl water	70.2 ± 0.4	1262.3 ± 1.3	274 ± 20.5	37.25 ± 0.2	6.4
DPPC	Propofol center	63.17 ± 0.4	1176.8 ± 1.5	319.5 ± 22.7	37 ± 0.7	17.5
	Propofol water	63.50 ± 0.5	1177.8 ± 0.9	243.1 ± 16.0	37.25 ± 0.9	14
	Fentanyl center	63.58 ± 0.4	1179 ± 1.1	236.2 ± 25.0	37.5 ± 0.8	8.3
	Fentanyl water	62.86 ± 0.6	1179 ± 1.0	331.2 ± 13.0	37.25 ± 0.70	6.4

TABLE 3.1: Averaged structural properties of pure and drug containing lipid bilayer systems where area per lipid = (A_L), volume per lipid = (V_L), isothermal area compressibility modulus = (K_A), bilayer thickness = (D_{HH}) and lateral lipid diffusion coefficient = (D_{xy}). Water and center refer to the starting positions of the drug molecule

3.2.2.2 Isothermal area compressibility modulus

The isothermal area compressibility modulus (K_A) is the stress required to induce an isotropic expansion in volume, which can be obtained from MD simulations by:

$$K_A = \frac{2k_BT\langle A_L\rangle}{n_{lipid}\sigma_A^2} \tag{3.1}$$

where k_B is the Boltzmann constant, T is the system temperature, $\langle A_L\rangle$ is the average area per lipid, σ_A^2 is the variance in area per lipid over the simulation and n_{lipid} is the number of lipids in the simulation box. K_A is a standard indicator of the phase of the membrane where large values indicate the L_β gel phase, as the chains would be fully extended and their Van der Waals interactions would strengthen and lead to tighter, more ordered lipid packing.

The results for the K_A of the pure bilayers are in excellent agreement with the

experimentally observed values. When propofol starts in the center of either membrane and diffuses towards the carbonyl region, An increase in K_A which induces a closer packing of the lipid chains was observed. The conformational changes of the membrane chains increases the aforementioned interactions between them, causing the bilayer to stiffen. The largest increase in K_A is observed for DOPC, owing to the presence of the double bond in the chain which then drug molecule inhibits the fluidity of by binding in the upper chain region. During the diffusion process from the water phase into the membrane, a small increase in K_A was observed due to the fast diffusion through the head group region. This observation suggests that the process of stiffening is not instantaneous, and the direction of diffusion plays a key role. In the DOPC system a lower K_A for fentanyl compared to that for propofol was calculated, which indicates that fentanyl is causing more fluctuation within the head group region of the bilayer, (Figure 3.2).

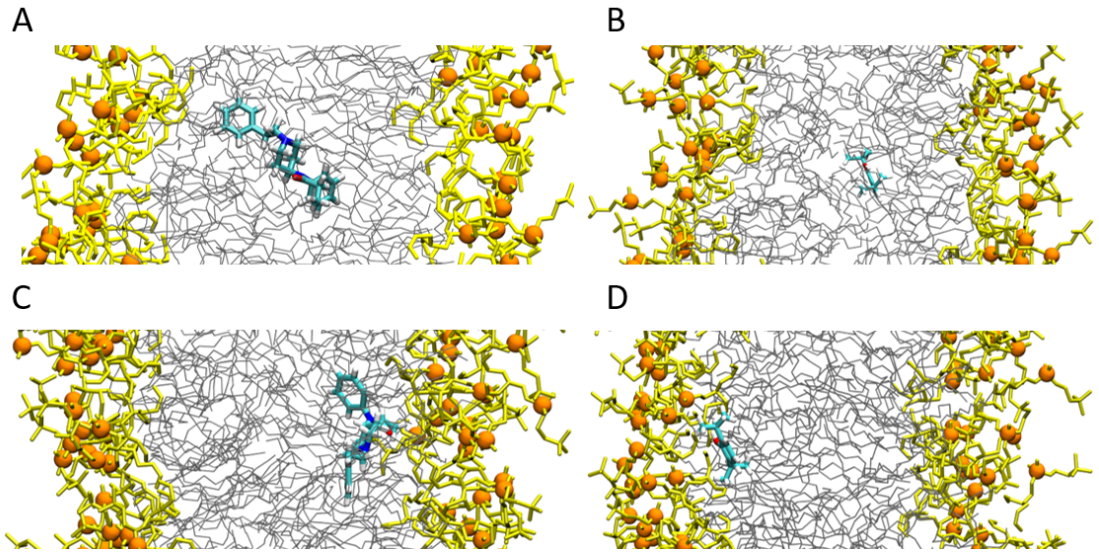

FIGURE 3.2: Starting positions for fentanyl (A) and propofol (B) in the bilayers. End positions after production simulation of fentanyl (C) and propofol (D), DOPC shown as positions were similar in both systems. Head groups shown as yellow sticks, head group phosphate shown as orange spheres, lipid chains shown as grey sticks

When fentanyl naturally diffuses into the DOPC bilayer, a small decrease in K_A by 11.2 mNm^{-1} compared to the pure bilayer was calculated, which shows that

the diffusion does not allow the chains to pack tighter together. For fentanyl in the DPPC bilayer a small 4.3 mNm^{-1} increase compared to the pure membrane was calculated, even though the drug molecule positions itself parallel to the head groups at the interface, as it does in DOPC. As such, the difference in chain structure plays a significant role in the way that the structural properties of lipid bilayers are affected by drug molecules. The most unexpected result found for fentanyl is the simulation where it fails to diffuse from the water phase into the membrane interior of DPPC which results in an increase in K_A of 99.3 mNm^{-1} over the pure bilayer. During the course of this simulation it was observed that several partial diffusion attempts where fentanyl enters the head group region for 1 - 4 ns before returning to the water phase. To confirm whether there was a change in the conformation of the head group region during these partial diffusion events, the angles between the P-N vector and the normal of the bilayer were calculated using the MEMBPLUGIN tool[141] for VMD.[133] For the pure DPPC bilayer, an angle of 69.0 $\pm$ 2.4^o was calculated which is almost identical to the fentanyl containing system. To study the specific conformation of the head groups which fentanyl causes disruptions in when it partially diffuses, head group molecules were selected which were 15 Å from the fentanyl molecule. The P-N vectors were calculated as 73.0 $\pm$ 2.0^o which shows that fentanyl causes local conformational changes within the head group region. No changes were observed for propofol due to the rapid diffusion into the membrane interior.

3.2.2.3 Lipid lateral diffusion

The lateral diffusion of a lipid bilayer is an important dynamical property, as it can affect many membrane parameters. For example, one study reported a connection between the lateral lipid diffusion and the viscosities in different parts of the membrane.[142] The lateral diffusion coefficients of the lipids without and with the drug molecules using the mean squared displacement (MSD) of the membrane in the xy direction was calculated, over 20 ns window lengths and averaged over time origins separated by 200 ps (Figure 3.3). This property is related to the

Einstein equation in two dimensions

$$D = \lim_{t\to\infty} \frac{1}{4} \frac{d}{dt} \langle |\Delta r(t)|^2 \rangle \tag{3.2}$$

where $\langle |\Delta r(t)|^2 \rangle$ is the MSD in the XY plane in time t and D represents the lateral diffusion coefficient. The diffusion coefficient can be obtained from the gradient of the linear portion of the MSD plot. Table 3.1 lists the calculated lateral diffusion coefficients for pure DOPC and DPPC, which are comparable to those calculated in the original lipid14 paper.[109] The production runs were performed in the NPT ensemble using Langevin dynamics to control the temperature by randomising particle velocities so can potentially affect dynamic membrane properties. Slightly more accurate results can be obtained using the microcanonical (NVE) ensemble, but as the results obtained under NPT conditions were within experimentally determined values, drug molecules simulations remained in the NPT ensemble.

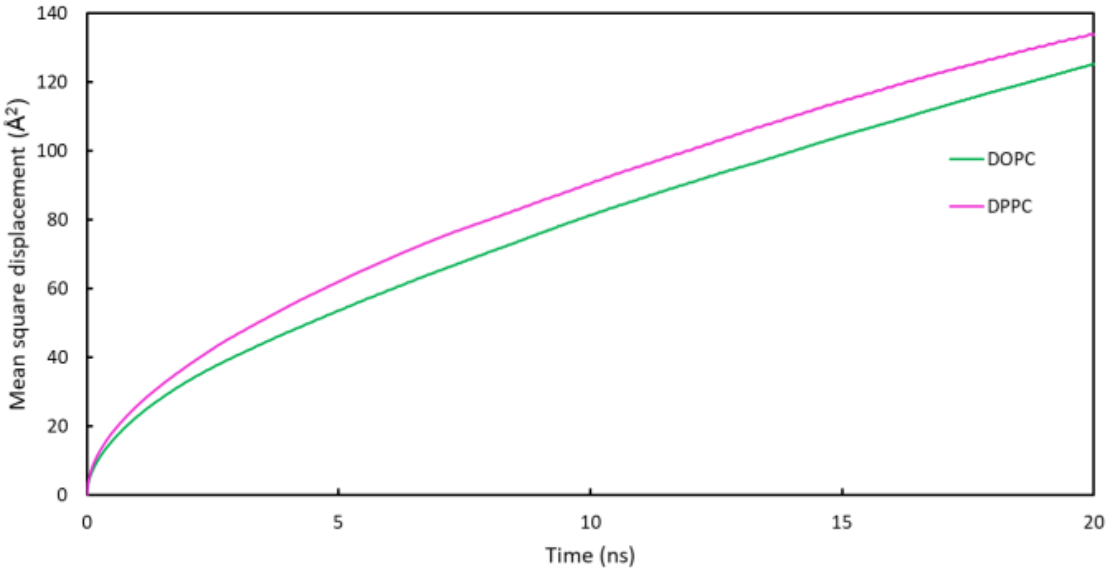

FIGURE 3.3: Time averaged mean squared displacement of the lipid center of mass versus simulation time

With the addition of propofol within the bilayer a slight increase in the lateral diffusion coefficient for both lipid systems (Table 3.1) was observed. This finding is unexpected since the drug molecules can penetrate the lipid bilayer where

they occupy a portion of the free volume within the membrane and reduce the lateral diffusion.[143] This hypothesis is observed when there is spontaneous diffusion of propofol from the water phase as it occupies free volume space within the head group region, whereas propofol starting in the center of the bilayer does not penetrate the head group space. For fentanyl a significant decrease in the lateral diffusion coefficient in both systems with respect to propofol was seen. This difference in behaviour can be explained by the larger size of the fentanyl molecule compare to propofol, which therefore occupies more free volume within the bilayer, hence limiting the fluidity of the membrane.

3.2.2.4 Lipid tail order parameters

The overall fluidity of a membrane comes from the hydrocarbon tails which form the hydrophobic interior of the bilayer.[144] The mobility of these chains at individual carbon positions can be evaluated by measuring the order parameter. A value of $S_{CD} = 0$ implies total random motion and a value of $S_{CD} = 1$ implies a position parallel to the bilayer normal. Experimentally, this can be determined with deuterium NMR quadrupole splitting which requires substitution of the hydrogen atoms at each carbon position with deuterium and measuring their dynamic variations by ^{2}H NMR. This property can be calculated from MD simulations where the carbon-deuterium order parameter is determined by the tensor S in the equation

$$S = \frac{1}{2}\langle 3cos^2\theta - 1\rangle \tag{3.3}$$

where θ represents the angle formed between the Z direction and the bilayer normal. Simulated results for the pure bilayers are shown in Figure 3.4 with comparison to literature values.[145–147]

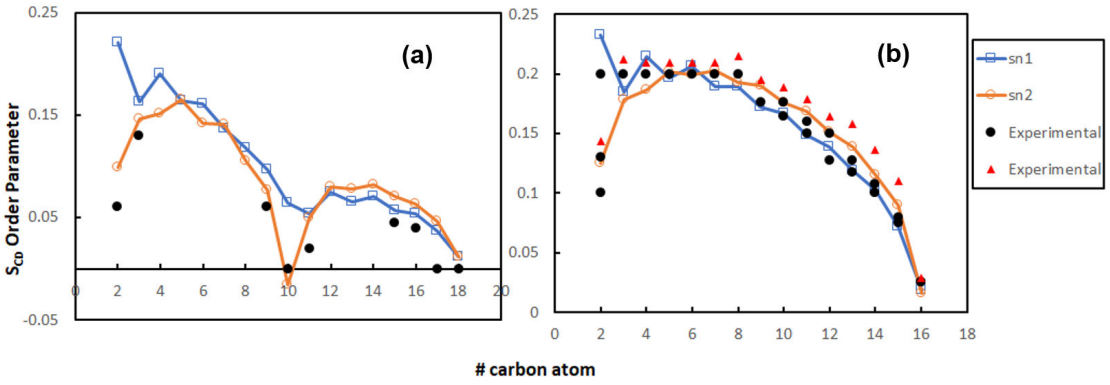

FIGURE 3.4: S_{CD} order parameters for (a) DOPC and (b) DPPC compared to experiment.

The results for the pure membrane systems are in excellent agreement with the trends which have been reported in the literature. Figure 3.5 shows the results which were obtained for the systems containing propofol and fentanyl. Very small changes in the sn-1 chain for the DOPC bilayer was observed when the drug molecules were present, compared to the pure system. A small increase in observed between C3 and C6, with respect to the pure system. This suggests a slight restriction in the mobility of the chain at this position due to the presence of the drug molecules. A small decrease in the order parameter for fentanyl between C10 and C11 suggests more mobility at these positions. This behaviour is also seen in the sn-2 chain for both anesthetic molecules, although note the lower values in C12-C14, which could account for the reduced area compressibility calculated for fentanyl due to the chains becoming more flexible and hence requiring less force to induce an isotropic expansion.

In the DPPC system there are clear differences between the drug-containing bilayers and the pure reference systems. In the sn-1 chain, it was observed that propofol increases the order parameter from C5 to C12, reducing the chain mobility and hence requiring more force to induce an isotropic expansion within the bilayer, in agreement with K_A. The introduction of fentanyl causes negligible changes in the order parameter of the DPPC bilayer. The sn-2 chain shows a clear difference in

the C6 to C13 region compared to the pure membrane. Propofol causes a higher order parameter for these carbons, as seen in the sn-2 chain, whereas fentanyl shows lower values at this region, which would suggest a more flexible chain and hence a lower K_A.

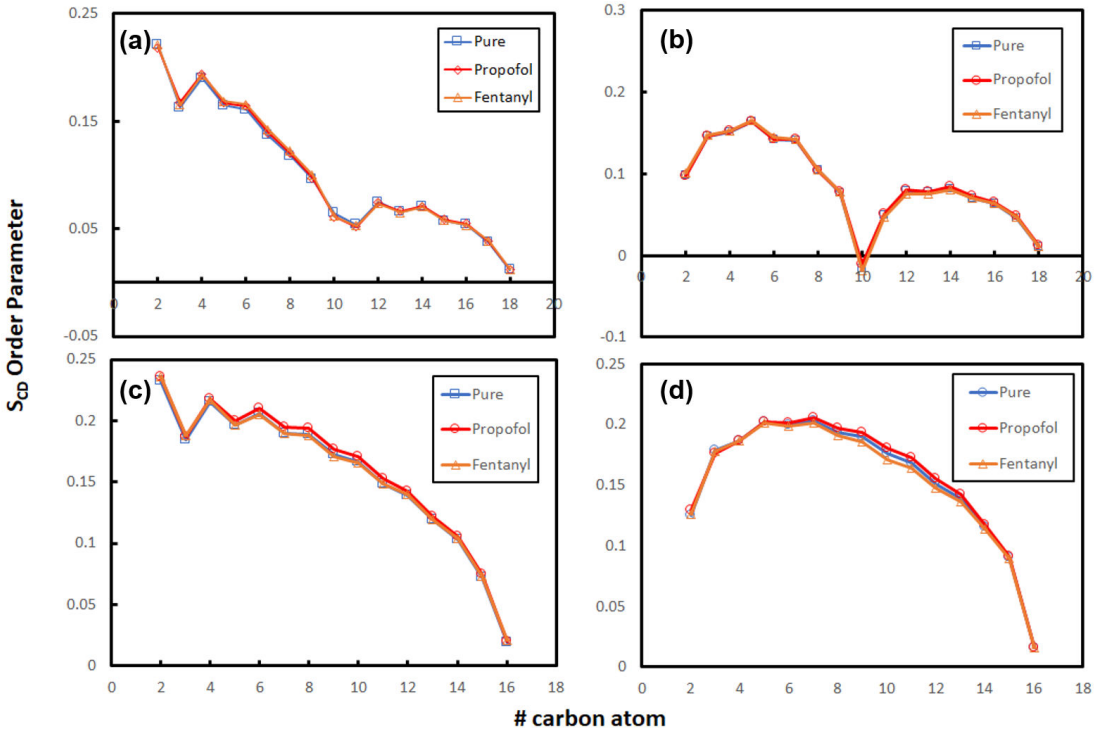

FIGURE 3.5: S_{CD} order parameters for (a) DOPC sn-1 chain, (b) DOPC sn-2 chain, (c) DPPC sn-1 chain and (d) DPPC sn-2 chain. Order parameters for drug-containing systems calculated when the drug was present in the hydrophobic phase of the bilayer.

Table 3.1 shows that there is no correlation between the lipid chain mobility and K_A, which indicates that the flexibility in the head group region could be the link between them. I should note here that a similar study conducted on the local anesthetic articaine in a DMPC bilayer found higher order parameter values for the neutral form of the molecule, similar to propofol in the DPPC bilayer.[148] The differences observed for articaine are larger, which is most likely due to the higher concentration of drug molecules inserted into the bilayer.

3.2.2.5 Hydrogen bonds

Hydrogen bonds were observed between the drug molecules and water, and propofol was also seen to form hydrogen bonds with the head groups of both membrane systems. The conditions used to determine if a hydrogen bond was formed were set by a bond distance of 2.5 Å between the donor hydrogen and the acceptor atom with a maximum angle of 30° between the donor hydrogen and the acceptor hydrogen vectors.[149]

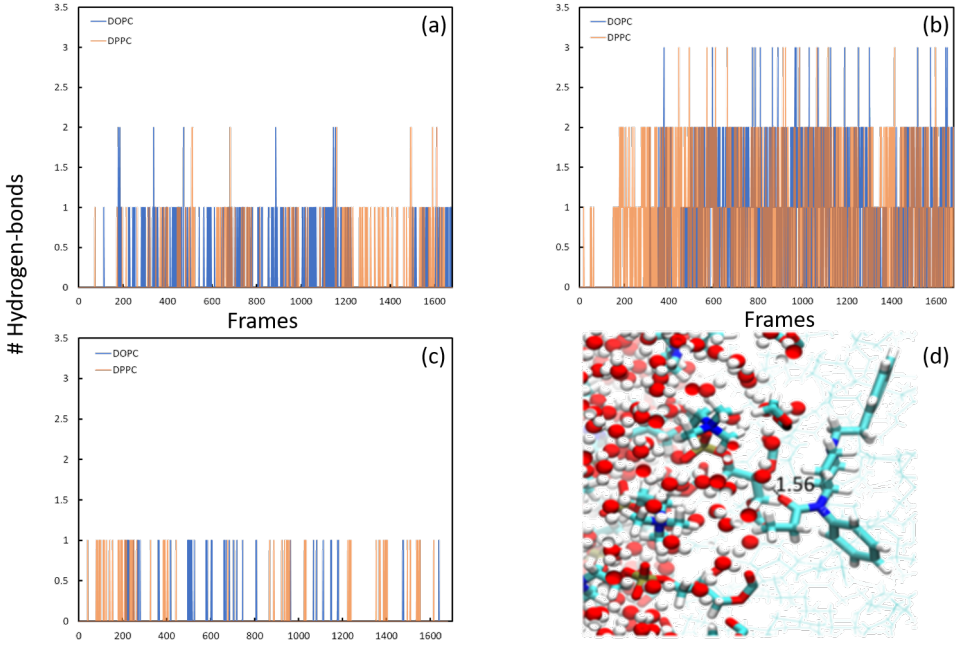

FIGURE 3.6: Hydrogen-bond plots of (a) propofol-to-water, (b) fentanyl-to-water, (c) propofol-to-lipid head groups; and (d) snapshot of fentanyl binding to water within the hydrophobic phase. Hydrogen bond distance is shown in panel in Angstroms (d).

Figure 3.6 A shows that the pattern of hydrogen bonding to water is similar in both membrane systems. Hydrogen bonds were mostly formed between the hydrogen of the propofol hydroxyl group and the oxygen of the water molecules. During the simulations, the conformation allowed the hydrogen from another water molecule to coordinate with the propofol hydroxyl oxygen. The average number of hydrogen bonds formed per frame was similar for DOPC (0.120) and DPPC

(0.119). Figure 3.6 B shows the hydrogen bonding pattern for fentanyl in both bilayers. Hydrogen bonds are formed faster within the DPPC bilayer as this is the most fluid membrane (Table 3.1) which allows the drug molecule to move faster toward the interface with water and hence form hydrogen bonds. Fentanyl has two extra hydrogen bonding sites, i.e., carbonyl oxygen and both nitrogens, compared to propofol that has only the hydroxyl oxygen site, which explains the different number of hydrogen bonds formed. Fentanyl forms bonds between both the carbonyl oxygen and the neighbouring nitrogen to water hydrogen. No bonds are formed to the piperidine nitrogen due to steric hindrance and the conformation adopted by fentanyl. A similar number of hydrogen bonds per frame in DOPC (0.758) and DPPC (0.715) were calculated for fentanyl. From Figure 3.6 C, it can be seen that propofol forms hydrogen bonds to the lipid head groups in both DOPC and DPPC, which fentanyl is unable to do. The carbonyl oxygen of the sn-1 chain is favoured in both lipids over the sn-2 chain, due to the conformation that the head group adopts throughout the simulations, which makes it better accessible for bonding. Figure 3.6 D shows a snapshot from the simulation of DOPC, where I noted a number of water molecules entering the hydrophobic bilayer core and forming "anchoring" hydrogen bonds to fentanyl. This behaviour was observed in both bilayers but to a greater extent in the DOPC membrane. This phenomenon was not seen with propofol, which could explain the higher membrane mobility compared to fentanyl. Table 3.2 shows the average number of

Lipid	Drug	Average bond per frame
DOPC	none	464.9
	fentanyl	481.3
	propofol	467.8
DPPC	none	396.4
	fentanyl	397.5
	propofol	399.4

TABLE 3.2: Number of hydrogen bonds formed between lipid head groups and water

hydrogen bonds per frame between lipid head groups and water molecules, which is used as a means to assess the effect of the drug molecules on the ability of the head groups to form hydrogen bonds to the surrounding aqueous environment. In

the DPPC bilayer containing either of the two drug molecules, very little change in the number of hydrogen bonds between the head groups and water compared to the pure bilayer was observed. The results for the DOPC system show a clear increase in the number of hydrogen bonds formed in the presence of fentanyl. This observation can be explained by the disruptions caused by fentanyl in the head group region (Figure 3.7), which can accommodate more water molecules at the interface, thereby increasing the potential for hydrogen bonding. These results highlight the different behaviour observed in the two different PC lipid bilayers despite their close structural similarity.

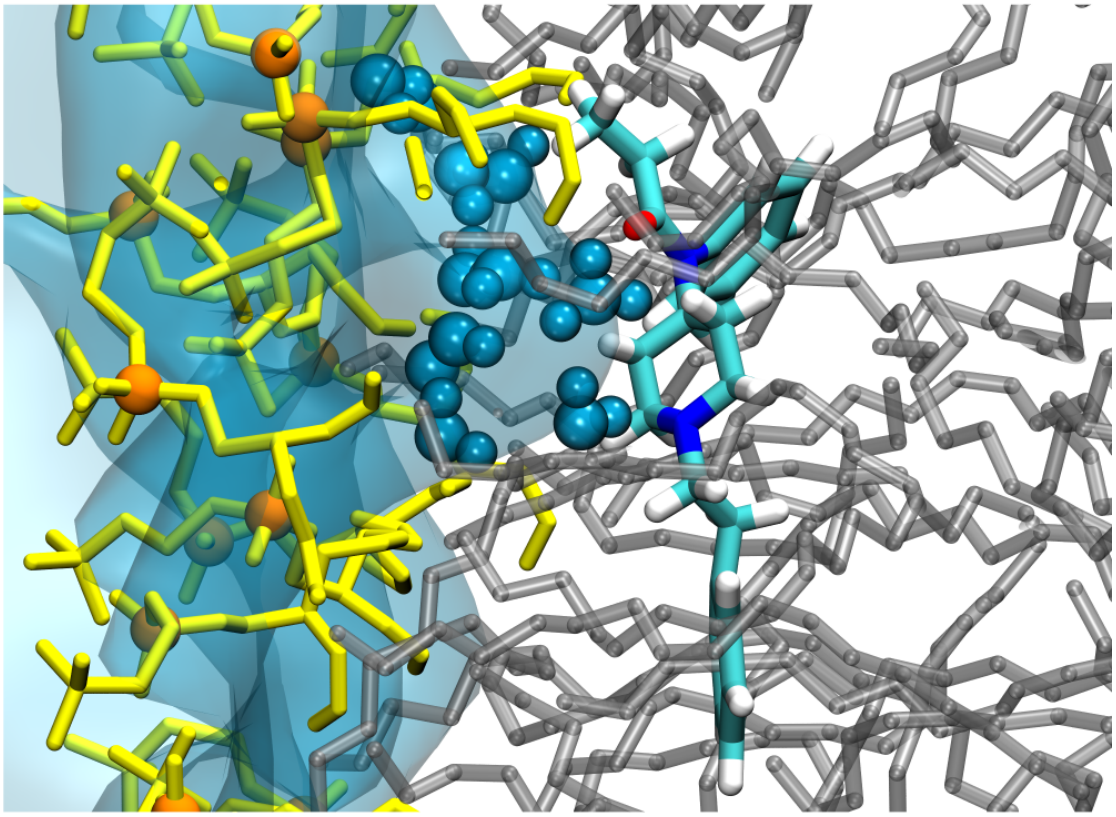

FIGURE 3.7: Multiple water molecules moving through the DOPC lipid head group into the hydrophobic phase of the bilayer. Lipid head group is shown as yellow sticks, lipid tails are shown as grey sticks, phosphorous atom of the phosphate group is shown as an orange sphere, water molecules within 5 Å of fentanyl are shown as blue spheres, and fentanyl is shown as sticks.

3.2.2.6 Radial distribution function

To further understand the distribution of water and the drug molecule around the bilayer, radial distribution function (RDF) analysis was carried out. Figure 3.8 shows the RDF plots for the oxygen atom of water around the phosphorous of the lipid head group. From the insets of each graph, it can be seen that when fentanyl is present in the membrane there is a higher density of water molecules around the phosphate group of the lipid head group. This difference is slightly larger in the DOPC membrane, which agrees with the observation that fentanyl causes more water molecules to penetrate the head groups and enter the hydrophobic phase. RDFs were also computed for the atoms in each drug molecule, which exhibited hydrogen bonding to water and, in the case of propofol, the lipid head groups themselves. Figure 3.9 A shows that water is more concentrated around the carbonyl oxygen of fentanyl in DOPC, with an average hydrogen bond distance to water of 1.75 Å. The peak for the oxygen-to-oxygen density is a further 1 Å away, which indicates the length of the O-H bond in the water molecule. Figure 3.9 B shows the same trend for DPPC as for DOPC, although the densities for N to H and N to O are close, with the O-to-O density slightly higher by 0.05. Figure 3.9 C shows the dominance of hydrogen bonding between propofol and the head group region. The conformation of the head group in DOPC increases the sn-1 lipid chain in such a way that it is better accessible to form hydrogen bonds to propofol. A higher density was found for sn-1 and sn-2 in DPPC due to the differences in chain mobility between between the two systems; see Figure 3.9 D. A sharp shoulder peak is observed at 1.95 Å in the propofol DPPC system, which is due to hydrogen bonds forming at different distances.

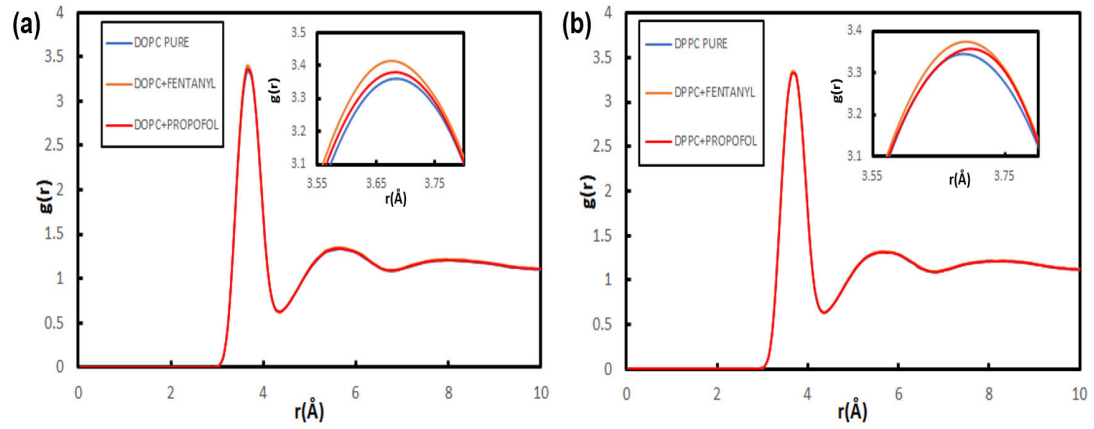

FIGURE 3.8: Radial distribution function plots of (a) water oxygen to phosphorous of DOPC and (b) DPPC lipid bilayers. The insets show the increase in density caused by the addition of the drug molecules.

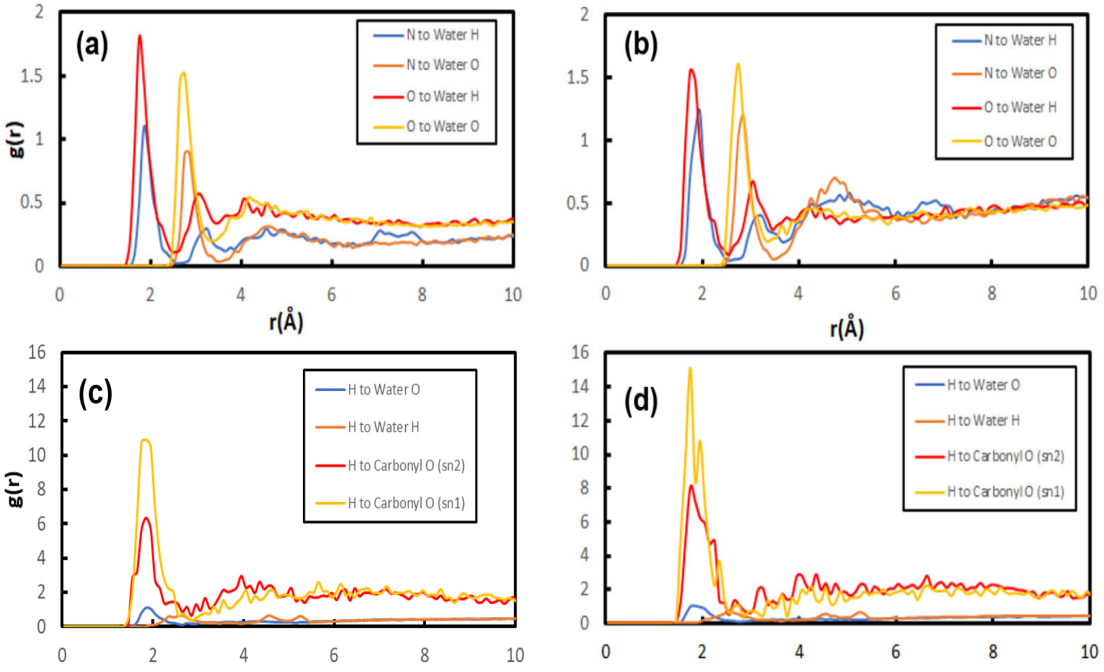

FIGURE 3.9: Radial distribution function plots of (a) fentanyl hydrogen bonding atoms to water hydrogen and oxygen in DOPC; (b) fentanyl hydrogen bonding atoms to water hydrogen and oxygen in DPPC; (c) propofol hydroxyl hydrogen to water hydrogen and oxygen, and sn-1 and sn-2 carbonyl oxygen in DOPC; and (d) propofol hydroxyl hydrogen to water hydrogen and oxygen, and sn-1 and sn-2 carbonyl oxygen in DPPC.

3.3 Clinical concentration simulations

The single drug-bilayer simulations allowed me to study the difference in the membrane mobility, positioning and strucutral changes that these drug molecules can exert and the differences between them. The changes in bulk membrane structure observed with a single molecule are small, and it is likely that these results are not statistically significant as calculations were largely performed on all of the lipids in the bilayer. In reality these concentrations are far below what would be used in general surgical applications so to obtain more realistic information on the interactions between these drug molecules and the membranes, and each other, I have conducted simulations at the drug concentrations commonly used in real life applications.

These simulations allow a more complete look at how these drug molecules alter the strucutral properties of these bilayer systems and how the drug molecules interact with each other in this environment.

3.3.1 Simulation set up

The set up for these simulations is the same as that described in section 3.2.1. The only difference is the number of drug molecules present in the system. The concentrations of these drug molecules in surgical applications in 7.1 μM for propofol[150] and 1.0 μM for fentanyl,[151] corresponds to 36 and 4 molecules respectively.

Calculations based on certain simplifying assumptions give the rough estimates for the number of drug molecules in a bilayer system of this size.[152,153] 7.1 μM and 1.0 μM give approximately 28 mol% and 4 mol% for propofol and fentanyl in a lipid membrane. The workings are as follows for propofol:

- An average person weighs 70kg so the body has volume 70 litres
- Drug does 7.1 μM Number of drug molecules = N_A x 7.1 x 10^{-6} x 70 = 2.8 x 10^{20}

- Conservative estimate of 1 x 10^{12} cells
- Therefore 2.8 x 10^{20} / 1 x 10^{12} = 2.8 x 10^{8} drugs per cell
- There are an estimated 1 x 10^{9} lipid molecules per cell[154]
- This results in a drug:lipid ratio of 2.8 x 10^{8} : 1 x 10^{9} = 28%
- This corresponds to approximately 36 molecules in a 128 lipid patch

The drug molecules were inserted randomly into the water phase of each system using a custom python script. The drug molecules were restrained with a force constant of 10 kcal/mol Å^2 during the equilibration procedure to allow the solvent to equilibrate around the drugs, any overlapping water molecules that remained after this were removed. The simulation procedure remained the same as that described in section 3.2.1.

3.3.2 Clinical concentration simulation results

The drug molecules immediately began to diffuse into the membrane interior from the aqueous phase. Figure 3.10 shows the final positions of the drug molecules within the membrane interior, the positioning was almost identical in DOPC and DPPC so only one system is shown.

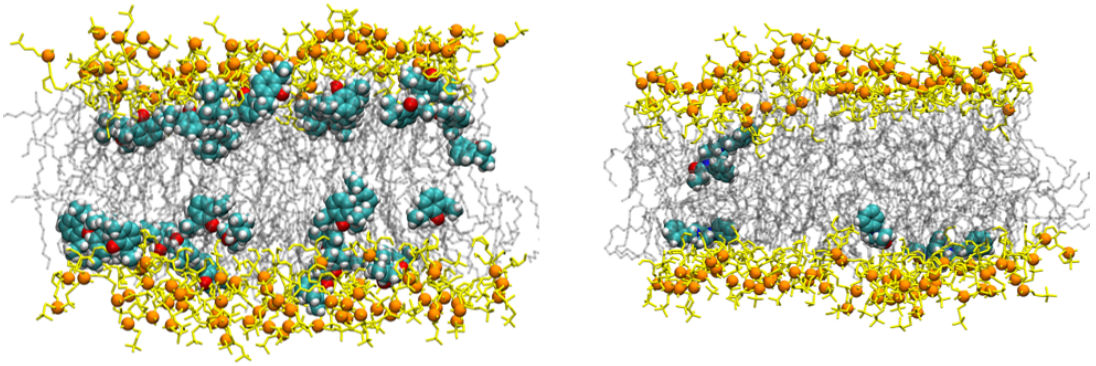

FIGURE 3.10: End states of propofol (left) and fentanyl (right) in the lipid bilayers. Phosphorous atoms are shown as orange spheres, lipid head groups are shown as yellow sticks, lipid tails are shown as grey sticks, and drug molecules are shown as VdW spheres.

3.3.2.1 Electron density profiles

The average positions of the drug molecules during the simulations were calculated with decomposed electron density profiles which were computed with CPPTRAJ.[132] These profiles (Figure 3.11) were constructed for each drug in each bilayer using an average over all replicates. Both drug molecules were located predominately under the lipid head groups in the hydrophobic phase. This observation is consistent with was has been observed for other anesthetic drugs, such as alcohols,[155] benzocaine,[156] and halothane.[157] The two drug molecules prefer slightly different depths within the bilayers, with propofol having a density maximum at approximately 10.3 Å from the bilayer center in both DOPC and DPPC, while fentanyl has a density maximum at approximately 9.1 Å in DPPC and 10.3 Å in DOPC. The density for fentanyl in both bilayers is higher than that for propofol in the center (0 Å), which indicates that the fentanyl molecules are able to cross the bilayer on the timescale of the simulation, as the free energy is lower in the center for fentanyl.

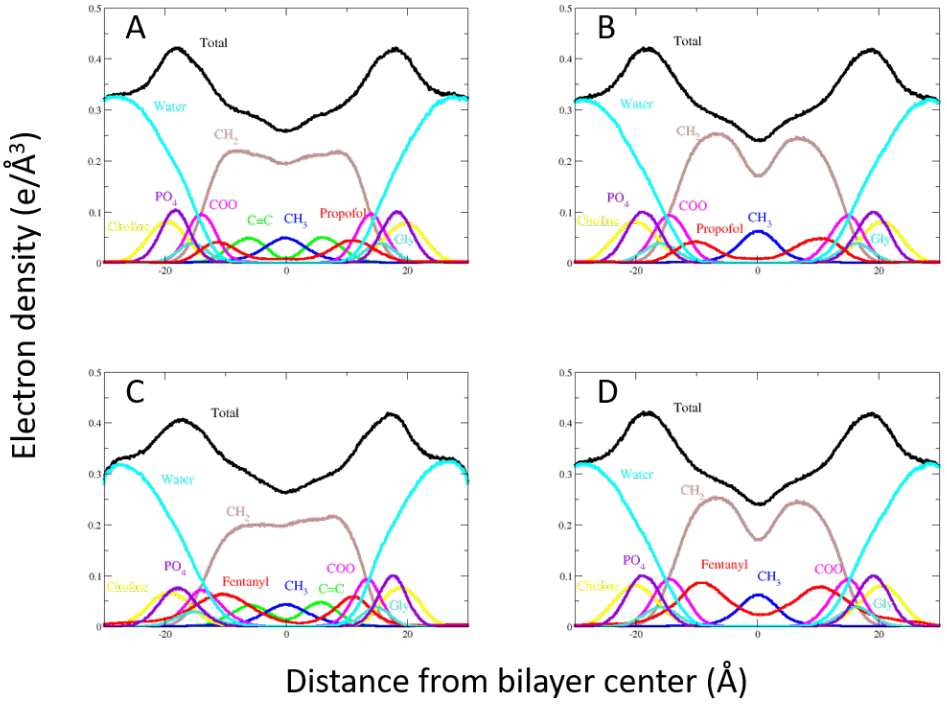

FIGURE 3.11: Total and decomposed electron density plots for propofol in DOPC (A) and DPPC (B), and fentanyl in DOPC (C) and DPPC (D). Contributions from water, choline, phosphate (PO4), glycerol (Gly), carbonyl (COO), methylene (CH_2), unsaturated CH=CH, and terminal methyls (CH_3).

3.3.2.2 Radial distribution function

To gain further insight into the hydration state and coordination of the drug molecules and the probability distribution of the water molecules around the drugs and the lipid head groups, RDFs of the water oxygen around the phosphate of the lipid head group have been calculated for both drug molecules in both lipid systems, as shown in Figure 3.12.

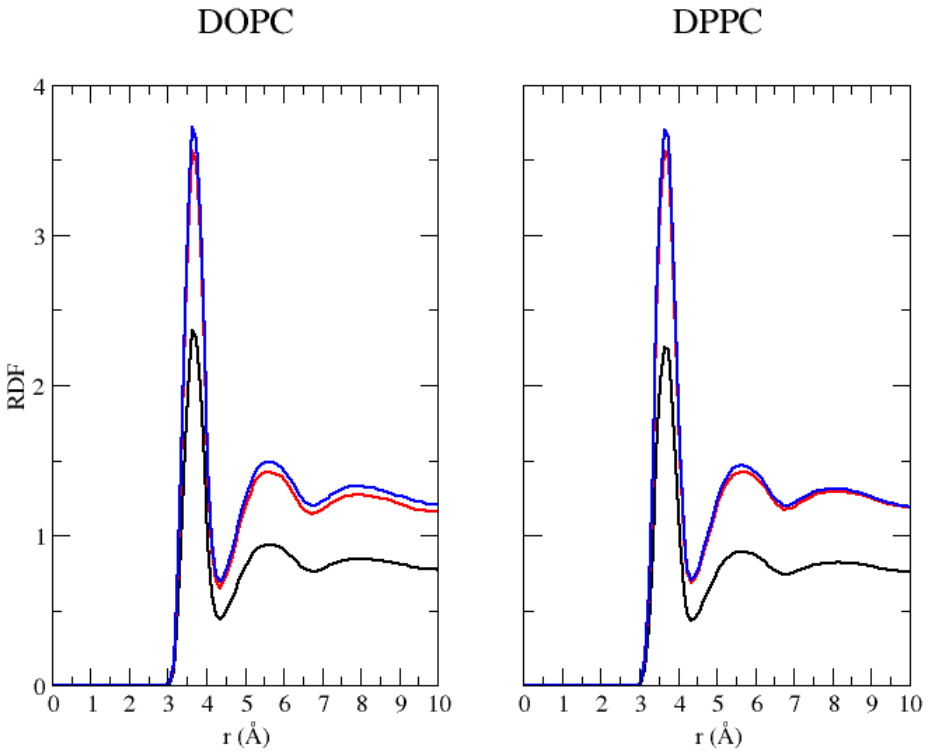

FIGURE 3.12: Radial distribution functions of water oxygen around the phosphate of the DOPC and DPPC lipid head groups in the pure system (black), propofol system (red), and fentanyl system (blue).

The RDF plots for the water oxygen around the phosphate group show similar behaviour for both lipid systems, with the first minimum indicating the hydrogen bond between water and the phosphate oxygen. The RDFs for the systems containing the drug molecules are considerably higher, which can be understood from the density plots, which show that both drug molecules are mostly located in the upper part of the lipid tail region and the ester group area. The presence of the drug molecules creates a larger area per lipid in all systems (Table 3.3), which allows more space in the head group region that can be filled with additional water molecules, thereby increasing the hydration at the head group/extracellular region.

System	A_L (Å^2)	V_L (Å^3)	K_A (m Nm^{-1})	D_{HH} (Å)	D_{xy} (10^{-8} cm^{2}s^{-1})
DOPC pure	70.1 ± 0.2	1274.2 ± 1.1	285.2 ± 19.7	37 ± 0.2	6.3
DPPC pure	62.9 ± 0.3	1175 ± 0.2	231.9 ± 22.7	37.8 ± 0.2	8.8
DOPC propofol	76.8 ± 0.4	1363.8 ± 2.3	666.7 ± 31.0	37.4 ± 0.3	5.8
DOPC fentanyl	71.0 ± 0.3	1283.4 ± 1.6	394.7 ± 15.9	37.25 ± 0.2	6.4
DPPC propofol	70.3 ± 0.4	1280 ± 0.9	312.1 ± 26.0	37.7 ± 0.4	6
DPPC fentanyl	66.0 ± 0.2	1242.2 ± 1.4	256.2 ± 14.0	37.6 ± 0.3	6.4

TABLE 3.3: Averaged strucutral properties of pure and clinical concentration systems, where area per lipid = (A_L), volume per lipid = (V_L), isothermal area compressibility modulus = (K_A), bilayer thickness = (D_{HH}) and lateral lipid diffusion coefficient = (D_{xy})

3.3.2.3 Ordering and dynamics

To understand how these drug molecules alter the membrane ordering and dynamics at clinical concentrations the head group tilt angles were calculated, S_{CD} order parameters (Figure 3.13), and lipid lateral diffusion coefficients (Table 3.3). Order parameter plots show little to no changes when a single drug molecule is incorporated into the system. But when clinical concentrations are used, far more significant changes to the chain dynamics are seen. The tilt angle of a phospholipid head group is an important property because of the dipole moment associated with the zwitterionic head group, which is involved in long-range electrostatics, which can affect many bilayer properties.[158] Drug molecules which are located within or close to the head group region, may cause disruption of this angle, which was observed for other anesthetic drugs like lidocaine[159] and articaine.[148] Table 3.4 shows the average calculated angles between the P-N head group vector and the bilayer normal for the two pure reference systems and the clinical concentration systems. Results were obtained using the MEMBPLUGIN tool[141] for VMD. For these calculations, all lipids were included as opposed to lipids located close to each drug molecule due to the greater number of drugs in each system.

System	P-N vector angle (deg)	Standard error (±)
Pure DOPC	66.88	2.30
Propofol DOPC	70.60	2.31
Fentanyl DOPC	70.14	2.30
Pure DPPC	69.0	2.40
Propofol DPPC	71.1	2.0
Fentanyl DPPC	70.02	2.4

TABLE 3.4: Average DOPC and DPPC angles between the P-N vector and the normal of the bilayers for pure and drug-containing systems

The results presented in Table 3.4 show small influences from the drug molecules, more so for propofol due to the increased number of molecules in the system compared to fentanyl. Results for the single molecule simulations were almost identical to those obtained for the pure systems. More significant results were obtained for the previously mentioned lidocaine and articaine studies[159,148] in which decreases of around 20° were seen due to the charged molecules located within the lipid head group region, so the positively charged drug molecules caused significant repulsions with the head group choline groups outwards towards the aqueous phase. Both propofol and fentanyl in my simulations are neutral, so they therefore reside in the upper chain region close to the ester group and slightly deeper towards the membrane center for fentanyl (Figure 3.11), so there are no charge-charge interactions to significantly alter the P-N vector. The increased hydration of the head groups (Figure 3.12) can therefore be explained by the drug molecules causing separation in the head group region, which is seen in the increase in the area per lipid, shown in table 3.3, which allows water molecules to penetrate deeper into the head group region where hydrogen bonds are formed to the drug molecules.

The calculated order parameters (Figure 3.13) shows that these drugs at clinical concentrations have a significant impact on the lipid chain dynamics. For DOPC-containing propofol, an increase in K_A can be seen, which suggests a rigid/stiff bilayer, an increase in thickness, and a decrease in lipid lateral diffusion. The S_{CD} plot shows a higher-order parameter in the upper chain region for propofol, more

apparent in the sn-1 chain, resulting from the propofol occupying this space, which reduces the density of the lipid chains in this region causing them to straighten.

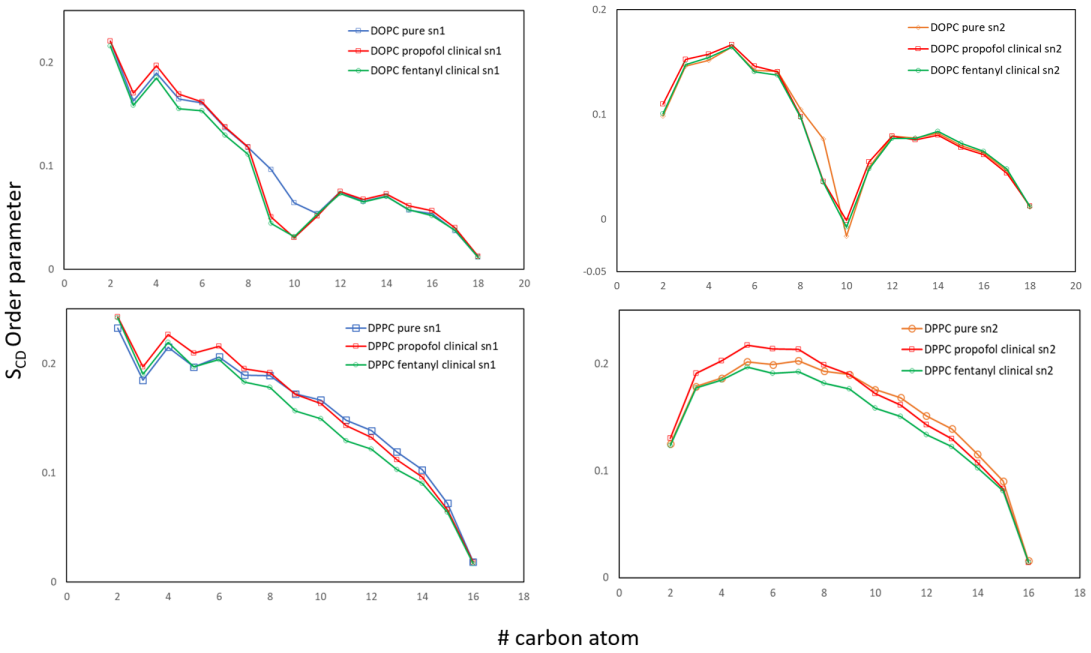

FIGURE 3.13: S_{CD} order parameters for DOPC (top) and DPPC (bottom) containing clinical concentrations of propofol and fentanyl

Similar results are seen for fentanyl, in which K_A and D_{HH} also increase but to a smaller extent compared to the results for propofol. The diffusion calculated for fentanyl in DOPC is almost identical to that of the pure system, which suggests that the number of molecules present in the system is a crucial factor in lipid lateral diffusion. The S_{CD} order parameter for carbons 9 and 10 in both DOPC systems show a significant decrease; these carbons form the double bond in the DOPC lipid chain, which is a region where the drug molecules do not spend any notable time. I suggest that this decrease in order is due to the positioning of the drug molecules near the ester groups, which disrupts the conventional packing of the lipid chains. For the DPPC systems, similar trends are seen in K_A, D_{HH} and D_{xy} compared to the DOPC systems. The upper region of the carbon chains in which propofol resides has an increased order parameter, which suggests stiffening of that region, as seen in the K_A value and lower diffusion coefficients. For fentanyl,

lower order parameters for carbon 6 onwards in both the sn-1 and sn-2 chains are seen, suggesting higher chain mobility in this area, but this is not what is seen in the diffusion coefficient, which shows a decrease in membrane fluidity.

3.4 Conclusion

In this chapter, I have utilised fully atomistic molecular dynamics simulations to model the physical and mechanical properties of pure and drug-containing lipid bilayers. Propofol and fentanyl show similar trends in the way that they alter the general properties of both DOPC and DPPC. I determined that propofol prefers to for hydrogen bonds with the carbonyl oxygens of the lipid head groups, especially with the sn-1 chain in both model membranes due to the chain orientation. Fentanyl orientates itself parallel to the head groups at the interface, where it forms hydrogen bonds with water, which are possible as a result of the disruption caused in the head group region due to the presence and positioning of fentanyl. Hydrogen bonding analysis showed an increase in water molecules within the head group region, most noticeably in the DOPC membrane. The calculated radial distribution functions also showed a higher density of water molecules around the phosphate group when fentanyl was present and to a lesser extent for propofol. The simulations involving the clinical concentrations of propofol and fentanyl show in detail that these drugs can cause significant perturbations to the membrane structure. At these concentrations, both drugs were shown to cause increased hydration of the lipid head groups, stiffening of the acyl chains, and hence a decrease in the membrane fluidity. The resulting strucutral defects from my simulations could provide the basis for investigations into the indirect modulation of membrane protein function by both of these drugs, which are the main components of total intravenous anesthesia.

Chapter 4

Interactions of fentanyl and propofol at the *Gloeobacter violaceus* ion channel

In this chapter, studies into the interactions of fentanyl with the *Gloeobacter violaceus* ion channel have been investigated using molecular dynamics simulations in combination with efficient end-state free energy calculations. It was found that fentanyl occupied a site approximately 9 Å below the orthosteric agonist-binding site in the extracellular domain, which is similar to the site occupied by the anesthetic/analgesic drug, ketamine. With fentanyl in this site structural rearrangements are seen in the transmembrane domain which lead to a closed conformation of the channel. Work describing this has been published as Faulkner *et al.*[2] Studies into the interaction of both fentanyl and propofol at this channel to determine whether the combination of these drugs altered their binding sites or pathways which will lead to a greater understanding of how fentanyl potentiates the effect of propofol. To investigate these interactions classical flooding style MD simulations were utilised with gaussian accelerated MD simulations. It was found that propofol bound within the transmembrane pore by an extracellular binding pathway, and fentanyl stabilised propofol in an extracellular binding site.

4.1 Modulation of the *Gloeobacter violaceus* ion channel by fentanyl

4.1.1 Introduction

The identification of opioid molecules, such as morphine and fentanyl, which cause desensitization to painful stimuli by acting upon G-protein-coupled receptors (GPCRs), has allowed great advances in modern medicine and invasive surgery. Other uses have also been identified for opioids such as fentanyl, i.e. in the potentiation of the general anesthetic propofol and as the main anesthetic component.[160,161] However, the mechanism of the anesthetic action of opioids remains unclear. Here, target ion channels have been investigated, specifically the Cys-loop family of pentameric ligand-gated ion channels (pLGIC). These proteins are sensitive to neurotransmitters from the pre synaptic axon terminal and are hence major drug targets.[162] Anesthetics are known to modulate both cation and anion-permeable channels, such as the gamma-butyric acid type A (GABAA) and nicotinic acetylcholine (nAChRs) receptors,[163,164] but high resolution structures of eukaryotic receptors have proved challenging to obtain. Crystal structures of the bacterial homologue (GLIC) have been obtained at reasonably high resolutions (2.4 – 4 Å),[165] which allows a valuable opportunity to study the modulation of pLGIC at the atomic level. This family of ion channels was chosen based on evidence from other studies, that show an "anesthetic binding pocket" which general anesthetics have been shown to occupy.[166,72] The analgesic/anesthetic drug ketamine has also been shown to bind to the GLIC structure[78] in a different, extracellular binding site compared to general anesthetics.

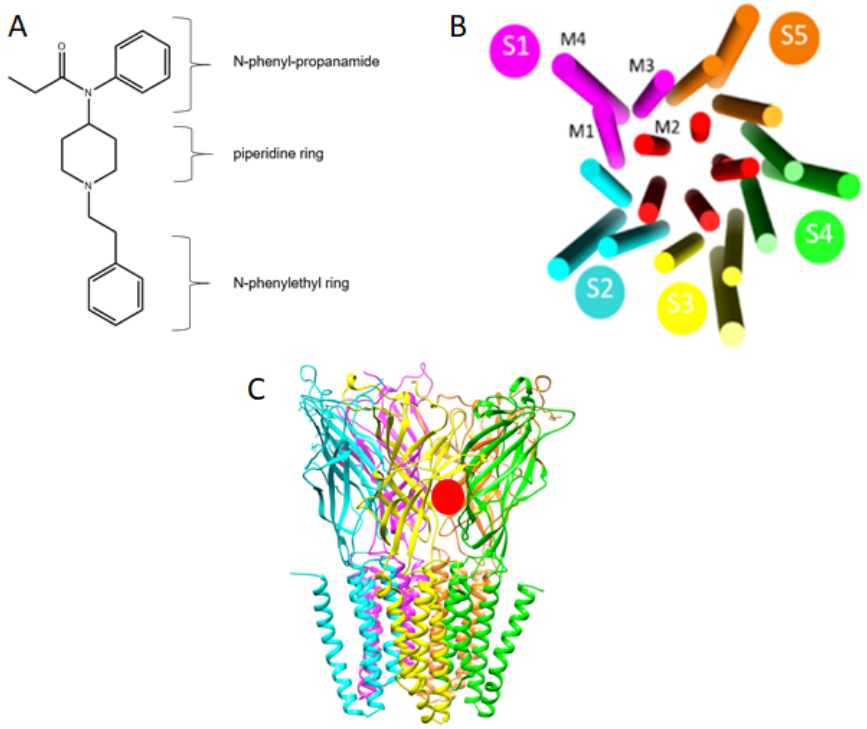

FIGURE 4.1: (A) Chemical structure of fentanyl. (B) Graphical representation of the transmembrane α helical domains showing the 5 symmetric subunits and the ion conducting M2 helices (red). (C) GLIC structure highlighting the fentanyl binding site in the extracellular domain (red sphere).

Figure 4.1 shows the structure of fentanyl and the transmembrane domain (TMD) of the GLIC. The TMD consists of four α-helices which span the entirety of the cell membrane (M1 – M4) in which the GLIC is embedded. The M2 α-helices are oriented towards the center of the pore which forms the ion-conducting, fully hydrated channel in the open state. The evidence of anesthetics interacting with and modulating these channels[73,167,75] provides an excellent starting point for the exploration of the anesthetic properties of fentanyl and how it can potentiate other general anesthetics. The GLIC open state structure at atomic resolution (2.4 Å) published by Sauguet et al[165] and the previous simulation studies of anesthetics interacting with ion channels[71,77,168] provide us with the opportunity to compare the effect of fentanyl on a GLIC structure with the binding and modulation of the channel by general anesthetics. I employed molecular dynamics (MD) simulations and efficient end-state free energy calculations to probe the interactions between fentanyl and the GLIC. My simulations reveal that fentanyl occupies multiple

extracellular binding sites similar to those observed for ketamine,[78] which lead to conformational changes within the M2 helix domain, causing pore closure and dehydration resulting in a non-conductive state.

4.1.2 Methods and theory

General simulation protocol

All simulations were carried out with the CUDA enabled Amber16 package.[128] The ff14SB forcefield[108] was used to describe the protein, the lipid14 forcefield[109] was used to describe the DOPC lipids and the GAFF2 forcefield[110] was used to describe the fentanyl molecules. The TIP3P water model[107] was used to describe the explicit waters. A constant pressure of 1.0 atm was maintained using the anisotropic Berendsen method with a pressure relaxation time of 1.0 ps. The temperature was maintained at 310 K using the Langevin thermostat with a collision frequency of $\gamma = 1.0$ ps^{-1}. Three dimensional periodic boundary conditions with the usual minimum image convention were used. The SHAKE algorithm was used to constrain covalent bonds to hydrogen, allowing the use of a 2 fs time step. Electrostatic interactions were treated with the PME method using a cutoff of 10 Å. Snapshots were taken every 10 frames for the MM-PBSA calculations. Secondary structure calculations were performed with CPPTRAJ.[132]

System set up

The high resolution crystal structure of GLIC (PDB code 4HFI)[165] was inserted into a DOPC bilayer consisting of 157 lipids in the lower leaflet and 150 lipids in the upper leaflet. The system was solvated with 150 mM NaCl aqueous solution giving a system containing approximately 232,000 atoms and initial dimensions of approximately 130 x 130 x 180 Å^3. This set up was carried out using the CHARMM-GUI webserver.[126] Protonation states were assigned based on literature values.[64] Fentanyl systems were created from the equilibrated pure system before production. Fentanyl molecules were added to the solvent phase using the gmx insert-molecules tool included with the Gromacs 2018.2 package.

System equilibration

The systems were minimised initially for 10000 steps with the steepest decent method and then 10000 steps with the conjugate gradient method. Heating was conducted in two stages, stage 1 involved heating the system to 100 K in the NVT ensemble with the protein and lipids restrained with a force constant of 10.0 kcal/mol Å^2. Stage 2 involved heating the system slowly to 303 K in the NPT ensemble again with the protein and lipids restrained with a force constant of 10.0 kcal/mol Å^2. Equilibration runs were performed by carrying out 10 individual 500 ps simulations, each with harmonic restraints on the protein and lipids which decreased by 1 kcal/mol Å^2 each simulation. Fully unrestrained production runs were carried out for 500 ns.

Simulations under applied electric field

To assess the ion conduction of the pure and fentanyl-bound GLIC systems, I carried out three separate simulations on each system at three different transmembrane potentials (100 mV, 270 mV and 510 mV) for 200 ns each, totalling 1.2 μs of simulation time under the electric field. The field was applied in the z-direction using the efz variable in the amber input file. High transmembrane potentials were used for computational efficiency. The equilibrated pure system was used as the starting structure for the pure simulations and the structure used for the fentanyl-bound system was taken after fentanyl had entered its binding pocket. Transmembrane potentials were chosen based on typical transmembrane voltages experienced physiologically ($\sim$ 100 mV),[169,170] voltage-clamp and computational electrophysiology studies on membrane proteins (270 mV)[171,172] and for computational efficiency (500 mV).[173,174]

MM-PBSA theory

Molecular Mechanics Poisson-Boltzmann Surface Area (MM-PBSA) calculations are post-processing end-state method used to calculate free energies of molecules in solution. There are several methods which have been developed to calculate free energies, the most theoretically rigorous methods are alchemical perturbation

(AP) methods which consist of Free Energy Perturbation[175] and Thermodynamic integration.[176] These methods, although thorough, are highly computationally demanding and become increasingly expensive as system size increases. End-state methods have been introduced to reduce the computational cost of free energy calculations by removing the need for simulating non-physical intermediate states which is required in AP methods. The cost is further reduced by replacing the explicit solvent environment with the use of implicit models like the Poisson-Boltzmann model. As a result, these methods have been extensively used in computational drug binding studies.[177,178]

These calculations are used for calculating the binding free energy in receptor-ligand complexes, shown as a thermodynamic cycle in Figure 4.2.

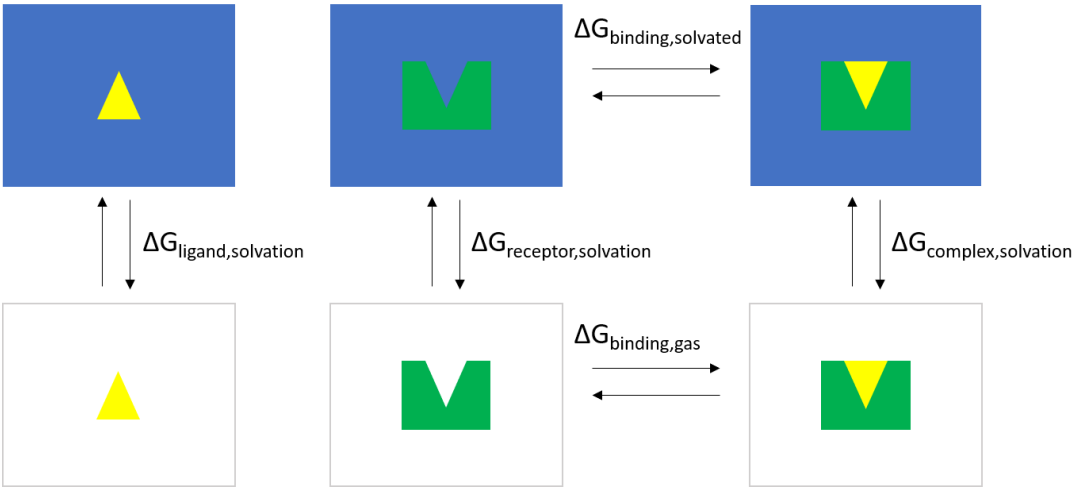

FIGURE 4.2: Thermodynamic cycle for binding free energy calculations for a protein-ligand complex. Solvated systems are shown in blue boxes and gas phase systems are shown in white boxes

Binding free energies are calculated by subtracting the free energies of the unbound receptor and ligand from the free energy of the bound complex:

$$\Delta G_{binding,solvated} = \Delta G_{complex,solvated} - [\Delta G_{receptor,solvated} + \Delta G_{ligand,solvated}] \quad (4.1)$$

The free energy change associated with each term on the right hand side of equation 4.1 is estimated according to equation 4.2:

$$\Delta G_{solvated} = E_{gas} + \Delta G_{solvation} - TS_{solute} \tag{4.2}$$

$\Delta G_{solvation}$ represents the true free energy as the solvent has been averaged as an implicit solvent model was used. The gas-phase energies (E_{gas}) are taken from the molecular mechanical (MM) energies calculated from the forcefield, while solvation free energies ($\Delta G_{solvation}$) are obtained from the implicit solvent model and the entropic contribution (S) is estimated using the quasi-harmonic approximation. The free energy of solvation is further decomposed as the sum of non polar and electrostatic contributions.

The energies described in the above equations are single point energies of the system, however, end-state calculations estimate these energies according to averages from an ensemble of structures generated from MD simulations in my case. Equation 4.2 can be expressed in terms of averages which yields equation 4.3:

$$\Delta G_{solvated} \cong \langle E_{gas} \rangle + \langle \Delta G_{solvation} \rangle - T\langle S_{solute} \rangle \tag{4.3}$$

$$= \frac{1}{N}\sum_{i=1}^{N} E_{i,gas} + \frac{1}{N}\sum_{i=1}^{N} \Delta G_{i,solvation} - \frac{T}{N}\sum_{i=1}^{N} S_{i,solute}$$

where i is the index of a particular frame and N is the total number of frames analysed.

In my studies, all ensembles were extracted from a single MD trajectory of the bound complex which is referred to as the single trajectory protocol (STP). Separate simulations can be used for each state which is referred to as the multiple trajectory protocol (MTP). The STP method is less computationally expensive due to only one trajectory being required to generate all ensembles. Additionally, the internal potential terms cancel exactly in STP due to the conformations in the bound and unbound states are the same, which leads to lower fluctuations and faster convergence. The MTP method has been shown to be much less accurate than the STP method[179,180] which was selected for this work.

4.1.3 Results and discussion

I initially performed three separate 500 ns MD simulations on the pure GLIC structure inserted into a 1,2-Dioleoyl-sn-glycero-3-phosphocholine (DOPC) lipid bilayer[165] as reference, followed by three 500 ns simulations in which four fentanyl molecules were added to the simulation box in each system, where the equilibrated pure GLIC system before its production run was used as the starting structure. From the pure GLIC simulation, root mean squared deviations (RMSDs) were calculated to assess whether the protein structure was stable within the membrane and the RMSD was also calculated for the fentanyl systems (Table 4.1).

System	Structure	RMSD (Å)
Pure	Protein	2.34 ± 0.21
	TMD S1	1.19 ± 0.21
	TMD S2	1.25 ± 0.22
	TMD S3	1.40 ± 0.23
	TMD S4	1.11 ± 0.17
	TMD S5	1.07 ± 0.22
Fentanyl	Protein	2.17 ± 0.36
	TMD S1	1.55 ± 0.40
	TMD S2	1.80 ± 0.30
	TMD S3	1.37 ± 0.28
	TMD S4	1.81 ± 0.38
	TMD S5	1.47 ± 0.28

TABLE 4.1: Root mean squared deviations for the back bone carbon atoms of the whole GLIC structure and each transmembrane domain (TMD) for the pure and fentanyl containing systems

Several binding sites were identified and molecular mechanics Poisson–Boltzmann surface area (MM-PBSA)[181] calculations were performed to assess the strength of binding at each site. Figure 4.3 shows the residues in the fentanyl binding site which has a calculated binding free energy of -27.35 ± 0.06 kcal/mol. The fentanyl

molecule showing the strongest binding energy initially interacts with the hairpin loop located at the top of the extracellular domain for $\sim$ 20 ns before diffusing into the channel, where it then enters the binding pocket. Fentanyl was neutral in these simulations, but it is possible that the piperidine ring nitrogen could be protonated, which raises the possibility of cation-pi interactions with aromatic residues which could alter the binding strength in the pocket. The energy value obtained for fentanyl using this methodology is comparable to results obtained for other ligands binding to pLGICs, such as the neurotransmitter gamma-aminobutyric acid,[182] the antidepressant drug vortioxetine,[183] general anesthetics[184] and benzodiazepines.[185] This agreement shows that the calculated energy for fentanyl are of sensible magnitude compared to those determined for other pLGIC ligands. It should be noted here that due to approximations used within the MM-PBSA methodology, and no fast way of calculating accurate solute entropies, MM-PBSA often overestimates binding energies (systematically more negative than experiments).[186–189] For strong binders we would expect a binding energy of $\sim$ - 10 kcal/mol in reality so we see a significant overestimation in the binding strength of fentanyl. However, the MM-PBSA method is still useful in calculating relative binding free energies for a series of ligands at a target protein, and the result obtained for fentanyl is comparable to that of other drugs which have been shown to bind to this channel.

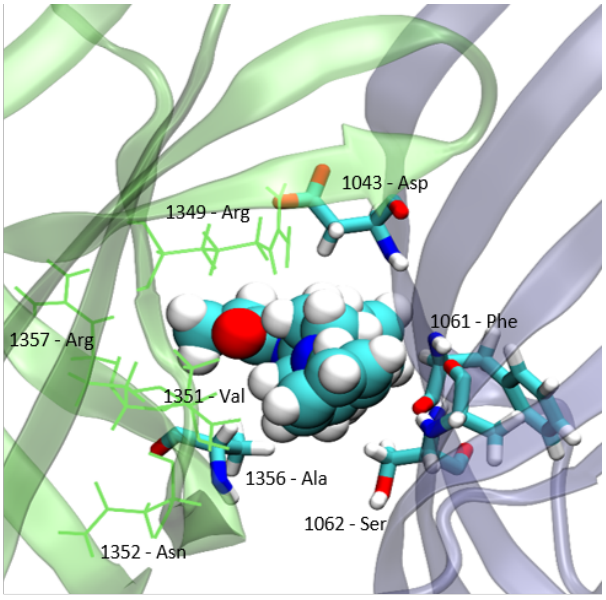

FIGURE 4.3: Detailed view of fentanyl binding in its intersubunit extracellular site. Fentanyl is shown in VdW sphere representation, strongest binding residues shown in licorice representation and additional residues shown in stick representation

This binding pocket is situated between two subunits in the extracellular domain above the lipid head group region. Fentanyl initiates binding at $\sim$ 40 ns in one simulation, and at $\sim$ 50 ns in another, they both remain within the binding site for the rest of the simulation time, totalling 460 ns and 450 ns of binding time respectively, with little structural deviations to the binding conformation (RMSD 1.7$\pm$0.8 Å with respect to the initial binding pose adopted by fentanyl after binding at $\sim$ 40 ns), indicating that this is a very stable binding site. Secondary structure calculations show that there is no appreciable change in the secondary structure of the binding pocket before or after fentanyl binding. Root mean squared fluctuation calculations for the two subunits which form the binding site show that fentanyl causes an increased fluctuation in S5, but stabilises loop C, which forms the top of the binding site (Figure 4.4). At the other binding sites, fentanyl dissociated and diffused into the membrane domain where it remained for the rest of the simulations.

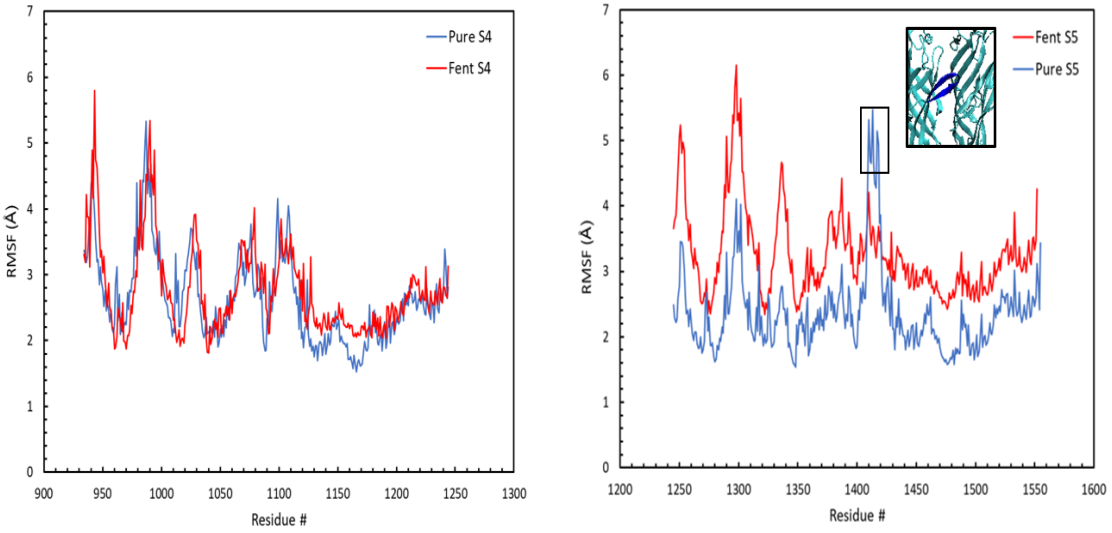

FIGURE 4.4: RMSF plots for S4 and S5 which fentanyl binds in between, loop C (blue) shown in insert

To assess the effects of the binding on the function of the GLIC, I computed the change in the number of pore water molecules, using an in house python script utilising the MDAnalysis python toolkit.[190] Pore water molecules were identified as those which occupied the M2 pore from 245-Asn residues at the top of each helix to 222-Glu residues at the bottom (slightly above the bulk water phase). Note that the pore is fully solvated in the pure GLIC systems. In the fentanyl-bound systems, de-wetting in the 240-Ile to 233-Ile hydrophobic gate region was observed. The remaining water molecules in the M2 pore in the fentanyl-bound systems are located above (245-Asn to 240-Ile) and below (233-Ile to 222-Glu) the hydrophobic gate. Full dehydration of the hydrophobic gate region was observed visually using VMD.[133] This methodology has previously been used to analyse hydrophobic gate formation in other channel proteins.[191] The analysis of the pure system confirmed that the channel was in the open state (Figure 4.5). To identify visually the formation of the hydrophobic gate, VMD[133] was used to identify the gating residues. From this information, I was able to identify residues 233-Ile and 240-Ile as the residues forming the hydrophobic gate and causing dehydration of the M2 pore, which is consistent with the GLIC hydrophobic gating residues identified from

other studies.[166,192,193] This gating mechanism is similar to that for acetylcholine receptors which rely on M2 helix rotations to control ion conduction.[194]

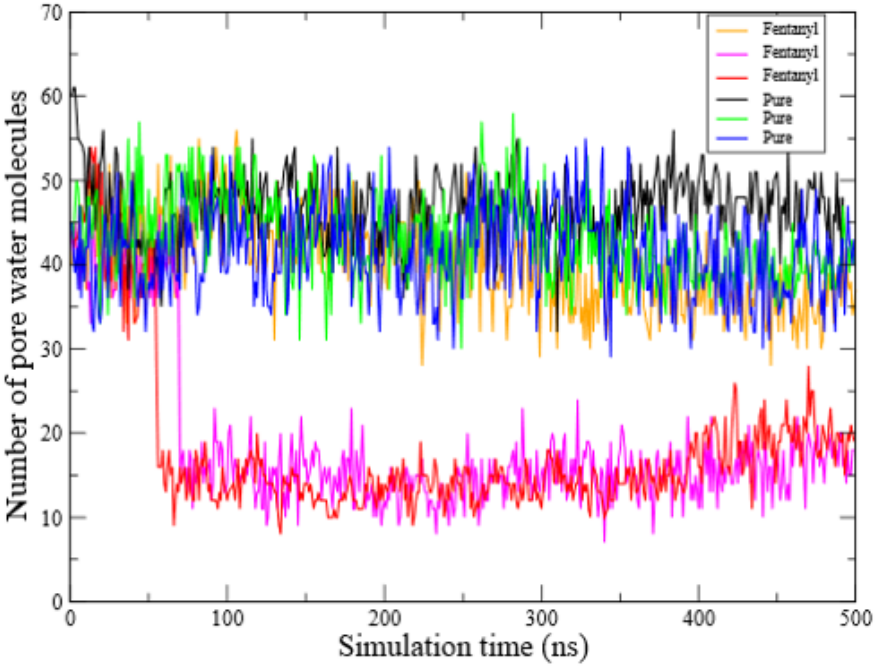

FIGURE 4.5: Plot highlighting the change in the number of pore water molecules within the M2 helix channel pore when fentanyl is bound

The analysis performed shows clearly the formation of a hydrophobic gate within the pore that is consistent with that observed for general anesthetics. In addition, the M2 pore radius of the pure simulation is less contracted than that of the fentanyl system, but instead resembles the open state of the crystal structure (Figure 4.6). As this change of state observed in the fentanyl simulation is not observed within the control simulation, I suggest that the hydrophobic gate formation is caused by the binding of the fentanyl molecule at $\sim$ 40 ns. It should be noted that the GLIC structure is determined to be in the open state based on the pore radius at the 233-Ile and 240-Ile gating region. In the profiles shown in Figure 4.6 there is an apparent constriction at the cytosol interface which is due to glutamic acid residues. In the crystal structure which was solved at pH 4.0, the 221-Glu residues from each subunit are in close contact with each other which blocks intracellular entry of the pore. Due to the low pH, the carboxylic groups will likely be partially protonated. In the simulations performed here, the unprotonated side chains can

repel each other and flip conformations rapidly. I should also note that ELIC and nAChR also have Glu residues at this region which are believed to account for favourable cation conduction in pLGICs.[195,192]

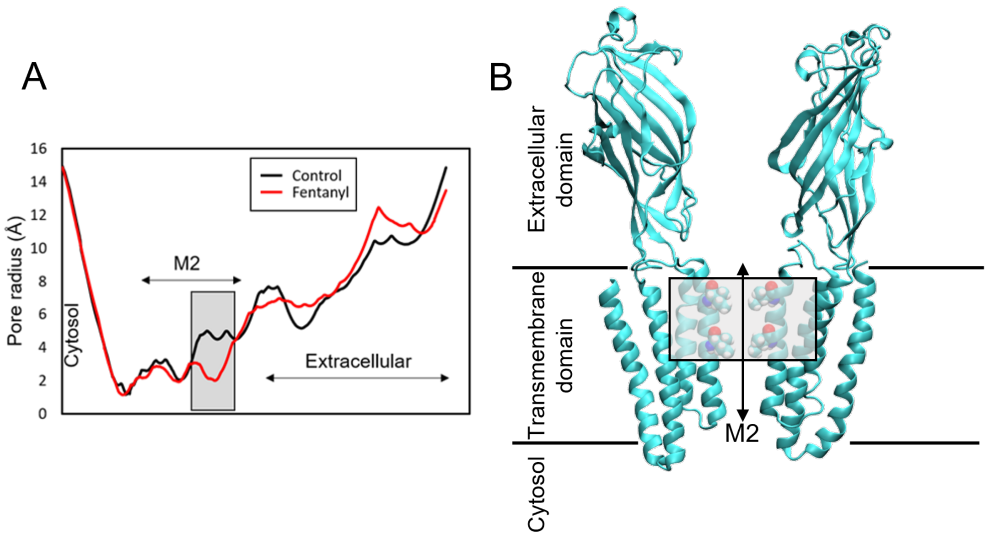

FIGURE 4.6: (A) M2 pore radius calculations for the pure/control and fentanyl simulations averaged over the trajectories. The grey box represents the hydrophobic gate region. Calculations performed using the HOLE program. (B) Gate region shown in the channel pore

To determine if the formation of the hydrophobic gate inhibited ion conduction through the channel, I have performed several applied electric field simulations. Ion conduction was observed in the pure GLIC system after ~ 60 ns at a transmembrane voltage of 270 mV, but no conduction was observed in the fentanyl-bound system, in which ions remained above the hydrophobic gate residues (Figure 4.7). Fentanyl remained bound throughout all of these simulations at all voltages, this observation is further evidence of fentanyls affinity for this intersubunit extracellular site. Transmembrane voltages up to 510 mV were used to increase computational efficiency, although this does not represent the transmembrane potential in a human neuronal cell membrane, the higher potentials allow ion conduction to be observed at computationally relevant timescales.

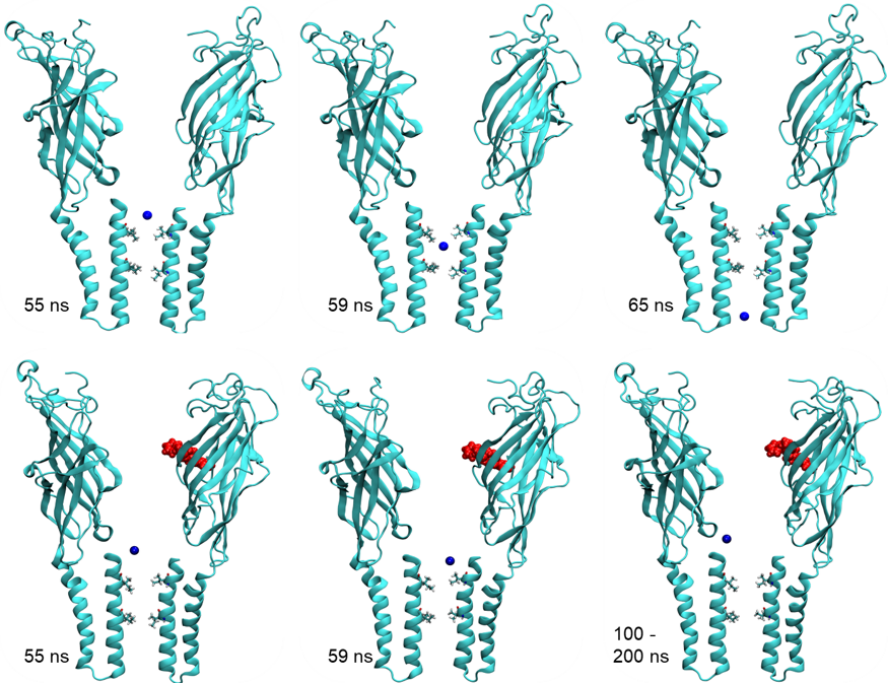

FIGURE 4.7: Top three images represent pure GLIC system under applied transmembrane voltage of 270 mV. Sodium ion shown in blue, hydrophobic gate residues shown in licorice representation. Bottom three images represent fentanyl bound system under applied transmembrane voltage of 270 mV. Fentanyl shown in red spheres.

The conformational change within the TMD associated with anesthetic binding is a $\sim 10^o$ tilt in the upper region of the M2 helix, causing an "iris-like" contraction.[166,192,196] To analyse the effect of fentanyl binding on the geometry of the M2 helix, I employed the TRAJELIX[197] module as incorporated in the Simulaid analysis program,[198] and the Bendix[199] plugin for VMD. I used this methodology to calculate the global helix x, y and z tilt angles; turn angle per residue; local helix tilt; helix rotation; and angle of curvature for each M2 transmembrane helix over the course of the 500 ns trajectories. Figure 4.8 shows the helix rotation for one of the five M2 helices, as they were all relatively similar. I consistently observed a rotation of 10° with a small degree of local helix tilting, which suggests a different method of pore contraction to that observed in binding general anesthetics.[166,192,196]From the curvature analysis I observed that the general trend for the pure system is perturbed by fentanyl binding. The most noticeable increase

in curvature is observed in the first 10 residues of the helix which include the hydrophobic gate region.

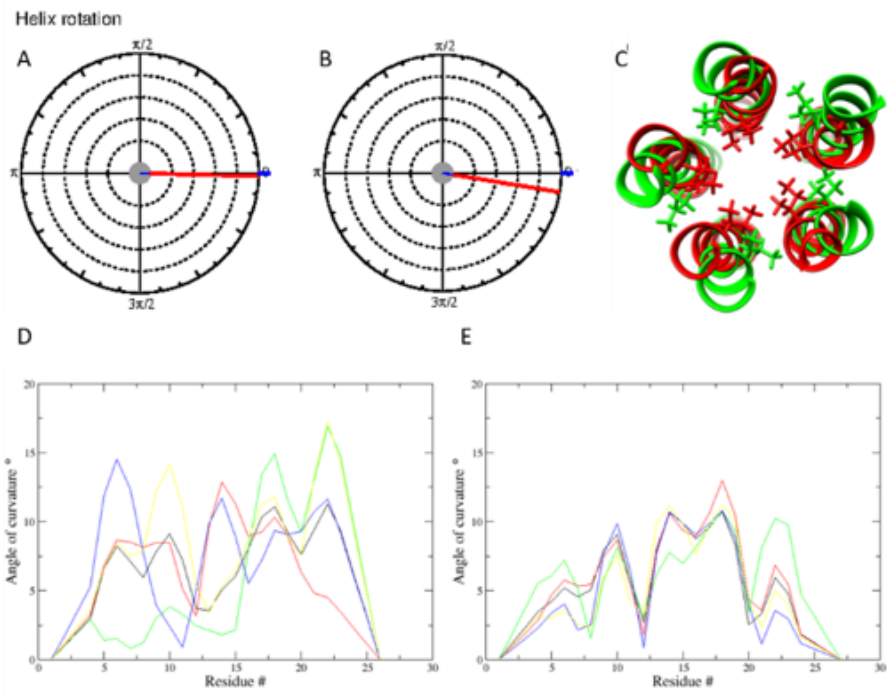

FIGURE 4.8: (A) Dial plot indicating the helix rotation of the S3 M2 helix in the pure GLIC system. (B) Dial plot indicating the helix rotation of the S3 M2 helix in the fentanyl-bound system. (C) Overlapped structures of the M2 TMD, with green indicating an open channel (fentanyl not bound) and red indicating a closed channel (fentanyl bound), Ile gating residues shown in stick representation (rendered with UCSF Chimera). (D-E) Helix curvature plots for fentanyl (D) and pure (E) simulations, where each line represents one subunit.

Although a full signalling pathway or mechanism of action for neurotransmitter and drug action on pLGICs still re-mains unclear, several studies have proposed conformational changes of certain regions of the channels. Salt bridge perturbation has been shown to be significant in the gating process for nicotinic and GABA receptors, as well as GLIC.[200,201] In the fentanyl-bound simulations, I computed the distance between the center of mass (COM) of the 32-Asp and 192-Arg salt bridge, which was shown to break after fentanyl binding. Loop C was also stabilised in the simulations (Figure 4.4), which is also seen in various pLGIC ligand studies where loop C is stabilised in structurally different conformations.

From this analysis I can hypothesize that the difference in helix conformational change is due to the extracellular binding site, which has no direct interaction with the helices themselves. In contrast, the anesthetic binding site, which is either in between TMD sub-units or within the four helices of the sub-units themselves,[202–204] does have direct interaction with the M2 pore helices, possibly causing the larger degree of tilting that has been observed previously. I should note here that a 2.99 Å crystal structure has been obtained, which shows the anesthetic/analgesic drug ketamine binding to a GLIC structure with binding sites situated between extracellular subunits,[72] which is consistent with the observations for fentanyl. Fentanyl remains deeper in the intersubunit site compared to ketamine, most likely due to the size of the fentanyl molecule. Although, during my simulations, fentanyl was seen to interact with 154-Asp which is the residue which contributes to the stabilisation of ketamine. Ketamine is similar to fentanyl in that it can act as both analgesic and anesthetic,[205,206] which suggests that these molecules may have independent binding sites, compared to those of general anesthetics, in the context of the GLIC structure.

4.1.4 Conclusion

In conclusion, I have presented a novel binding site for the opioid analgesic/anesthetic fentanyl, which, to the best of my knowledge, is the first evidence provided of fentanyl interacting with and modulating the conductance state of GLIC. My simulations have shown that fentanyl binding induces the closure of the helix pore by causing helix rotation and curvature with minimal tilting, leading to the 233-Ile and 240-Ile residues forming a hydrophobic gate blocking the pore conductance, which is similar behaviour to that identified for general anesthetics. However, with the use of the TRAJELIX module I was able to identify a rotational motion of the helices which is not observed for anesthetic binding. Discovery of this modulation of GLIC by fentanyl should stimulate further investigations at an atomic level into the role of opioid analgesics in general anesthesia to provide a more complete description of the mechanisms of general anesthesia.

4.2 Interactions between propofol and fentanyl at the *Gloeobacter violaceus* ion channel

4.2.1 Introduction

As stated in Section 4.1.1, the GLIC channel is a pentameric ligand gated ion channel which is responsible for converting synaptic chemical signals into electrical impulses within the peripheral and central nervous systems and as such they are a target for general anesthetics. Propofol has already been shown to bind and modulate the function of this channel,[203,72] along with several other anesthetic molecules (ethanol,[165] ketamine,[78] desflurane,[72] and halothane[75]) which bind to the extracellular and transmembrane domains of the protein structure. These discoveries have provided the strongest evidence thus far that anesthetics exert their main function by modulating the activity of these ion channels. My previous work has shown that the opioid analgesic/anesthetic fentanyl can also bind to and modulate the function of this channel.[2] Fentanyl is an extremely interesting drug as it can be used as a highly effective analgesic, an adjunct to general anesthesia or as the primary anesthetic. Fentanyl has also been shown to potentiate the effect of propofol when both drugs are used in combination to induce and maintain anesthesia.[116,207,208] But knowledge of the specific interactions between propofol and fentanyl at the molecular level is severely lacking. Understanding the interactions between these drugs at their site of action, however, could lead to further development of safer and more efficient anesthetic drugs which will reduce the risk of anesthesia- related complications and help uncover the mechanisms behind this phenomenon.

In this study I have utilised extensive enhanced sampling molecular dynamics techniques, namely conformational flooding and Gaussian accelerated molecular dynamics (GaMD), to probe the interactions between propofol and fentanyl at the GLIC channel. The theory behind these methods are discussed in the coming sections along with the simulation methodology used. This is the first time that

MD simulations and enhanced sampling methods have been used to study the explicit interactions between these two drug molecules and this has allowed us to identify multiple sites in GLIC where both molecules appear to act together and alter the protein structure and function. The paper that arose from this study can be found here.[209]

4.2.2 Methods and theory

4.2.2.1 System preparation and MD simulation methodology

All systems used for the MD simulations were based on the high-resolution open-state crystal structure (PDB: 4HFI) of GLIC.[165] The structure was embedded in a DOPC lipid bilayer and fully hydrated with TIP3P water molecules[210] using the CHARMM-GUI web server[126] and data from the orientation of proteins in membranes (OPM) database.[211] DOPC was chosen as the lipid component as it has been previously used by the publishers of the crystal structure.[165] Each system has the approximate dimensions of 128 x 130 x 180 Å where the z-axis is normal to the bilayer, and contains 1 GLIC, 307 lipid molecules, and approximately 54,000 water molecules. Sodium and chloride ions were added to give a 150 mM salt concentration. 50 propofol and 10 fentanyl were added to the aqueous solution for the flooding and GaMD simulations. Each system contained approximately 230,000 atoms.

Protonation states of the ionisable residues of the protein were assigned based on calculations performed by Bocquet et al.[64] Parameters and atomic point charges for each drug molecule were assigned using the antechamber program from AmberTools and the General Amber ForceField (GAFF)[110] for small organic molecules.

All MD simulations were performed using the CUDA enabled Amber16 molecular dynamics package.[127] The ff14SB forcefield[108] was used for the protein, solvent and ions, the lipid14 forcefield[109] was used for the lipids and the GAFF2 forcefield[110] was used for the drug molecules. The systems were energy minimised for 20,000 steps (10,000 steepest descent then 10,000 conjugate gradient). Heating

was conducted in two stages, where stage 1 involved heating the system to 100 K in the NVT ensemble with the protein, lipids and drug molecules restrained with a force constant of 10.0 kcal/mol Å^2. Stage 2 involved heating the system slowly to 303 K in the NPT ensemble with the same force constant applied to the protein, lipids and drug molecules. Equilibration was initially performed with multiple 2 ns simulations where the lipid restraints were gradually reduced from 10 to 0 kcal/mol Å^2 over 22 ns. The was then repeated while reducing restraints on the protein backbone totalling another 22 ns. The unrestrained conformational flooding simulations were run for 1 μs and the GaMD simulations were run for 500 ns. Three repeats were carried out for each method. One simulation was carried out on the pure GLIC structure as a control to determine if the system was constructed correctly, which was run for 500 ns. All simulations were carried out at a constant pressure of 1.0 atm, which was maintained using the anisotropic Berendsen method with a pressure relaxation time of 1.0 ps. The temperature was maintained at 303 K using the Langevin thermostat with a collision frequency of $\gamma = 1.0$ ps^{-1}. Three dimensional periodic boundary conditions with the usual minimum image convention were used. The SHAKE algorithm was employed to constrain covalent bonds to hydrogen, allowing the use of a 2 fs time step. Electrostatic interactions were treated with with the PME method using a cutoff of 10 Å. Data analysis was carried out using VMD,[133] CPPTRAJ[132] and custom scripts. UCSF Chimera[212] was used to render images.

4.2.2.2 Flooding simulations

Simulation studies of the GLIC system in the past have mostly focused on the anesthetic binding site from the the published crystal structure,[72] which often involve docking the drug molecule within the observed site. However, this methodology does not take into account the pathway of the drug molecule, or any other binding sites that can be occupied. The flooding methodology investigates the possibility of of these alternative binding sites and pathways by implementing three independent 1 μs flooding simulations in which 50 propofol molecules and 10 fentanyl molecules were added to the solvent phase randomly; this methodology is similar

to other studies carried out on different anesthetics.[166,71] The drug molecules were added to the system at random initial positions using the gmx insert-molecules tool available with the GROMACS package.[213] Propofol was used in excess in my simulations to mimic the higher concentration of propofol used in the general anesthesia process. I note that the ratio of opioid to anesthetic is higher here than would be used clinically, but the goal of using a higher ratio is to increase the probability of finding a site of opioid-anesthetic interaction during the simulations. The MD flooding approach provides a dynamic, flexible and physical dock which is a significant advantage over traditional docking procedures.[71,214]

4.2.2.3 Gaussian accelerated molecular dynamics

GaMD is an accelerated MD method which allows unconstrained sampling and accurate reconstruction of free energy profiles, thereby allowing long timescale events which would normally occur over hundreds of microseconds to milliseconds to be investigated in more realistic simulation times.[215,216] GaMD enhances the conformational sampling of biomolecules by adding a harmonic boost potential to smooth the system potential energy surface (Figure 4.9). Consider a system with N atoms at positions $\vec{r} = \{\vec{r_1},...,\vec{r_N}\}$. When the system potential $V(\vec{r})$ is lower than a threshold energy E, a boost potential is added as:

$$\Delta V(\vec{r}) = \frac{1}{2}k(E - V(\vec{r}))^2, V(\vec{r}) < E, \tag{4.4}$$

where k is the harmonic force constant. The modified system potential, $V^*(\vec{r}) = V(\vec{r}) + \Delta V(\vec{r})$ is given by:

$$V^*(\vec{r}) = V(\vec{r}) + \frac{1}{2}k(E - V(\vec{r}))^2, V(\vec{r}) < E \tag{4.5}$$

Otherwise, when the potential of the system is greater than the threshold energy, i.e., $V(\vec{r}) \geq E$, the boost potential is set to zero and $V^*(\vec{r}) = V(\vec{r})$.

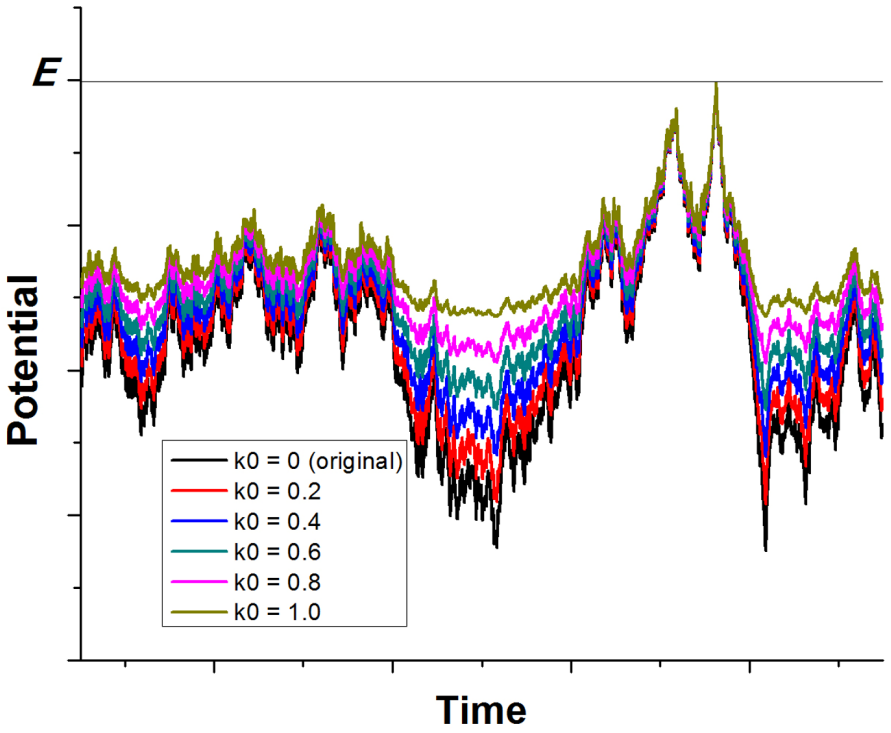

FIGURE 4.9: Schematic illustration of GaMD. When the threshold energy E is set to the maximum potential (E=V_{max}), the systems potential energy surface is smoothened by adding a harmonic boost potential that follows a Gaussian distribution. The coefficient k_0, which falls in the range of 0 - 1.0, determines the magnitude of the applied boost potential. Copyright Journal of Chemical Theory and Computation (2015).[1]

In order to smooth the PES for enhanced sampling, the boost potential needs to meet a defined criteria. First, for any two arbitrary potential values $V_1(\vec{r})$ and $V_2(\vec{r})$ found on the unmodified energy surface, if $V_1(\vec{r}) < V_2(\vec{r})$, ΔV should be a monotonic function that does not change the relative order of the biased potential values, i.e., $V_1^*(\vec{r}) < V_2^*(\vec{r})$. By replacing $V^*(\vec{r})$ with Eq. (4.5) and isolating E, we then get:

$$E < \frac{1}{2}[V_1(\vec{r}) + V_2(\vec{r})] + \frac{1}{k} \tag{4.6}$$

Second, if $V_1(\vec{r}) < V_2(\vec{r})$, the difference in potential observed on the smoothened energy surface should be lower than that of the unmodified surface, i.e., $V_2^*(\vec{r})$ - $V_1^*(\vec{r}) < V_2(\vec{r})$ - $V_1(\vec{r})$. Similarly, by replacing $V^*(\vec{r})$ with Eq. (4.5), we can derive:

$$E > \frac{1}{2}[V_1(\vec{r}) + V_2(\vec{r})] \tag{4.7}$$

With $V_{min} \leq V_1(\vec{r}) < V_2(\vec{r}) \leq V_{max}$, the threshold energy E has to be set in the following range by combining Eqs. (4.6) and (4.7):

$$V_{max} \leq E \leq V_{min} + \frac{1}{k}, \tag{4.8}$$

where V_{min} and V_{max} are the system minimum and maximum potential energies, respectively. To make sure that Eq. (4.8) is correct, $V_{max} \leq V_{min} + \frac{1}{k}$ and k have to satisfy:

$$k \leq \frac{1}{V_{max} - V_{min}} \tag{4.9}$$

Let us define $k \equiv k_0 \cdot \frac{1}{V_{max} - V_{min}}$, then $0 < k_0 \leq 1$. As shown in Figure 4.9, k_0 determines the size of the boost potential which is to be added. With greater k_0, a larger boost potential is added to the PES, which leads to lover energy barriers allowing enhanced sampling to be achieved.

Third, the standard deviation of ΔV needs to be small enough (narrow distribution) to allow accurate reweighting using cumulant expansion to the second order to be performed:

$$\sigma_{\Delta V} = \sqrt{\left(\frac{\delta \Delta V}{\delta V}\bigg|_{V=V_{avg}} \right)^2 \sigma_V^2} = k(E - V_{avg})\sigma_V \leq \sigma_0, \tag{4.10}$$

where V_{avg} and σ_V are the average and standard deviation of the system potential energies, respectively, $\sigma_{\Delta V}$ is the standard deviation of ΔV with σ_0 is an upper limit (e.g., $10 k_B T$) for accurate reweighting which is defined by the user.

If Eq. (4.8) gives the range of threshold energy E, when E is set to the lower bound $E = V_{max}$, E and k can be substituted in, to give:

$$k_0 \leq \frac{\sigma_0}{\sigma_V} \cdot \frac{V_{max} - V_{min}}{V_{max} - V_{avg}} \tag{4.11}$$

The right hand side of equation 4.11 can be represented as $k_0' = \frac{\sigma_0}{\sigma_V} \cdot \frac{V_{max} - V_{min}}{V_{max} - V_{avg}}$. To allow for efficient sampling with the greatest possible acceleration, k_0 can then

be set to its upper bound as:

$$k_0 = min(1.0, k_0^{'}) = min\left(1.0, \frac{\sigma_0}{\sigma_V}.\frac{V_{max} - V_{min}}{V_{max} - V_{avg}}\right). \tag{4.12}$$

The greater $\sigma_{\Delta V}$ that is obtained from the unmodified PES (particularly for larger systems), the smaller k_0 may be able to allow for accurate reweighting. As another option, when the threshold energy E is set to its upper bound $E = V_{min} + \frac{1}{k}$ according to Eq. 4.8, E and k can be subbed into Eq. 4.10 and give:

$$k_0 \geq \left(1 - \frac{\sigma_0}{\sigma_V}\right).\frac{V_{max} - V_{min}}{V_{avg} - V_{min}} \tag{4.13}$$

The right hand side of Eq. 4.13 can be defined as $k_0^{''} \equiv \left(1 - \frac{\sigma_0}{\sigma_V}\right) . \frac{V_{max}-V_{min}}{V_{avg}-V_{min}}$. It should be noted that a smaller k_0 will lead to a higher threshold energy E being obtained, but smaller force constant k. When $0 < k_0^{''} \leq 1$, k_0 can be set to either $k_0^{''}$ for the highest threshold energy E or its upper bound 1.0 for the greatest force constant k. In this regard, $k_0 = k_0^{''}$ is applied in the current simulation.[1]

Similar to traditional accelerated molecular dynamics (aMD), GaMD makes it possible to add only the total boost potential ΔV_p, only dihedral boost potential ΔV_d, or the dual boost potential (both ΔV_p and ΔV_d). The dual boost method gives greater acceleration than the other two types for enhanced sampling. The simulation parameters comprise of the threshold energy values and the effective harmonic force constant, k_{0P} and k_{0D} for the total and dihedral boost potential, respectively.[1]

When performing simulations of biomolecular systems, the probability distribution along a selected reaction coordinate A(r) is written as p*(A), where r denotes the atomic positions $r_1,...,r_N$. Given the boost potential $\Delta V(r)$ of each frame, p*(A) can be reweighted to recover the canonical ensemble distribution, p(A),[215] as:

$$p(A_j) = p^*(A_j)\frac{\langle e^{\beta\Delta V(r)}\rangle}{\sum_{i=l}^{M}\langle p^*(A_i)e^{\beta\Delta V(r)}\rangle_i}, j = 1, ..., M, \tag{4.14}$$

where M is the number of bins, $\beta = k_B T$ and $\langle e^{\beta\Delta V(r)}\rangle_j$ is the ensemble average

Boltzmann factor of ΔV(r) for simulation frames found in the jth bin. To minimise the energetic noise, the ensemble-averaged reweighting factor can be approximated using cumulant expansion:

$$\langle e^{\beta \Delta V} \rangle = exp\Big\{ \sum_{k=1}^{\infty} \frac{\beta^k}{k!} C_k \Big\}, \tag{4.15}$$

where the first three cumulants are given by:

$$\begin{aligned} C_1 &= \langle \Delta V \rangle, \\ C_2 &= \langle \Delta V^2 \rangle - \langle \Delta V \rangle^2 = \sigma^2_{\Delta V}, \\ C_3 &= \langle \Delta V^3 \rangle - 3\langle \Delta V^2 \rangle + 2\langle \Delta V \rangle^3. \end{aligned} \tag{4.16}$$

When the boost potential follows near-Gaussian distribution, cumulant expansion to the second order (or "Gaussian Approximation") provides the accurate approximation for free energy calculations. The reweighted free energy F(A) = -$k_B$ln p(A) is calculated as:

$$F(A) = F^*(A) - \frac{1}{\beta} \sum_{k=1}^{2} \frac{\beta^k}{k!} C_k + F_C, \tag{4.17}$$

where F*(A) = -k_BTln p*(A) is the modified free energy obtained from GaMD simulation and F_c is a constant.

To characterize the extent to which ΔV follows Gaussian distribution, its distribution anharmonicity γ is calculated as:

$$\gamma = S_{max} - S_{\Delta V} = \frac{1}{2} ln(2\pi e \sigma^2_{\Delta V}) + \int_0^{\infty} p(\Delta V) ln(p(\Delta V)) d\Delta V, \tag{4.18}$$

where ΔV is dimensionless as divided by k_BT where k_B and T is the Boltzmann constant and system temperature, respectively, and $S_{max} = \frac{1}{2}\ln(2\pi e \sigma^2_{\Delta V})$ is the maximum entropy of ΔV. When γ is zero, ΔV follows exact Gaussian distribution with enough sampling. Reweighting by approximating the exponential average term with cumulant expansion to the second order makes it possible to reconstruct the unmodified energy landscape. As γ increases, the ΔV distribution becomes

less harmonic and the constructed profile calculated from second order cumulant expansion would deviate from the original significantly. The anharmonicity of ΔV distribution acts as a gauge of the convergence of the sampling and accuracy of the reweighted free energy.[215]

For all of my simulations, the system energy was set to E = V_{max}. The dual boost scheme was used, in which the acceleration potential was applied to the dihedrals and the whole system potential. V_{max}, V_{min}, V_{avg} and σ_V were obtained from an initial 8 ns NPT simulation without a boost potential applied. Each GaMD simulation then underwent a 40 ns run in which the boost potential was updated every 1.6 ns, thus reaching equilibration values. Production runs were carried out for 500 ns for all three simulations, in which each was started with random particle velocities. The same number of drug molecules as in the flooding simulations were included here. Trajectory frames were saved every 1 ps.

4.2.3 Results and discussion

4.2.3.1 Flooding simulations

Within the first few nanoseconds of the production simulations, both drug molecules begin to partition into the hydrophobic region of the membrane (Figure 4.10), often forming small clusters in which multiple propofol molecules bind to one fentanyl molecule. To assess the strucutral stability of the GLIC structure within the membrane environment, the RMSD of the protein backbone was calculated to be less than 3.0 Å over the total length of simulation with an average of 1.92 $\pm$ 0.21 Å, based on which the simulations were deemed to be stable the protein remained in its native structure. Multiple regions were identified where propofol binds to the protein structure for several nanoseconds of the simulations. Of these potential interaction sites, only one was observed over multiple subunits for several hundred nanoseconds. This site was located in the transmembrane domain (TMD) close to the binding site which was identified experimentally, see Figure 4.11. The other

sites, where shorter interactions were observed, most likely represent non-specific adhesion of propofol to the protein surface rather than a functional binding site.

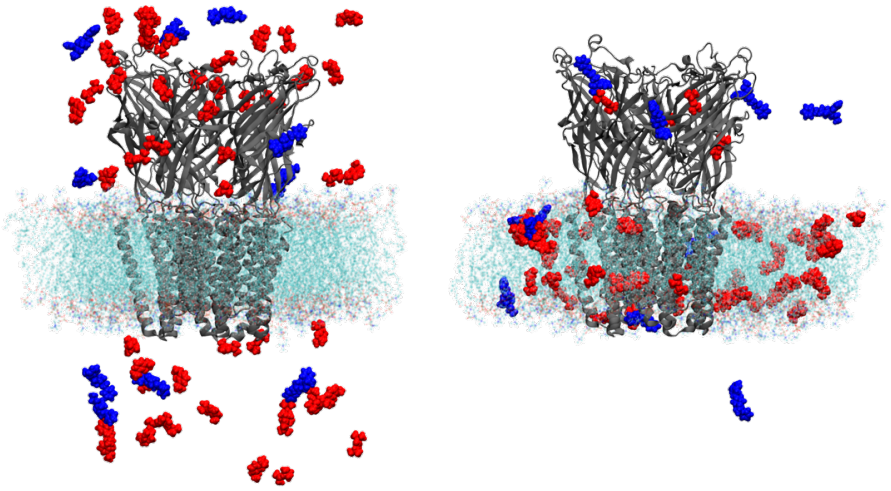

FIGURE 4.10: (A) First and (B) final frame of 1 μs of production simulation. Blue represents fentanyl and red represents propofol

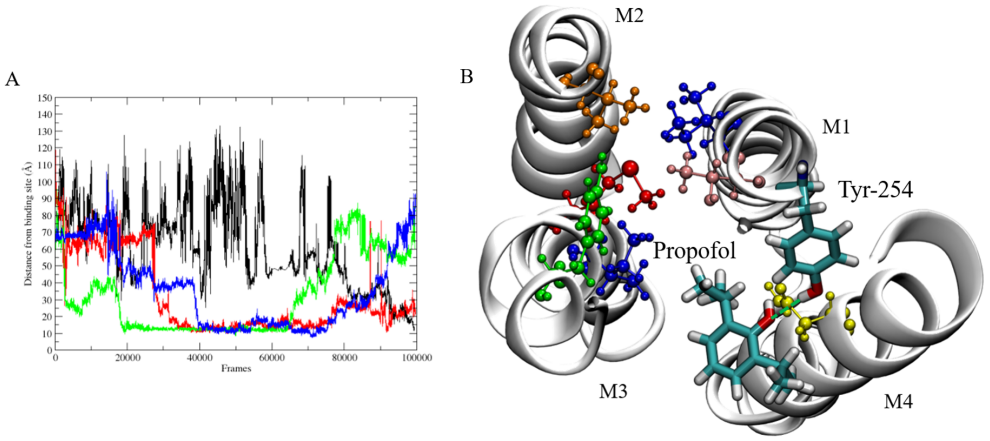

FIGURE 4.11: (A) Distance between interacting propofol molecules and COM of experimental binding site. Each line represents one propofol molecule. (B) Snapshot showing the binding site in which propofol (licorice representation) interacts with Tyr-254 (licorice representation) and Asn-307 (yellow). The anesthetic binding site residues are shown; Tyr-193 (green), Ile-202 (blue), Met-205 (red), Val-242 (orange), Thr-255 (pink) and Ile-259 (blue). M1-M4 are the transmembrane helices located in each subunit. Hydrogen-bond between propofol and Tyr-254 shown by green dashed line

The site where most stability is observed is identical to that which was observed by Arcario *et al.*,[166] where they observed the binding of desflurane to GLIC by forming a hydrogen bond to Tyr-254 during their simulations. The stability associated with propofol at this site (Figure 4.11 B) is due to the formation of a hydrogen bond between the hydrogen of the Tyr-254 hydroxyl group and the oxygen of the propofol hydroxyl group, which was calculated for the propofol molecule at subunit 3 (Figure 4.12).

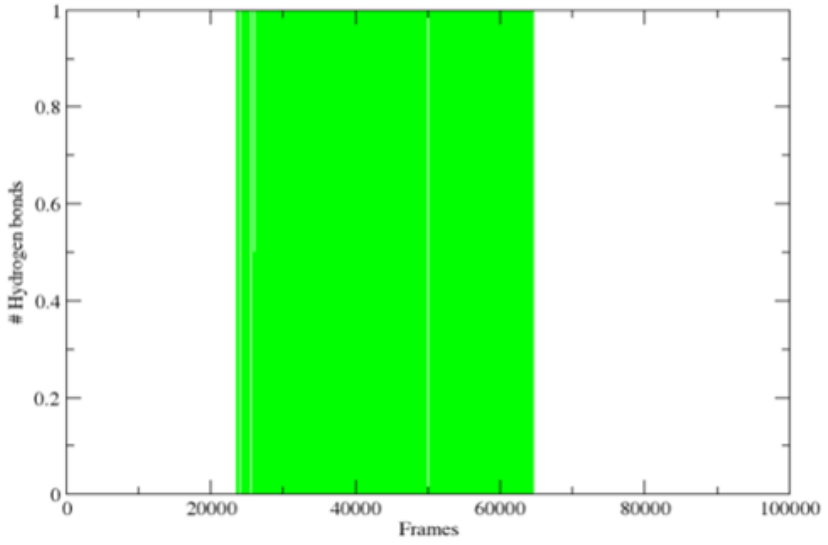

FIGURE 4.12: Plot of the hydrogen bond between propofol and Tyr-254

The hydrogen bond remains dominant over the full time in which propofol remains bound at this site, which is approximately 400 ns. The stability was shown by calculating the distance between the propofol molecules which were observed to interact at this site in each subunit, and the COM of the experimental anesthetic binding site, in which propofol has been shown to bind.[72] The propofol molecule which binds at S3 remains bound from $\sim$ 200 ns to $\sim$ 650 ns, where the hydrogen bond to Tyr-254 contributes to the binding stability here. Three molecules where observed to bind to the same site at the same time in different subunits, and this asymmetric ligand binding has been shown to play a role in channel function.[168] The distance calculations have shown that this binding site holds the propofol molecules at $\sim$ 10 Å from the deeper transmembrane site, indicating the possibility of a transition pathway, although this was not observed in any of the simulations.

Another possibility is that a allosteric binding site has to be filled before propofol can transition to this deeper site. Throughout the flooding simulations, multiple bound anesthetics were observed at multiple subunits which helps to explain why large amounts of general anesthetic are required to induce the desired clinical effect. This behaviour strengthens the argument that these drugs indiscriminately bind to several targets.[217–219]

An interesting observation made during the flooding simulations was propofol occupying the exact same binding site in the extracellular domain that the general anesthetic ketamine has been shown to occupy.[78] This site is approximately 10 Å below the orthosteric agonist-binding site in the extracellular domain. Ketamine binding in this site was also shown to modulate the function of the GLIC channel.[79] Previously identified binding sites for propofol were located in the upper transmembrane domain within a subunit which is very different from that identified for ketamine. I observed propofol binding in this extracellular site within the first 100 ns of the simulation and it remained in this site for the rest of the simulation, totalling $\sim$ 900 ns of residence time within the site. Propofol remains fairly mobile within the site with an RMSD of 5.0 $\pm$ 1.4 Å, which is due to the small molecular volume of propofol ($\sim$ 191 Å^3) compared to the ketamine site ($\sim$ 248 Å^3). The residues within 4 Å of propofol displayed a RMSD of 1.7 $\pm$ 0.5 Å, which shows that the structure in this flexible loop region is fairly resilient to propofol binding. Identification of multiple binding sites presents a compelling case for the allosteric action of molecules which possess anesthetic properties.

4.2.3.2 GaMD

The GaMD simulations were able to capture the complete binding pathway of one propofol molecule which binds within the channel pore above the hydrophobic gate region. Binding was captured within $\sim$ 50 ns in all three replicate GaMD simulations, whereas no propofol molecules were observed to bind within the pore in any of the flooding simulations. Propofol diffused from the bulk solvent to the β-3 loop in the upper extracellular domain of S1, before moving to the β-8 loop

between S1 and S2 in the extracellular domain, and finally into the center of the M2 helix pore above the Ile-239 gating residues, see Figure 4.13. By aligning the C-terminal domain of the GLIC, the RMSD of the diffusing propofol molecule relative to the position in the pore in the last frame of the simulations reaches a minimum of 1.1 Å. It forms hydrophobic interactions with several residues in and around the opening of the pore, see Figure 4.13.

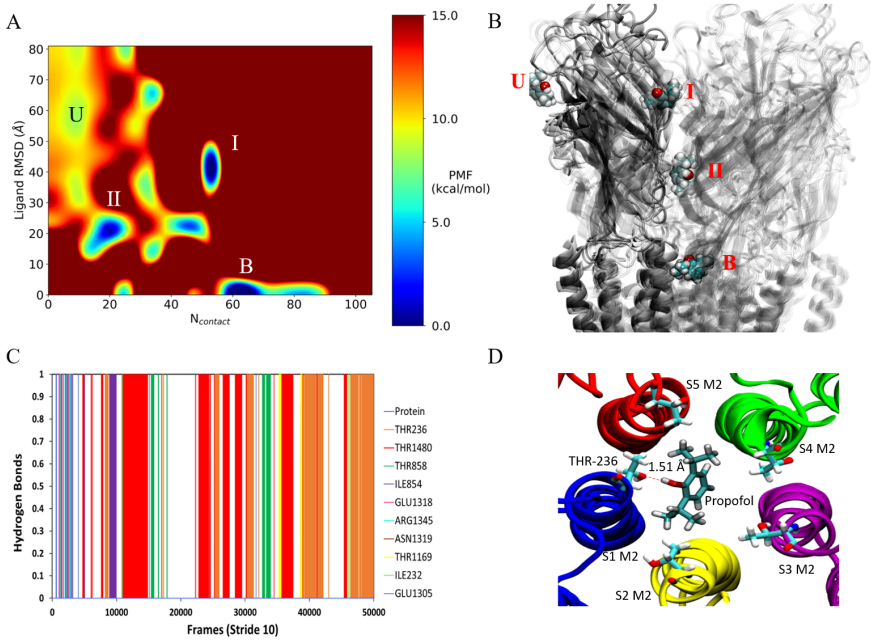

FIGURE 4.13: (A) 2D ($N_{contact}$, propofol RMSD) PMF calculated by reweighting the 500 ns GaMD simulation. (B) Pathway of propofol diffusion into the M2 helix pore in all 3 replicates. (C) Hydrogen-bonds formed between propofol and the GLIC, where bonds formed after 10000 steps are in the pore. Protein refers to short lived h-bonds formed on the protein exterior. Data combined from all three replicates. (D) Final frame snapshot showing propofol hydrogen-bonding to Thr-236 in S1

The boost potential applied during the GaMD simulations follows a Gaussian distribution and its distribution anharmonicity γ equals 1.94 x 10^{-2}. The average and standard deviation of ΔV are 15.3 kcal/mol and 4.7 kcal/mol, respectively. Such a narrow distribution will ensure accurate reweighting for the free energy calculations using cumulant expansion to the 2nd order. Using the number of protein heavy atoms that were within 5 Å of propofol ($N_{contact}$) and the RMSD of propofol relative to the final frame pose, a 2D potential of mean force (PMF) profile

was calculated by reweighting the three independent GaMD simulations using the PyReweighting toolkit.[220] As the pore blocking pathway was observed in all three replicates, the data were combined to produce the PMF. The reweighted PMF allows us to identify four low-energy states: the unbound ("U"), intermediate 1 ("I"), intermediate 2 ("II") and bound ("B") states. The maximum energy was capped at 15 kcal/mol to clearly identify distinct unique states. The unbound state is located in a local energy well centred at $\sim$ (10, 60 Å), the I state is centred at $\sim$ (50, 40 Å), the II state is centred at $\sim$ (20, 20 Å) and the B state is located at the global energy minimum $\sim$ (60, 0 Å). As the propofol binding was observed in all three replicate simulations, I can assume that the calculated energies between the individual states have a low degree of error. Propofol forms hydrogen-bonds within the channel pore with residues Thr-236, Thr-1480, Thr-858 and Thr-1169 (Figure 4.13). Hydrogen-bonds are also formed along the pathway to the pore with residues Ile-854, Arg-1345, Asn-1319 and Glu-1305.

Anesthetic transmembrane binding site

Most studies which have been carried out on the GLIC system have focused on the experimental bind site which was observed in the crystal structure,[72] using docking methods which do not take into account the binding pathway to the site. To assess whether any propofol molecules in the system entered this site, I defined the binding site by the following residues: Tyr-193, Ile-198, Met-201, Val-238, Thr-251 and Ile-255. I used the center of mass (COM) of these binding site residues and calculated the distance between the COM, and any propofol molecules which were identified as being close to the site through visual inspection in VMD.[133] During the distance calculations, a step size of 10 was used. Figure 4.14 shows the distances between the propofol molecules and the COM of the anesthetic transmembrane site. No molecules were identified for subunit 2.

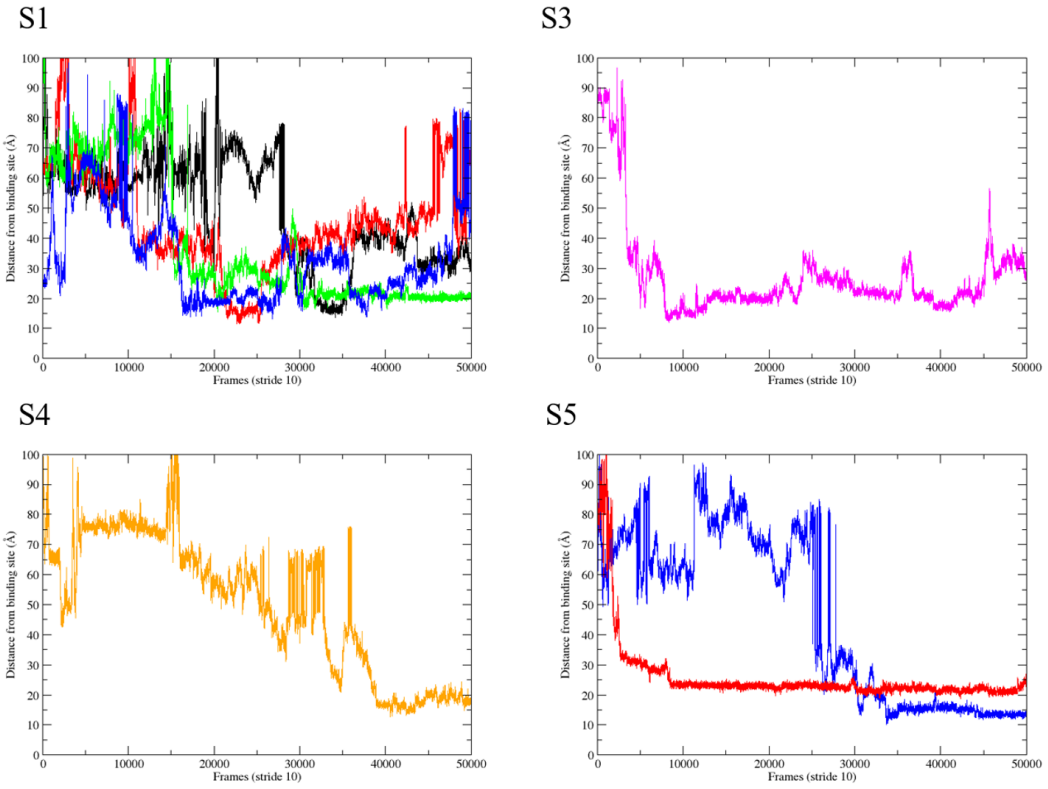

FIGURE 4.14: Calculated distances between the binding site COM and identified propofol molecules. Each line in the graphs represents an individual propofol molecule. Data taken from one replicate in which most interactions were observed

Figure 4.15 shows multiple propofol molecules interacting at S1, although I noticed that none of these molecules get close to the binding site. Regions of propofol stability are located between 10 and 20 Å from the crystal structure binding site. The initial thoughts behind the reason for this distance was due to multiple propofol molecules interacting with each other and forming small clusters, as has been observed before in the membrane region.[221] Further investigations revealed the same distances were present for S3 and S4 in which only one molecule was present which ruled out the hypothesis that it was caused by intermolecular interactions between multiple propofol molecules. When investigating the site at which the propofol molecules remain stable, I observed a site formed by residues Phe-261, Phe-295 and Val-264 (Figure 4.15 B).

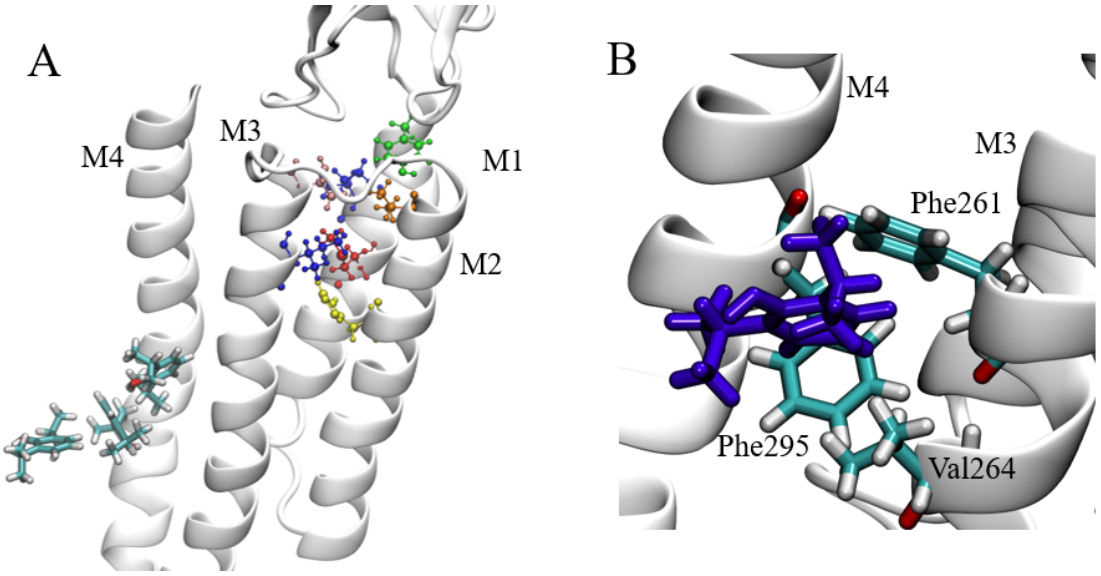

FIGURE 4.15: Interaction site of propofol at GLIC subunits: (A) Sites of propofol interaction in relation to the anesthetic binding site in which residues are coloured; Tyr (green), Ile (blue), Met (red), Val (orange), Thr (pink) and His (yellow). Propofol molecules are shown in licorice representation. (B) Blocking residues inhibiting the path to the anesthetic binding site, propofol (violet) shown in licorice representation

These residues form a barrier which block the propofol molecule from entering the upper region of the transmembrane where the anesthetic binding site is located. The phenylalanine residues appear to form π-π interactions with each other and the propofol molecule, which is likely to contribute to the observed stability of the propofol molecule at this site. If I assumed that the binding site observed in the crystal structure was correct, I must assume that either longer timescales are required to observe the passage of the propofol molecule into the binding site, or an allosteric mechanism in which another binding site has to be occupied to allow propofol to pass the Phe-261 Phe-295 gate, although none of this was observed in multiple microseconds of cMD and GaMD simulations. It should be noted that no propofol molecules were observed to enter from the other side of the M4 helix, between M4 and M1.

To investigate the dynamical consequences on GLIC induced by drug molecule binding, the distance between Asp-32 and Arg-192 which form a salt bridge. It

has been shown that salt bridge perturbation is a key factor in the channel gating process; this was shown in a nAChR channel,[222] and GLIC where the volatile anesthetic halothane caused disruption of this salt bridge, which led to instability within the channel.[75]

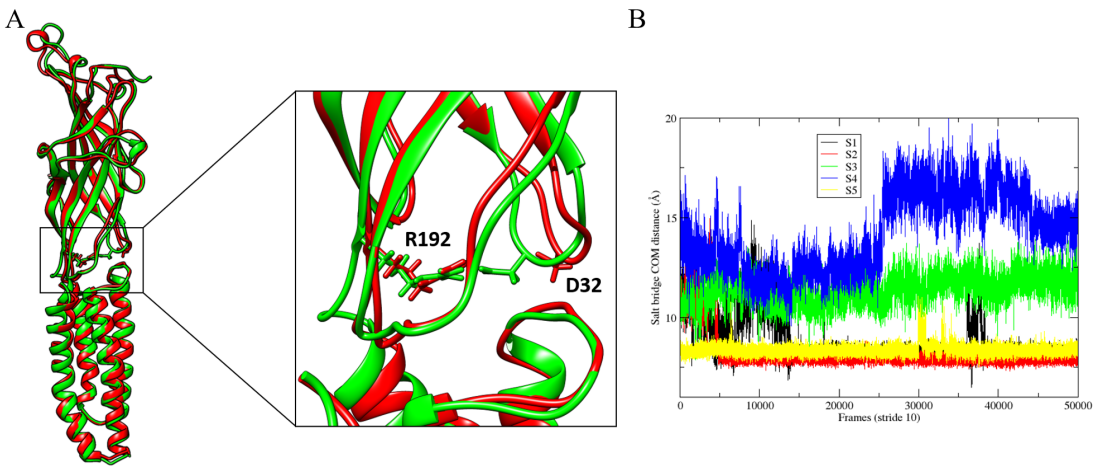

FIGURE 4.16: (A) Overlapped structure of a GLIC subunit in which the Asp-32 Arg-192 salt bridge is stable (green) and broken (red). (B) Distance between the COM of the salt bridge residues in each subunit

Figure 4.16 B shows that the salt bridge was broken at multiple subunits, and the times at which the salt bridge was broken, drug molecules were bound at the respective subunits. This shows that these drug molecules can make significant changes in the GLIC structure that are important to channel gating, even when no molecules were present in the experimental binding site.

To identify whether fentanyl and propofol share common binding sites, density maps were constructed using the VOLMAP plugin for VMD.[133] The density maps shown in Figure 4.17 were averaged over the whole simulation trajectories, apart from the first 50 ns which were discarded for system equilibration. The regions of high density which were identified reflect locations where drug molecules reside for long periods of time.

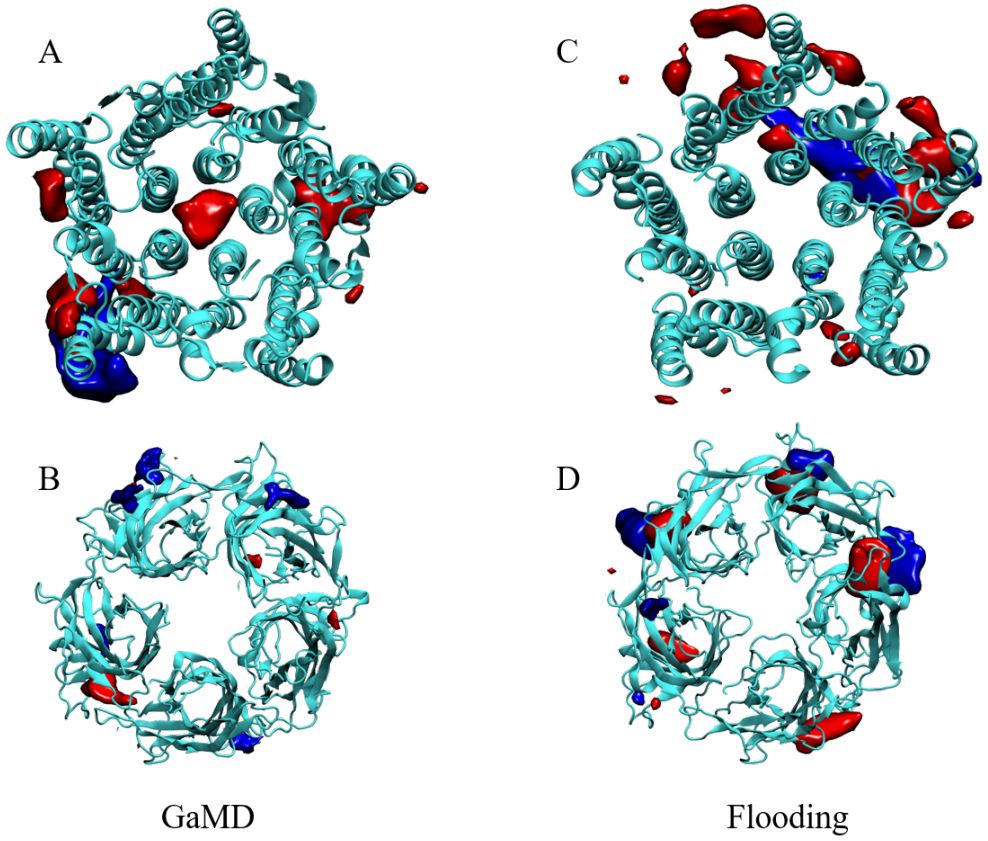

FIGURE 4.17: Regions of prolonged occupation by fentanyl (blue) and propofol (red) in GLIC. (A and B) represent the TM and EC domains of the GLIC, respectively, from the GaMD simulations. (C and D) represent the TM and EC domains of the GLIC, respectively, from the cMD simulations

Density maps were constructed for both the GaMD and flooding simulations, which allowed us to determine if the accelerated simulations were able to discover binding sites which were not attainable in the conventional simulations. The main difference that was observed is the occupation of the ion channel pore by propofol in the GaMD simulations. The pore is occupied by one propofol molecule which resides above the hydrophobic gating residues that form the upper part of the hydrophobic gate in GLIC.[192] The propofol molecule remains fairly mobile within the pore with a RMSD of 6.06 $\pm$ 0.76 Å. The propofol molecule blocks the majority of the channel pore which disrupts the flow of water through the

pore, effectively stopping all function. The propofol molecule forms hydrogen-bonds with the threonine residues at the top of the M2 helices, hydrogen-bonding calculations show that these residues form the majority of the interactions within the pore (Figure 4.13 C). It has previously been shown that the general anesthetic isoflurane blocks the pore of GLIC and nAChR as a dimer,[71] but this behaviour was not seen for propofol in my simulations, most likely due to the larger size of propofol compared to isoflurane. LeBard *et al.*[77] predicted the physical blocking of the GLIC pore by propofol, which was shown to bind with high affinity, as calculated from free energy perturbation (FEP) calculations. They predicted that it would bind as a dimer in a similar way to isoflurane, but this was not observed in any of my simulations. A structure of propofol bound to the pore of GLIC has not yet been resolved experimentally, most likely due to the binding of detergents (dodecylmaltoside, DDM) within the pore.[64] The GaMD simulations revealed the binding pathway that propofol takes when it binds within the channel pore, Figure 4.18 shows the sites associated with the intermediate states calculated from the reweighted GaMD simulations.

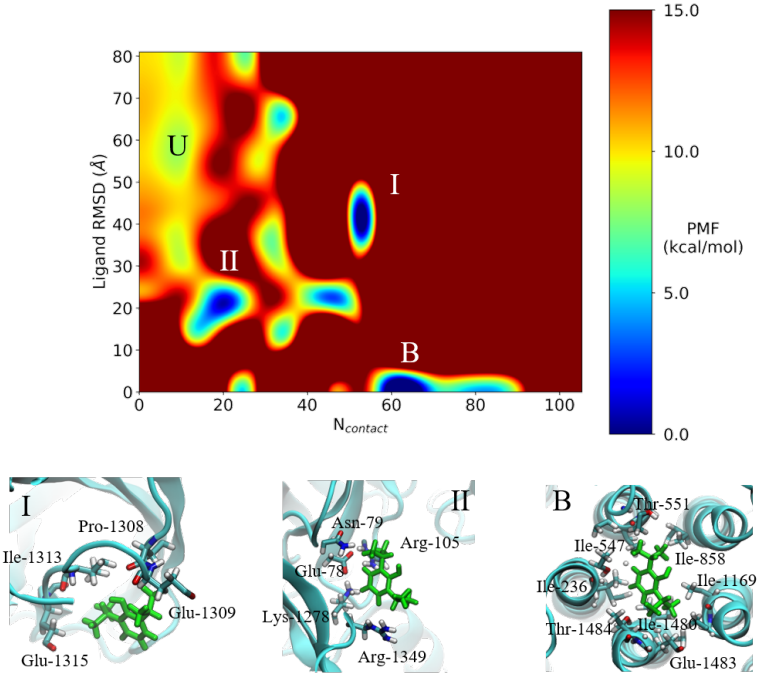

FIGURE 4.18: Graphical representations of the intermediate states of propofol (green) calculated from the reweighted GaMD simulations. Contact residues shown explicitly. Heat map reproduced from Figure 4.13.

The first intermediate state of the binding pathway is located in the β3 loop region at the top of the extracellular domain, where propofol forms short-lived hydrogen-bonds to the glutamic acid residues before moving to the next intermediate state. The next state is found between the β1-β2 loop and the β4-β5 loop in the inner region of the extracellular vestibule, where propofol remains bound for 36 ns before moving to the top of the ion conducting pore where it resides for the rest of the simulations.

Propofol molecules which were observed to bind close to the transmembrane intra-subunit anesthetic binding site showed some interesting dynamics within the binding site during the GaMD simulations, where the molecule would "jump" from one intra-subunit site to the adjacent intra-subunit site. The drug molecule would pass through a linking tunnel between the M3 helix of one subunit and the M1 helix of the adjacent subunit into an inter-subunit site initially, then into the intra-subunit site (Figure 4.19).

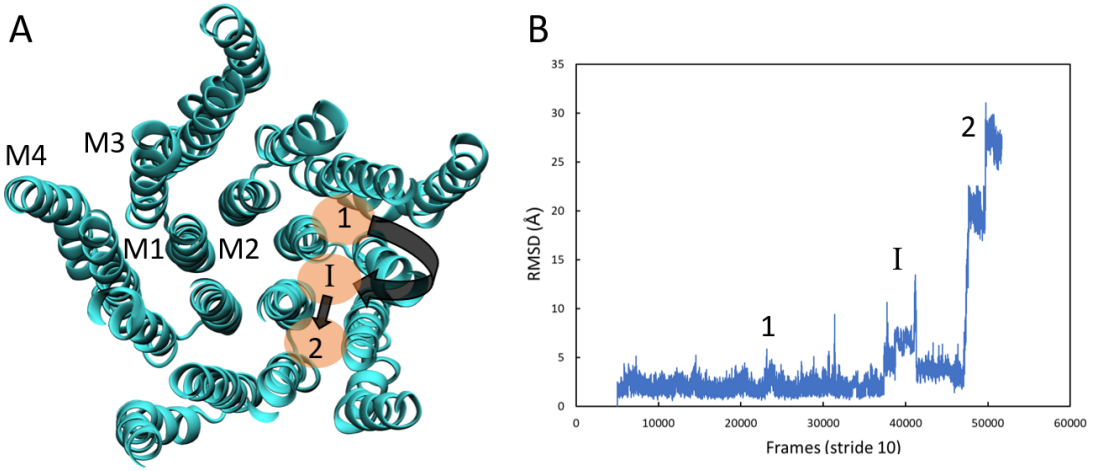

FIGURE 4.19: (A) Graphical representation of the propofol subunit jumping pathway in the TMD. (B) RMSD plot showing the change in position of propofol from the initial site (1) to the intermediate site (I) and then to the adjacent intra-subunit site (2). Reference for the RMSD calculation was taken from propofol in site 1. Data shown from one trajectory.

Multiple occupancy within transmembrane sites where up to three propofol molecules occupy the intra-subunit site was observed. This was initiated by small clusters

of propofol molecules which form within the lipid bilayer environment and then diffuse towards the TMD where they then bind to the helices. Fentanyl was not observed to bind within the M2 helix pore; I previously showed that fentanyl binds within a inter-subunit site in the extracellular region,[2] when propofol is not present. During the simulations I observed multiple sites where fentanyl and propofol share the same binding site, this was mostly observed in the extracellular domain during the flooding simulations (Figure 4.17). Multiple propofol molecules were seen to interact with a single fentanyl molecule in the extracellular domain, as this cluster of molecules moves towards the ion channel, the propofol molecules begin to separate from fentanyl and the remaining propofol molecule forms a stable hydrogen-bond with Asp-1418 located on loop C (Figure 4.20 C).

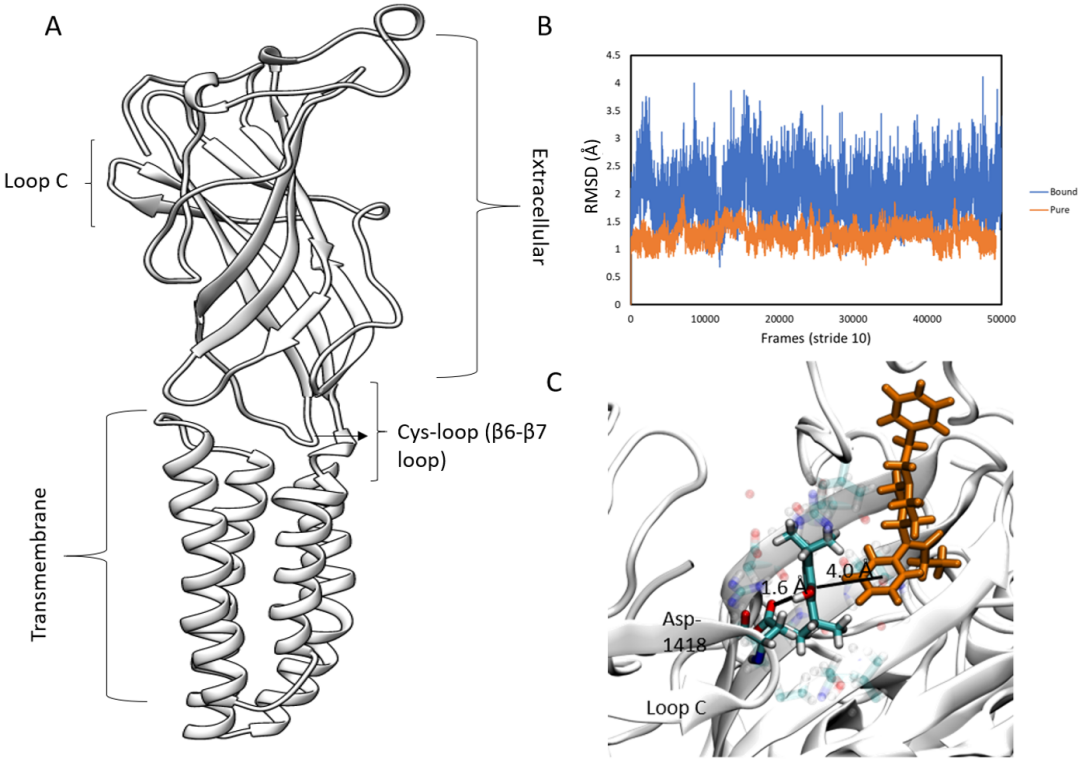

FIGURE 4.20: (A) Structure of one subunit highlighting key areas of the protein. (B) Cys-loop RMSD plot for pure and drug-bound systems. (C) π-π interaction of the fentanyl N-phenyl-propanamide ring and the propofol aromatic ring and the hydrogen-bond between propofol and Asp-1418 on loop C.

This hydrogen-bond remains stable for the majority of the simulations, where the fentanyl molecule, which I believe acts as a stabiliser for the bound propofol molecule which has an RMSD of 2.04 ± 0.4 Å. Table 4.2 shows the RMSD values for propofol when bound to Asp-1418, before and after the interaction with fentanyl. I can see that there is a stabilisation effect on propofol when the fentanyl molecule is present at the binding site. When I look at the flexibility of loop C, where propofol binds, I see that the flexibility is almost identical to the pure structure when fentanyl is present. When only one propofol molecule binds in this site, the flexibility of the binding region significantly increases. This shows that fentanyl not only stabilises the propofol molecule, but also a structurally important section of the GLIC extracellular region. The flexibility of the cys-loop (Figure 4.20) in the pure system and compared it to the systems in which propofol and fentanyl are bound. The cys-loop is thought to be a crucial component in the gating mechanism of pLGICs,[223–225] and my analysis clearly shows an increase in the cys-loop mobility (Figure 4.20 B) when the drugs are bound.

Region/molecule	RMSD (Å)
Propofol + Fentanyl[a]	2.04 ± 0.40
Propofol[a]	2.84 ± 0.44
Loop C (Pure)[b]	2.03 ± 0.17
Loop C (Propofol + Fentanyl)[a]	1.97 ± 0.36
Loop C (Propofol)[a]	3.41 ± 0.32

[a] Data averaged over flooding and GaMD trajectories where interaction was observed

[b] Data obtained from pure GLIC trajectory

TABLE 4.2: RMSD values for propofol binding to Asp-1418 with and without fentanyl, and loop C which Asp-1418 is part of

This shows that the combination of these drug molecules could play a role in the modulation of channel function. The backbone of fentanyl remains flexible throughout the simulations, but the N-phenyl-propanamide ring remains at an approximate 90 degree angle to the aromatic ring of the propofol molecule, forming a proposed π-π interaction to stabilise the propofol in this site. From the density

maps (Figure 4.17) I can see that there is many sites where there is overlap of the two drugs in both the extracellular and transmembrane domains. Within the TM domain I observed similar interactions as those shown in Figure 4.20 C, where fentanyl forms π-π interactions with propofol and holding it in specific sites. The TM sites where these interactions were observed were located near the bottom of the M2 helices, close to the head group region of the bilayer. The fentanyl molecules stabilise the propofol molecule in the lower M2 intra-subunit site before diffusing to the next subunit. This was observed in both the GaMD and flooding simulations.

4.2.4 Conclusions

In this study flooding style and Gaussian accelerated molecular dynamics simulations were used to study how the general anesthetic propofol and the opioid analgesic/anesthetic fentanyl interact with the GLIC protein and each other. The GaMD simulations reveal a detailed pathway for the pore blocking mechanism by propofol, which has not been observed previously when conventional MD simulations have been used. The GaMD simulations also showed that propofol can hop between TM intra-subunit binding sites by diffusing through a binding tunnel formed by helices of the occupied and adjacent TM subunits. Fentanyl was shown to play an important role in the stabilisation of propofol molecules in several binding sites. Initial interactions between fentanyl and propofol lead to the accurate mutation of a small number of propofol molecules with a fentanyl molecule. These small clusters either diffuse rapidly into the membrane environment and separate or diffuse towards the protein where the fentanyl molecule with interact with a propofol molecule and stabilise it in a binding site. The other propofol molecules move towards the extracellular domain of GLIC, binding close to the orthosteric agonist-binding site, where I again observed ligand stabilisation by fentanyl. These results show the first evidence of the opioid fentanyl interacting with, and altering,

propofol binding in GLIC. The structural results of propofol and fentanyl interacting at GLIC present a compelling case for the allosteric action of anesthetics and opioids at pLGICs.

Chapter 5

Fentanyl analogues

In this chapter, studies into how the analogues of fentanyl permeate phospholipid bilayers and interact with the *Gloeobacter violaceus* ion channel have been carried out using atomistic molecular dynamics simulations, and various free energy methods. The first part of this chapter will look at how accurately we can predict the membrane permeability coefficients for fentanyl and three of its analogues using simple membrane models and the umbrella sampling methodology. It was clear that good predictions can be made using this methodology and that the choice of phospholipid makes a significant difference to the results of these calculations. The ability to make accurate predictions of this fundamental pharmacological process, using simple models, for these opioid molecules is crucial for the future design of new drug molecules. The second part of this chapter focuses on how these molecules bind to, and modulate the function of the *Gloeobacter violaceus* ion channel. The simulations reveal that the analogues of fentanyl occupy a slightly different binding site to that which I have shown for fentanyl previously, but modulation of the channel function could still be observed.

5.1 Predicting the membrane permeability of fentanyl and its analogues

5.1.1 Introduction

As has been mentioned in previous chapters, there has been no widely accepted mechanism discovered which explains how fentanyl based opioids exert their anesthetic effect, even though it has been linked to direct binding with various membrane protein families, and interactions with lipid membranes which is commonly associated with inhalational anesthetics.[49,226] There was strong evidence, put forward by Stone et al,[227] which showed that the lipid membrane is a highly important piece of the puzzle in the opioid anesthesia process. What they found was a relation between the brain lipid membrane concentration of opiates with a defined minimum alveolar concentration (MAC) and electroencephalographic changes, which suggests a possible lipid membrane site for the anesthetic action of these types of drugs, at least up to the 50 % MAC reduction level. The relationship shown between the anesthetic effects and the membrane lipid component, as opposed to serum opioid levels, highlights the importance in studying opioid-lipid interactions which is lacking in the literature. The lipid membrane has been shown to be crucial for fentanyl binding to G-protein-coupled receptors; because od the high lipophilicity of fentanyl based drug molecules, the lipid membrane can act as a route for the drug molecules to bind to the transmembrane sites of the proteins.[228,229]

The lipid membrane is a highly complex environment which contains phospholipids, cholesterol, proteins and carbohydrates. It acts as a barrier to passive diffusion of small molecules, ions and water, although many small molecules, such as pharmaceuticals, can pass through the membrane. Fentanyl based drug molecules are lipophilic in nature, so they are expected to be able to enter the membrane environment with ease. In this section, four drug molecules are studied, that is, fentanyl, remifentanil, sufentanil and alfentanil (Figure 5.1) in four

simple model membrane bilayer systems, namely, 1-palmitoyl-2-oleoyl-glycero-3-phosphocholine (POPC), 1,2-dimyristoyl-snglycero-3-phosphocholine (DMPC), 1,2-dioleoyl-sn-glycero-3-phosphocholine (DOPC), and 1,2-dipalmitoyl-sn-glycero-3-phosphocholine (DPPC).

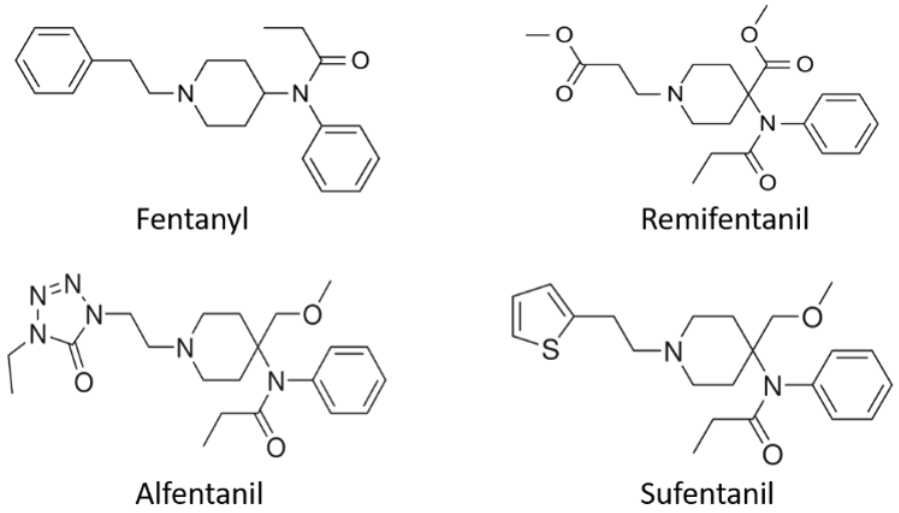

FIGURE 5.1: Chemical structures of the four drug molecules studied.

To try and model a "realistic" mammalian phospholipid membrane would require highly specific knowledge of which different lipids are present and at what concentrations they would be present at the system size used for the simulations, which is not available currently, there would also be no experimental results to compare against to see if the model was accurate. So instead of blindly constructing systems to try and claim they are more "realistic", I have chosen four lipids which have differing chain lengths and saturation to ascertain which model is best for predicting the permeability coefficients for these drug molecules.

Investigations into the permeation of drug molecules into the cell membrane are important to understand the delivery of drug molecules to their molecular targets. There are many experimental techniques which have been developed to investigate this property, such as parallel artificial permeability assay (PAMPA)[230] and cell-based CaCo-2 assay.[231] These methodologies are widely used throughout academia and industry to calculate the permeabilities of various types of compounds, but they are not able to provide any information on the biophysics of

membrane permeation.[232] Many linear response models and mathematical models, such as quantitative structure permeability relationship[233] and steady-state models,[234] have been developed to make predictions based on experimental test sets, but their performance has been relatively poor, and no detailed information can be obtained on the processes of permeation.[235] To gain atomistic insight into the passive permeation of fentanyl and its analogues, I have used fully atomistic molecular dynamics (MD) simulations in combination with the umbrella sampling technique and the weighted histogram analysis method (WHAM) to construct the potential of mean force (PMF) curves for the drug permeation. This section has two main goals: First I wish to ascertain whether this MD methodology can accurately predict permeability coefficients for fentanyl and its analogues using simple bilayer models, and second, I wish to determine if the lipid used in the model makes a difference to the permeability predictions and what lipid is most reliable for simulation of the systems.

5.1.2 Methods and theory

5.1.2.1 System preparation and simulation setup

All of the model membrane systems were constructed using the CHARMM-GUI membrane builder.[126] Each bilayer system contained 64 lipid molecules per leaflet with a water buffer of 35 Å on either side. The TIP3P water model[210] was used for all simulations along with the lipid14 parameters[109] for the lipids. The drug molecule parameters were generated using antechamber with the AM1-BCC charge model and the GAFF2 forcefield.[110] Pure membrane systems with no drug molecules were minimised and equilibrated in multiple stages. In stage 1, the system was minimised for 10,000 steps using the steepest descent method, the 10,000 steps using the conjugate gradient method. The systems were then heated initially to 100 K using a Langevin thermostat[129] with a 10 kcal/(mol Å^2) harmonic restraint applied to the lipid molecules. The systems were then heated to the desired production temperature (303 K for DOPC, POPC, and DMPC and

323 K for DPPC) for 100 ps. The equilibration stage involved slowly reducing the harmonic restraints to 0 over 10 ns of NPT simulation. 225 ns production runs were then carried out on all the pure membranes, which were then analysed to confirm if the models were in the correct, biologically relevant Lα phase. All of the simulations were carried out using the GPU enabled AMBER18 code. Three-dimensional periodic boundary conditions were used with the usual minimum image convention, and the SHAKE algorithm was used to constrain bonds involving hydrogen allowing for a 2 fs timestep. PME was used with a cutoff of 10 Å to treat the electrostatic interactions, and a long range analytical dispersion correction was applied to the pressure and energy. For the drug molecule simulations, the drug was added to the center of the bilayer, and a harmonic restraint of 10 kcal/(mol Å^2) was applied. A 10 ns simulation was carried out to equilibrate the lipid with the drug molecules. Steered MD simulations were used to pull each drug molecule through each bilayer into the water phase at a speed of 1.0 Å/ns (35 ns for each drug in each system). Coordinates of the system with the drug molecule at equally spaced locations over the pathway were extracted and used as starting states for the umbrella sampling simulations. Full profiles were obtained by symmetrizing the data as I am not using asymmetric or multicomponent bilayers, where it would be important to pull in both directions to study the differences between each leaflet.

5.1.2.2 Umbrella sampling simulation setup

The reaction coordinate for the drug permeation was defined as the z-component of the distance between the center of mass of the lipid nitrogen atoms and the heavy atoms in the drug molecules. For each drug in each bilayer, a total of 35 windows separated by 1.0 Å were used with a biasing harmonic restraint of 2.5 kcal/(mol Å^2) using the AMBER umbrella COM restraint code. Each window for each drug molecule was simulated for 100 ns, totalling 3.5 μs of sampling per drug molecule per bilayer, which totals 56 μs of sampling for all systems. The probability distributions obtained from these simulations were reweighted using the WHAM method. Umbrella sampling histograms were unbiased by the WHAM

with 720 bins and a tolerance of 1 x 10^{-8} for window offsets. The statistical uncertainty at each bin was estimated using bootstrapping, with 100 bootstrap trails for each PMF.

5.1.2.3 Umbrella sampling theory

Umbrella sampling[236,237] is an enhanced sampling method used in computational research to sample the conformational dynamics of a system along a reaction coordinate which allows the estimates of the relative free energy of different states along the defined reaction coordinate. A reaction coordinate (ξ) could be a kind of continuous parameter which could describe the system from a higher dimensional space. If the chosen reaction coordinate is suitable to differentiate distinct states, by biasing the system along this reaction coordinate, it is possible to calculate the free energy differences between the distinct states.

In the umbrella sampling methodology, multiple windows are set with initial structures with different reaction coordinate values. These windows can be created with steered molecular dynamics like is described in section 5.1.2.1 to create states within different parts of the bilayer. A bias potential is applied to each window according to a harmonic bias function. Therefore, the system in each window is constrained to sample a narrow phase space along the reaction coordinate to ensure potential energy distribution overlap between the adjacent windows. Once the simulations have been completed for all individual windows, a post-processing method, such as the weighted histogram analysis method, is required to recover the unbiased free energy profile.

When a reaction coordinate dependant bias potential $\omega_i(\xi)$ is added to the system in a window, the total biased energy can be expressed as:

$$E_{bias} = E_{unbiased} + \omega_i(\xi) \tag{5.1}$$

where i represents the ith window of the umbrella sampling. The harmonic bias potential which is added to the system is a simple bias potential expressed as:

$$\omega_i(\xi) = \frac{1}{2}K(\xi - \xi_i)^2 \tag{5.2}$$

Here ξ_i is used as a reference coordinate point. During the window simulations, if the system is escaping the reaction coordinate, then a bias potential is added to correct the system.

To calculate the unbiased free energy, the unbiased distribution of the reaction coordinate has to be found, this can be done according to the following equation:

$$P_i^u(\xi) = \frac{\int exp[-\beta E(r)]\delta[\xi^r(r) - \xi]d^{N_r}}{\int exp[-\beta E(r)]d^{N_r}} \tag{5.3}$$

Furthermore, the unbiased probability $P_i^u(\xi)$ could be determined by:

$$P_i^u(\xi) = P_i^b(\xi)exp[\beta\omega_i(\xi)]exp[-\beta\omega(\xi)] \tag{5.4}$$

From the simulations in each umbrella sampling window, the biased probability $P_i^b(\xi)$ is known, and the free energy of each window could thus be found by:

$$E_{unbiased} = -\left(\frac{1}{\beta}\right) ln\ P_i^b(\xi) - \omega_i(\xi) + F_i \tag{5.5}$$

where F_i is a constant which could be solved by self-iteration until convergence is reached.

The local diffusivity for each window can also be estimated using the Hummer positional autocorrelation extension to the Woolf-Roux estimator:

$$D(z) = \frac{\langle \delta Z^2 \rangle^2}{\int_0^\infty \langle \delta Z(t)\delta Z(0) \rangle dt} \tag{5.6}$$

where δZ(t) = z(t) - $\langle$Z$\rangle$ and Z is a position on the z-axis and z(t) is a position on the z-axis at time t. The obtained PMF from the umbrella sampling and D(Z) values were interpolated at 1.0 Å intervals, and the results can be used to calculate

the resistivity (R) and permeability (P) by:

$$R = \frac{1}{P} = \int_{Z_1}^{Z_2} \frac{exp[\beta W(z)]}{D(z)}\, dz \tag{5.7}$$

where $\beta = 1/k_B T$ and z is the position of the drug molecule along the transmembrane axis, and W(z) is the PMF. The lower and upper integration bounds are points in the center of the membrane and water phase.

5.1.3 Results and discussion

The free energy profiles for the four fentanyl analogue drug molecules permeating into the DOPC, DPPC, DMPC and POPC bilayers are shown in Figure 5.2.

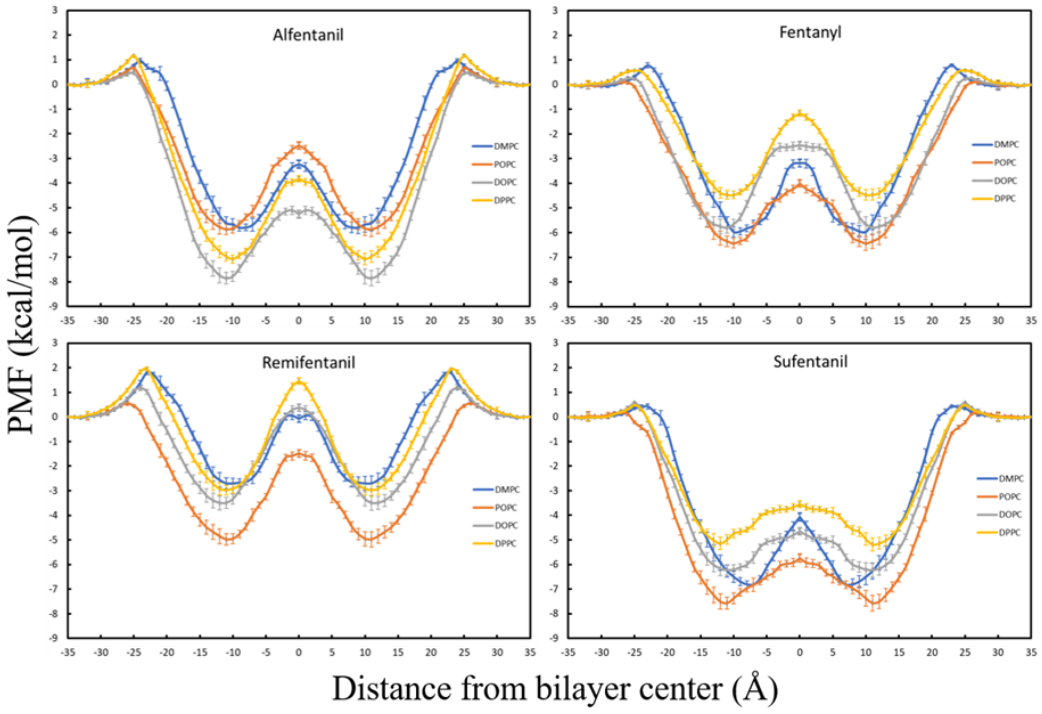

FIGURE 5.2: Free energy profiles calculated for all four drug molecules in all four bilayers

All of these fentanyl based opioid molecules are hydrophobic in nature, to varying extents, but I can see in the PMF profiles the expected behaviour of these molecules

due to their inherent hydrophobicity. There is a small positive energetic barrier, the largest being 1.94 ± 0.10 kcal/mol for remifentanil in the DPPC bilayer, when the drug molecules permeate into the hydrophilic phosphatidylcholine head group region of the bilayer, followed by a global minimum within the interior of the bilayer, with the lowest being observed at -7.86 ± 0.24 kcal/mol for alfentanil in the DOPC bilayer.

To understand the shape and positions of the minima in the calculated PMF profiles, the four-region model can be utilised.[238,239] The different regions of the membrane systems were defined as follows:

Region 1, which is the region of low head group density in the water phase at the entry into the membrane;

Region 2, which is the region of high phosphatidylcholine head group density;

Region 3, which is the region of high tail carbonyl group density; and

Region 4, which is the region of low-density acyl chains.

Using this model, region 3 is from 6 to 13 Å from the bilayer center is the high tail carbonyl chain group density region in the upper parts of the acyl chains. Hydrophobic molecules will form many favourable hydrophobic interactions with the lipid tails in this region, so the difference in free energy here can be explained by the formation of many favourable interactions between the drug molecules and the lipid tails. The barrier which can be observed at the center of the bilayers for all drug molecules could be a consequence of entropic factors, such as a reduction in the mobility of the lipid tails when the drug molecule is present. However, the more likely explanation is the reduction in the number of drug-lipid interactions at the center of the bilayer, because of a lower density of atoms in this region, where the lower interaction energies would therefore disfavour the presence of the

drug molecule in this region. This has previously been shown to be the main factor for the local anesthetic, benzocaine, and the antiepileptic drug, phenytoin.[240] The small variations in the shape of the PMF profiles between certain drug/lipid combinations is due to the diversity in the structure and properties of each drug molecule and the differences in the structure of the lipid chains. The different packing arrangements and dynamics of each chain will lead to different interactions with each drug molecule and hence slight changes in the PMF shape.

From the PMF profiles, it can be clearly seen that even though all systems have the same phosphatidylcholine head group, the difference in the tails clearly alter the permeation process. When the trajectories of the umbrella sampling windows were visually inspected, differences in the mobility of the head groups were observed due to the different structures of the lipid tails causing local rearrangements to the extent that exposure of the drug molecule to the tail regions varies. Water molecules were observed entering the through the head group into the hydrophobic region with both alfentanil and remifentanil, which stabilises these molecules through the formation of hydrogen bonds and accounts for the observed energetic barriers (Figure 5.3). These two analogues have the most hydrogen-bond acceptor sites, and hence they interact with more water molecules than sufentanil and fentanyl. Hydrogen bonding-plots (Figure 5.3 B and C) confirm that more water molecules are bound to both remifentanil and alfentanil in the head group/hydrophobic interface region, where the data was taken from. I should also note that the extent of sampling was greater here than in many other studies of solute permeation, hence it is therefore more likely to observe rearrangements that are not achievable in shorter simulations.

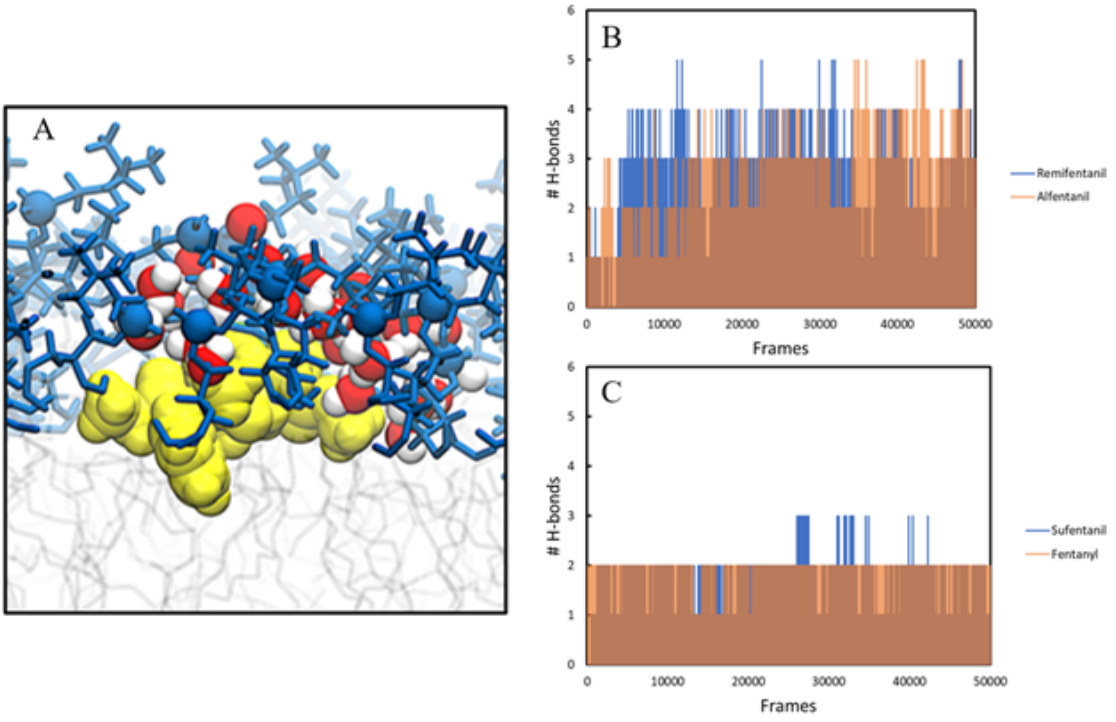

FIGURE 5.3: (A) Water molecules solvating remifentanil (yellow) at the head group/hydrophobic interface (blue). (B) Hydrogen-bond plot for remifentanil and alfentanil. (C) Hydrogen-bond plot for sufentanil and fentanyl. Hydrogen-bonding data was calculated in the 21-25 Å windows, where energetic barriers were observed and averaged for each drug molecule.

The position-dependent diffusion coefficients for the drug molecules do not vary significantly form each other (Figure 5.4). The average diffusion within the hydrophobic part of the membrane (z = -20 to 20 Å) for the drug molecules range from $\sim$ 1 x 10^{-6} to $\sim$ 2 x 10^{-6} cm^2/s. Within the core of the bilayer, the values for the diffusion coefficients for the drug molecules plateau at their minimum values at $z \approx$ 5 - 10 Å , but slightly increase as the drug molecule approaches the center of the bilayer (z = 0 Å), which is the most disordered area of the hydrophobic region of the membrane. All of the drug molecules show an increase in diffusion coefficient in the aqueous phase outside of the membrane that is close to an order of magnitude greater than the values obtained at the membrane core. This observation is consistent with previous biased MD simulation studies of drug molecules passing through lipid bilayers,[241] and the results obtained for these molecules are as expected for lipophilic drug molecules.

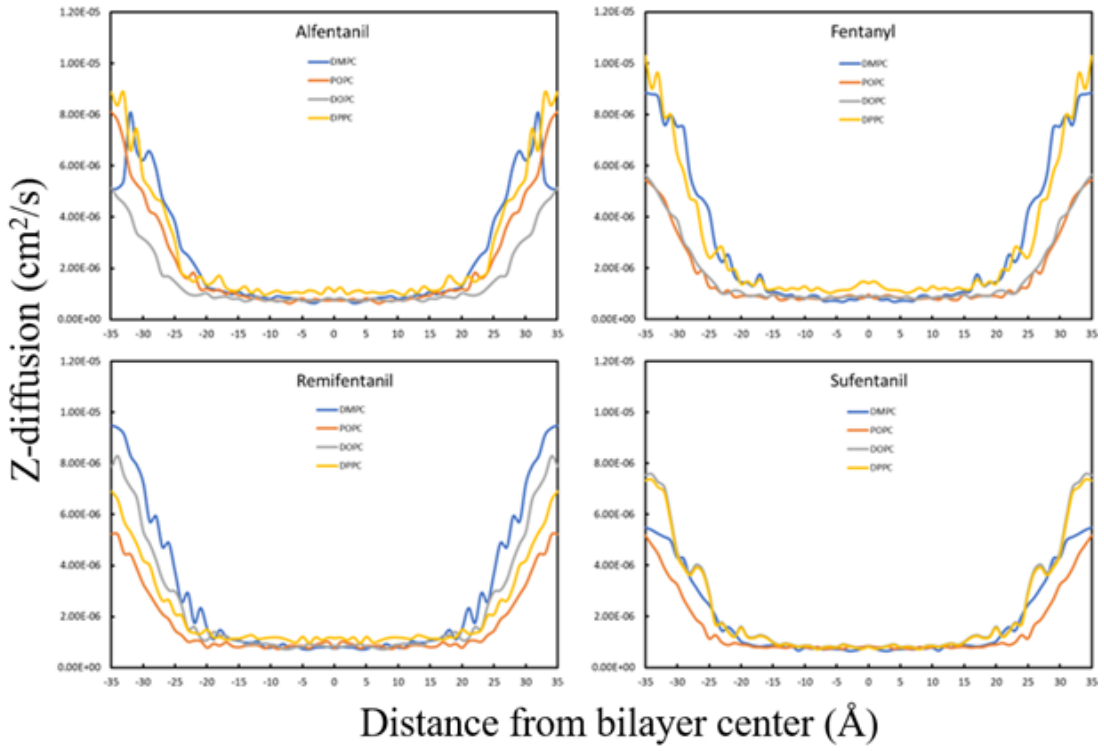

FIGURE 5.4: z-diffusion profiles calculated for all drug molecules in all bilayers.

Resistance to permeation profiles were calculated for each drug molecule in each bilayer, (Figure 5.5). As stated previously, fentanyl and its analogues are lipophilic drugs, and I would therefore expect the largest resistance to permeation to occur at the lipid-water interface, which is what I can see from the plots. The head group region of the membrane is polar and partially charged, which for hydrophobic molecules offers the largest resistance to permeation. The resistance plots follow the free energy profiles for all of the drug molecules, shown particularly clearly for remifentanil. This good agreement between resistance and free energy profiles is expected, and seeing this is therefore important for the validation of the simulations and methodology. The resistance increases steeply as the molecules pass through the head group region and again increase slightly at the disordered center of the bilayer, indicating that the resistance is dominated by the free energy component. This behaviour shows that higher free energy contributions lead to higher resistance to permeation for fentanyl-based opioids.

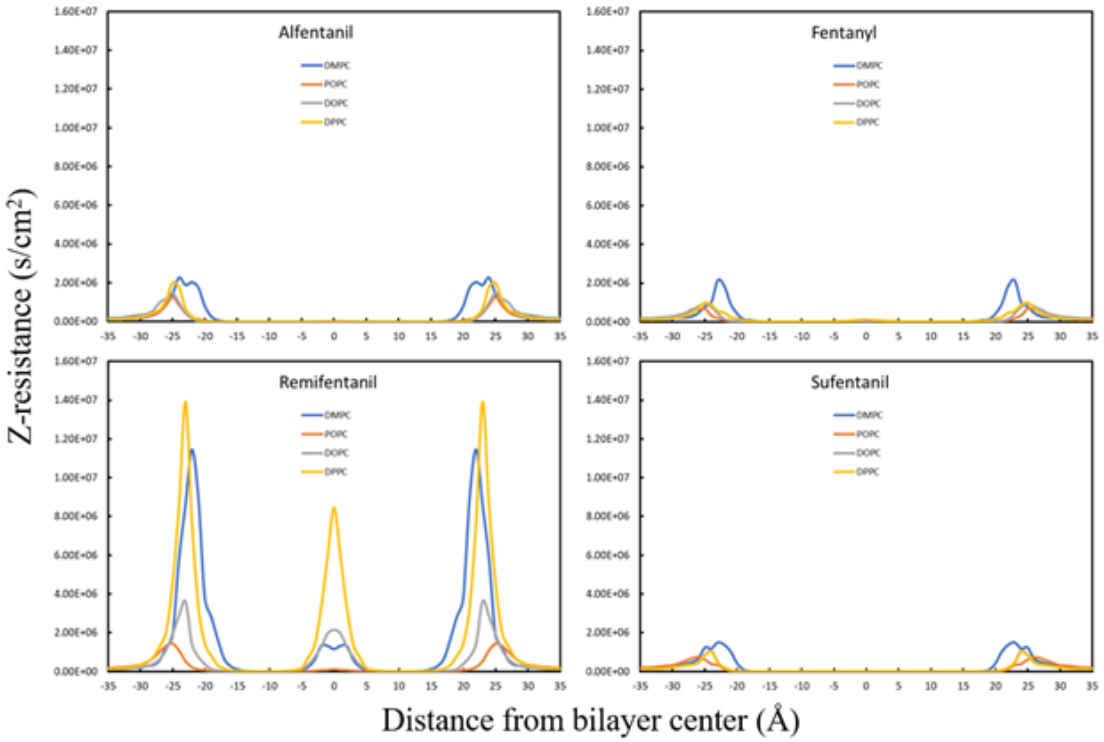

FIGURE 5.5: Resistance to permeation calculated for each drug molecule in each bilayer.

The calculated permeability coefficients calculated from the simulations are presented in Table 5.1 along with the experimentally determined permeability coefficients from a variety of different experimental techniques. It is clear from the calculated results that the umbrella sampling method that was used here can predict the correct trend in permeability coefficients for these fentanyl based drug molecules. The main experimental techniques that are used in both academic and industrial pharmaceutical research to calculate permeability coefficients for drug molecules are PAMPA, BBB-PAMPA (blood-brain barrier), and Caco-2 methods, and the data in Table 5.1 show that the simulations can produce results that compare well with the available experimental values.

Drug	Calculated permeability coefficient (cm/s)	Experimental permeability coefficient (cm/s)
alfentanil	-6.49 (DOPC) -6.15 (DPPC) -8.35 (POPC) -3.73 (DMPC)	-0.06 (porcine polar brain lipid)[242] -2.11 (microvessel lipid)[242] -2.88 (microvessel lipid + cholesterol)[242] -1.75 (dodecane)[242] -4.42 (spinal meninges)[243] -3.53 (PAMPA)[244] -3.49 (Caco-2)[244] -3.54 (Caco-2/MDCK)[245]
fentanyl	-8.67 (DOPC) -8.12 (DPPC) -10.94 (POPC) -5.42 (DMPC)	-2.31 (porcine polar brain lipid)[242] -2.48 (microvessel lipid)[242] -3.60 (microvessel lipid + cholesterol)[242] -4.81 (spinal meninges)[243] -4.32 (BBB-PAMPA)[246] -5.81 (human skin)[247] -6.16 (PAMPA)[248] -4.89 (human skin)[249] -3.22 (BBB-PAMPA)[245]
sufentanil	-10.09 (DOPC) -8.09 (DPPC) -9.33 (POPC) -5.00 (DMPC)	-3.15 (porcine polar brain lipid)[242] -2.69 (microvessel lipid)[242] -2.78 (microvessel lipid + cholesterol)[242] -3.57 (dodecane)[242] -4.90 (spinal meninges)[243] -5.48 (human skin)[247] -4.84 (human skin)[249] -3.87 (BBB-PAMPA)[250]
remifentanil	-2.49 (DOPC) -0.80 (DPPC) -5.81 (POPC) -0.93 (DMPC)	-0.33 (porcine polar brain lipid)[242] -2.49 (microvessel lipid)[242] -2.40 (microvessel lipid + cholesterol)[242] -3.76 (dodecane)[242]

TABLE 5.1: Calculated and experimentally determined permeability coefficients for fentanyl and the analogues studied

The simulation results compare very well with the experimental values for alfentanil (-3.73 (DMPC), -3.53 (PAMPA), -3.49 (Caco-2), -3.54 (Caco-2/MDCK)), fentanyl (-5.42 (DMPC), -4.32 (BBB-PAMPA), -6.16 (PAMPA)), and sufentanil (-5.00 (DMPC), -3.87 (BBB-PAMPA)). The results for remifentanil agree less well with the available data in the literature because of the uncertainty in the charge state of the drug molecule due to its susceptibility to hydrolysis. Remifentanil was modelled in its neutral phase, which is its expected state in the studies for which experimental data is available. I also see fairly good comparisons between the calculated results and other experimental techniques, for example, from spinal meninges and human skin. This is unexpected as the models to try and mimic these systems would normally include cholesterol at varying concentrations and other lipids, whereas I can see good correlation with the simple bilayer models using a large amount of sampling. It has previously been shown that inadequate sampling leads to inaccurate free energies, which can lead to an order of magnitude of difference in permeability owing to exponential dependence.[251,252] If cholesterol was added to the systems, it would be expected that the lipid tails would become more ordered due to the favourable van der Waals interactions that would be formed between the cholesterol and the lipid tails. Thus, when the drug molecule is added to the system, strong van der Waals contacts would be disrupted which would cause large voids around the drug molecule. A previous experimental study[253] looked into this and found that the addition of cholesterol into a DMPC bilayer caused an increase in the hydrophobicity of the bilayer center, which in turn caused a large hydrophobic barrier to the permeation of polar molecules. With regard to the fentanyl based opioid molecules which are hydrophobic in nature, high concentrations of cholesterol could cause an increase in the barrier and decrease their permeability, which has been shown to occur for other hydrophobic drug molecules.[254] Obtaining good comparisons with spinal meninges and human skin comparisons are important for research into opioid pharmacology, as these drugs are often administered though transdermal patches as analgesics for various chronic conditions and as epidural anesthetics. Different routes of administration will lead to slightly different mechanisms of action, and understanding as many of

these as possible is vital for the design of safer pharmaceuticals. The differences in permeability obtained in each bilayer system show that basic dynamical and strucutral properties of simple single component bilayers can cause a significant impact on the membrane permeability of these drug molecules. The systems which contain the shorter, full saturated tails give the best comparisons, which suggests that the higher degree of lipid tail packing in saturated lipids are an important factor for drug permeability. The results obtained from the simulations suggest that the DMPC lipid bilayer is best suited for the prediction of permeability coefficients for these drug molecules as it gives the best comparisons to the available experimental data, which is an important finding as many studies only utilise one model bilayer to make predictions, which could introduce large errors into the results that the simulations produce. The results obtained from the simulations suggest that the testing of multiple bilayers in simulation studies is a more thorough procedure and, where possible, should be carried out to find the best model bilayer for the target drug molecule which will lead to more consistent results that minimise errors when comparing simulated results to experimental data.

5.1.4 Conclusions

In this section, extensive umbrella sampling simulations of fentanyl and three of its analogues in four different simple phospholipid bilayers were performed to calculate their membrane permeability coefficients and determine which bilayer provides the most accurate results compared to available experimental data. The simulations showed that for all four drug molecules, the main resistance to permeation was observed to occur at the lipid head group interface because of its partially charged, polar nature and the hydrophobic nature of the drug molecules. The simulations were able to identify the DMPC bilayer system as the most reliable one to to use in the simulation of these drug molecules as the results compared best with the literature values from PAMPA and Caco-2 methods which are most used in pharmaceutical research. Using the umbrella sampling methodology, properties such as free energy, local resistance and diffusion can be calculated for the drug

molecules in atomic-level detail in all regions of the system, and produce accurate permeability coefficients. This methodology could therefore be of importance in the future design of new fentanyl-derived anesthetic/analgesic drugs.

5.2 Interactions between fentanyl analogues and the *Gloeobacter violaceus* ion channel

In this chapter, studies into the interactions between the three fentanyl analogues and the *Gloeobacter violaceus* have been investigated using atomistic molecular dynamics simulations and efficient end-state free energy calculations. I have previously shown that fentanyl binds to in a site located approximately 9 Å below the orthosteric agonist-binding site, and that binding within this site causes conformational changes in the protein structure, which causes the formation of a hydrophobic gate blocking the conductance of ions from the extracellular region to the intracellular region.[2] This behaviour was very similar to that which has been observed for the analgesic/anesthetic drug ketamine when it binds in this site. Studying how the different analogues of fentanyl interact with this channel will lead to a greater understanding about the different clinical effects observed when these analogues are used. It was found that these analogues bound within an intersubunit site located in "β-sandwich" region of one subunit and above the β9-β10 loop (loop C) of the adjacent subunit. Discovering different binding sites for these types of drug molecules will be very useful for the future design of opioid-based drugs.

5.2.1 Introduction

Since the discovery of fentanyl which was shown to be around 100 times more potent than morphine, it has been routinely used in general surgery for pain management in the general anesthesia process and as a pure anesthetic. The mechanisms by which fentanyl exerts in anesthetic properties is not understood. Fentanyl has been shown to act at G-protein coupled receptors[255] and various ion channels, such as voltage-operated sodium channels,[256] Ca^{2+} channels,[257] hERG potassium channel,[258] and the *Gloeobacter violaceus* ion channel.[2] Since various examples have been shown of molecules which possess anesthetic properties acting on ion channel proteins and modulating their function, they are currently the prime target for investigations into mechanisms of general anesthesia.

Various fentanyl analogues have been developed which have different pharmacological properties. The most commonly used fentanyl analogues are alfentanil, remifentanil and sufentanil which are studied in this work (Figure 5.1). Another analogue named carfentanil which has been developed is around 100 times more potent than fentanyl and is used in veterinary medicine to anaesthetise large animals. There is also concerns over its use as a drug of abuse and as a chemical weapon.[259]

Alfentanil is a synthetic opioid analgesic/anesthetic which was derived from fentanyl. It is very widely used as the analgesic component in the general anesthesia process, or as a primary anesthetic when used in very high dosages during cardiac surgery. Compared to other anesthetics like fentanyl and sufentanil, alfentanil is the least potent with a potency of around a quarter of that of fentanyl. Alfentanil has the fastest onset of action and the shortest duration of action so is therefore often chosen for use in short procedures or procedures in which rapid changes in the level of consciousness is necessary.[260]

Sufentanil is another synthetic opioid analgesic/anesthetic which has actions and therapeutic effects that are similar to those seen for fentanyl. Sufentanil is around 5 to 10 times more potent than fentanyl and is the most potent opioid which is

used in clinical practice.[261] Sufentanil differs from fentanyl through the addition of a methoxymethyl group on the piperidine ring which is believed to increase the potency and reduce its duration of action,[262] and the phenyl ring is replaced with a thiophene. Sufentanil is highly lipid soluble which allows it to rapidly cross the blood-brain barrier which increases its onset of action time slightly when compared to fentanyl.[263]

Remifentanil is the most recently developed synthetic opioid analgesic/anesthetic which is studied here. Remifentanil is similar to fentanyl in terms of potency and has a very short duration of action. Remifentanil is a derivative of fentanyl that contains an ester linkage to propanoic acid with gives it a very unique pharmacokinetic profile. The presence of this ester linkage allows remifentanil to be rapidly and extensively metabolised by non-specific blood and tissue esterases. The metabolites are very easily eliminated in the urine which gives a low terminal elimination half-life. These properties therefore allow high dose opioid anesthesia to be performed with continuous infusion. The recovery profile from remifentanil anesthesia has also been shown to be highly favourable.[264]

The discovery of high resolution crystal structures of the *Gloeobacter violaceus* ion channel allows a valuable opportunity to study the modulation of pLGICs at the atomic level. This channel was chosen based on the evidence from other studies which show that anesthetics can bind in various sites (Figure 5.6) and alter the state of the ion channel. I was also able to show that fentanyl can bind to and modulate the function of this channel[2] so by studying the binding of the analogues here, I will be able to see potential differences in binding site and changes to the protein structure and function.

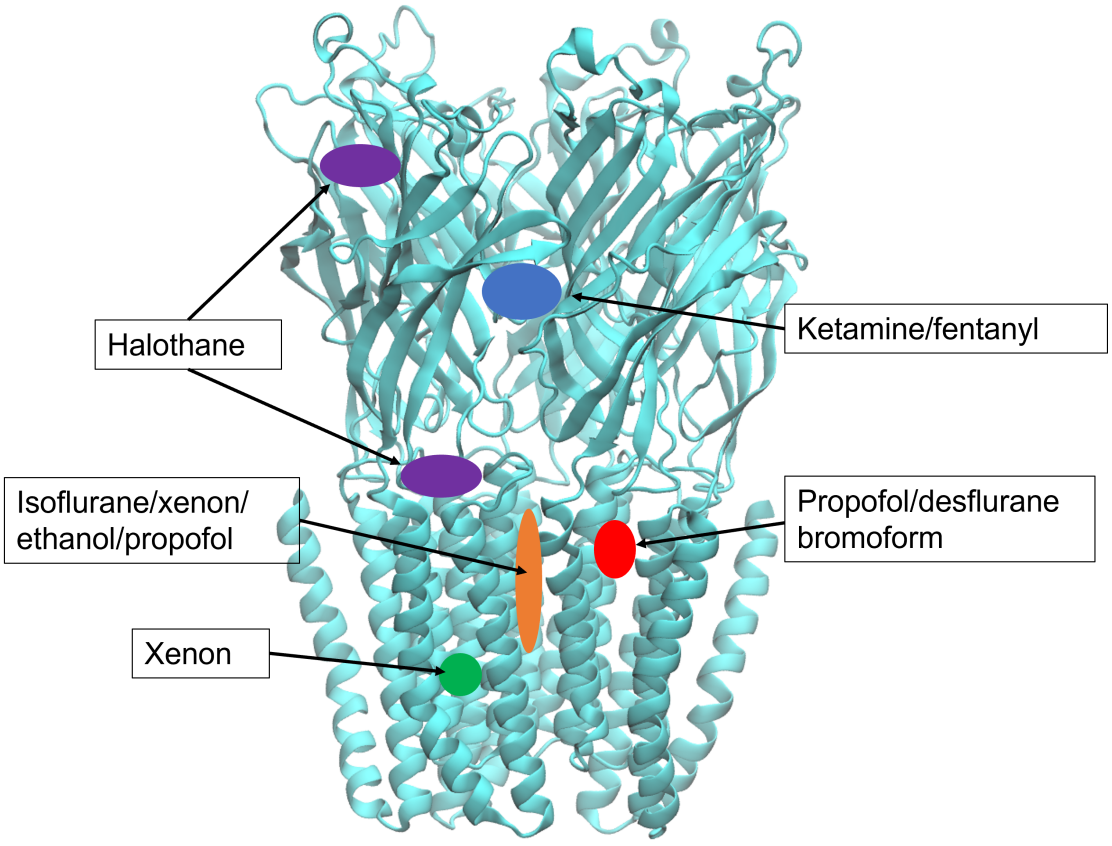

FIGURE 5.6: Binding sites found on the GLIC structure for various anesthetics using experimental and computational methods

Atomistic molecular dynamics simulations in combination with efficient end-state free energy reveal a novel extracellular intersubunit site in which these analogues bind. The strength of binding within this site is weaker for the analogues compared to fentanyl in its site. Binding of these drug molecules in this site cause conformational changes in the protein which cause channel closure and strucutral changes in the extracellular domain.

5.3 Methods and theory

5.3.1 General simulation protocol

All simulations performed here were carried out using the CUDA enabled Amber18 molecular dynamics package on NVIDIA tesla V100 gpu cards. The ff14SB forcefield[108] was used to describe the ion channel protein, the lipid14 forcefield[109] was used to describe the DOPC lipids which form the bilayer and the GAFF2 forcefield[110] was used to describe the fentanyl analogue molecules. The TIP3P water model[107] was used to describe the explicit water molecules and ions. The simulations were performed at a constant pressure of 1.0 atm and was maintained using the anisotropic Berendsen method with a pressure relaxation time of 1.0 ps. The temperature was maintained at 303.15 K using the Langevin thermostat with a collision frequency of $\gamma = 1.0$ ps^{-1}. Three dimensional periodic boundary conditions with the usual minimum image convention were used. The SHAKE algorithm was used to constrain covalent bonds to hydrogen, allowing the use of a 2 fs timestep. Electrostatic interactions were treated with the PME method using a cutoff of 10 Å. Snapshots were taken every frame for the MM-PBSA calculations.

5.3.2 System set up

The high resolution crystal structure of GLIC in the open state (4HFI)[165] was inserted into a DOPC lipid bilayer which was composed of 157 lipids in the lower leaflet and 150 lipids in the upper leaflet. The system was solvated with 150 mM NaCl aqueous solution giving a system of approximately 232,000 atoms and dimensions of approximately 130 x 130 x 180 Å^3. The set up for this system was performed using the CHARMM-GUI webserver.[126] Protonation states were assigned using PDB2PQR[265] and PROPKA.[266]. Four fentanyl analogue molecules were added to the solvent phase using the gmx insert-molecules tool included with the Gromacs 2018.2 package.

5.3.3 System equilibration

The systems were initially minimised for 10000 steps with the steepest decent method and then 10000 steps with the conjugate gradient method. The equilibration procedure was carried in 6 steps. Step 1 was carried out for 250 ps in the NVT ensemble with 10.0 kcal/(mol Å^2) restraints applied to the protein, membrane and drug molecules. Step 2 was carried out for 250 ps in the NVT ensemble with 5.0 kcal/(mol Å^2) restraints on the protein and membrane atoms and 10.0 kcal/(mol Å^2) restraints on the drug molecules. Step 3 was carried out for 250 ps in the NPT ensemble with 2.50 kcal/(mol Å^2) restraints on the protein and membrane atoms and 10.0 kcal/(mol Å^2) restraints on the drug molecules. Step 4 was carried out for 1000 ps in the NPT ensemble with 1.0 kcal/(mol Å^2) restraints on the protein and membrane atoms and 10.0 kcal/(mol Å^2) restraints on the drug molecules. Step 5 was carried out for 1000 ps in the NPT ensemble with 0.5 kcal/(mol Å^2) restraints on the protein and membrane atoms and 10.0 kcal/(mol Å^2) restraints on the drug molecules. Step 6 was carried out for 10000 ps in the NPT ensemble with no restraints on the protein and membrane atoms and 10.0 kcal/(mol Å^2) restraints on the drug molecules. Fully unrestrained production runs were carried out for 1 μs for 3 replicates for each system.

5.3.4 MM-PBSA

The underlying theory of the MM-PBSA free energy method can be found in section 4.1.2. In this study, a ligand, receptor and complex ensemble were extracted from a single MD trajectory of the bound complex which is referred to as the single trajectory protocol (STP). This method is less computationally expensive compared to the multiple trajectory protocol and the internal potential terms cancel out exactly which leads to lower fluctuations and faster convergence. The MMPBSA.py.MPI script was used for these calculations which is available in the AMBER18 package. Ionic strength was set to 0.15 M, external dielectric constant was set to 80.0, internal dielectric constant was set to 1.0, cavity surface

tension was left at the default value of 0.0378 kcal/mol Å^2, cavity offset was left at the default value of -0.5692, fill ratio was set at 4.0, the resolution of the Poisson Boltzmann grid was set at 2.0, solvent probe radius was set at 1.4 Å and the atomic radii was set according to the prmtop.

5.4 Results and discussion

Three simulations of 1 μs were initially conducted on the pure GLIC structure in the DOPC lipid bilayer to assess the systems stability, and to obtain strucutral information on the protein structure which could be used as comparisons for the drug containing systems. The backbone RMSD was calculated for the pure GLIC system as an indicator of the protein stability within the membrane, over the course of the 3 μs simulation time, the protein RMSD was calculated as 2.23 $\pm$ 0.53 Å which indicates good stability. Visual inspections showed that the protein also remained stable in its position and did not drift or tilt within the membrane and no other anomalies were observed.

The simulations carried out on the systems containing the fentanyl analogues showed the drug molecules forming short-lived, non-specific interactions with the the protein exterior and penetrating into the membrane in which they remain for the majority of the simulations, this is expected behaviour due to the lipophilicity of the drug molecules.[267] It was however observed that a molecule of each analogue was seen to bind for a long period of time in a site located in the extracellular domain in multiple simulation replicates (Figure 5.7).

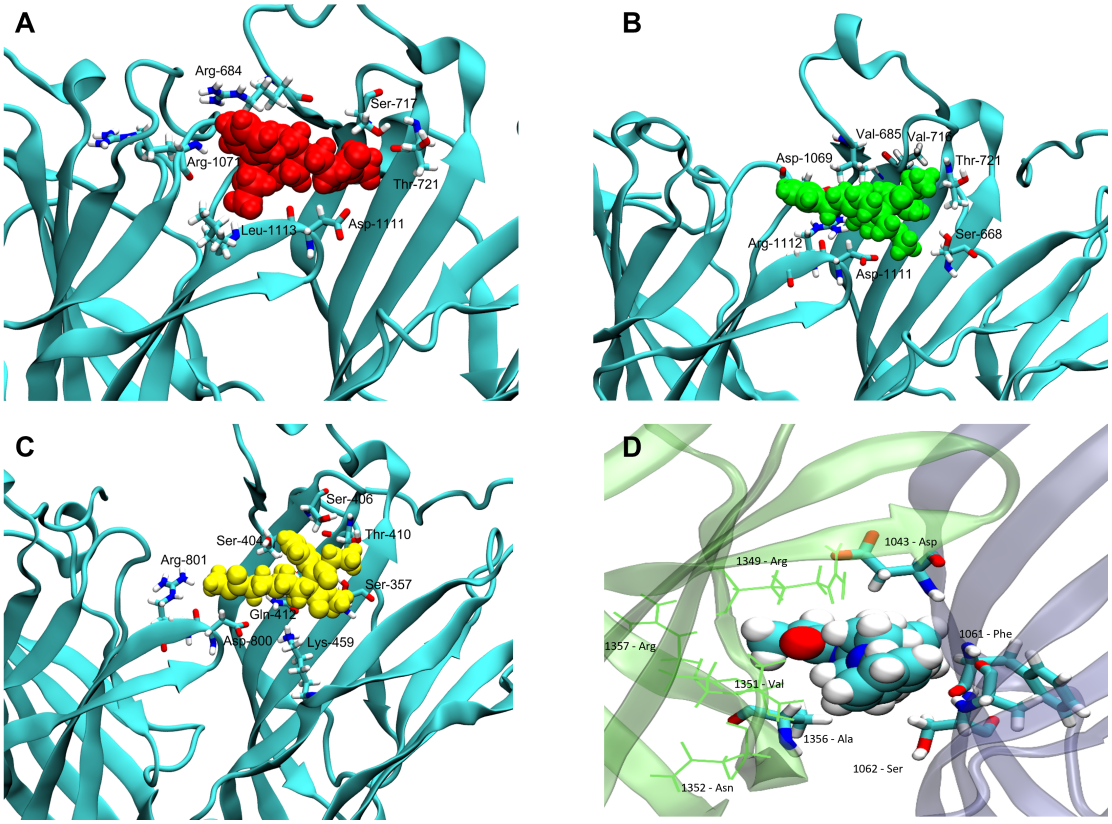

FIGURE 5.7: Detailed view of the alfentanil (A), remifentanil (B) and sufentanil (C) binding sites. (D) The fentanyl binding site[2] is shown for reference. The drug molecules are shown in VdW sphere representation with binding residues shown in licorice representation

This binding site is located between two subunits in the extracellular domain much like the site that was found for fentanyl in Section 4.1.3. That site was located approximately 9 Å below the orthosteric-agonist binding site which is not what I observed for the analogues. The analogue binding site located approximately 6 Å to the upper right of the orthosteric-agonist site in the "β-sandwich" region with interacting residues also from the upper loop region and loop C. All of the analogues entered this site directly from the solvent with no diffusion into the channel. Alfentanil initially bound in this site after $\sim$ 550 ns of the simulation and left the site after $\sim$ 900 ns. After alfentanil left the site, it re-entered and exited multiple times until the end of the simulation but did not transition into the fentanyl site. Remifentanil bound within this site after $\sim$ 190 ns and left the

site after $\sim$ 950 ns where it remained in the solvent until the end of the simulation. Sufentanil entered the binding site after $\sim$ 330 ns and unbound after $\sim$ 831 ns where it diffused into the membrane environment. The drug molecules remained fairly stable in this site with RMSDs of around 2 to 2.5Å for all bound drug molecules.

To ascertain whether the binding of the analogues had any affect on the structure of the β-sandwich region, secondary structure calculations were carried out on the whole of that region (Figure 5.8).

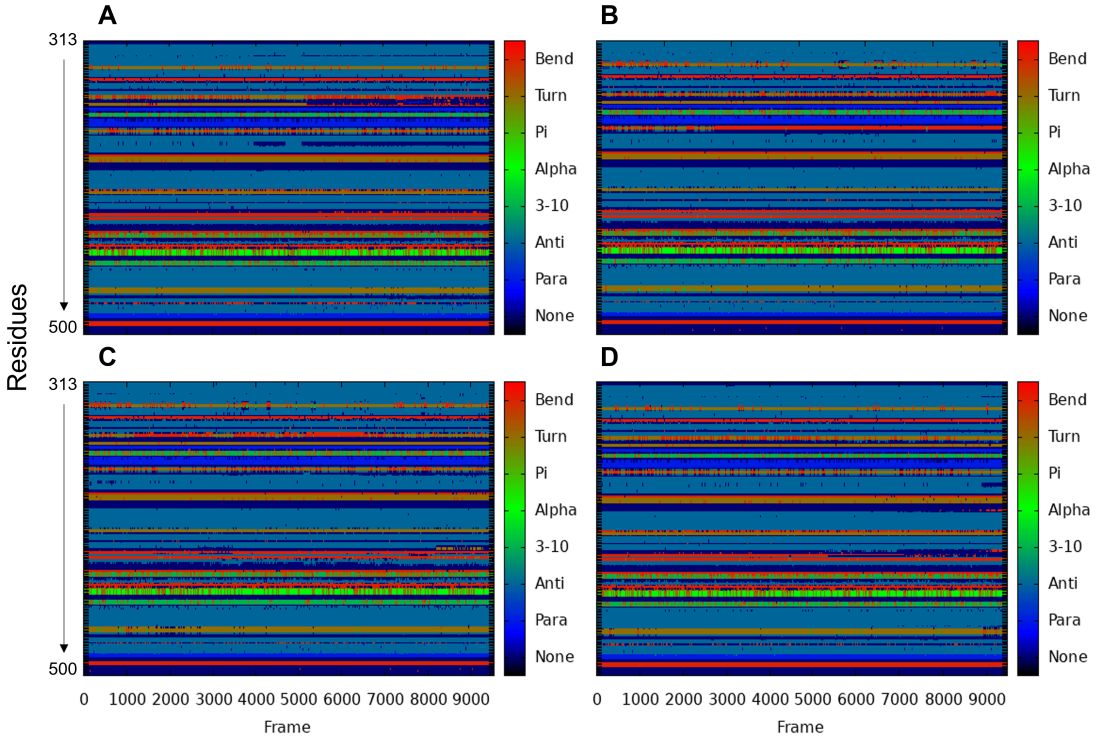

FIGURE 5.8: Secondary structure of the β-sandwich region for (A) the pure system, (B) the sufentanil system, the alfentanil system and the remifentanil system

The secondary structure calculations show that the binding of the analogues in this region does not affect the anti-parallel and parallel beta sheets in any appreciable way. There are small changes seen in areas with bends changing to turns but these areas are highly flexible and any small changes cannot be attributed to the binding of the drug molecules. The drug molecules also interact with loop C which forms

the top of the fentanyl binding site, RMSD calculations show that the binding of the analogues in the site to the upper right of loop C cause destabilisation of the loop (Figure 5.9).

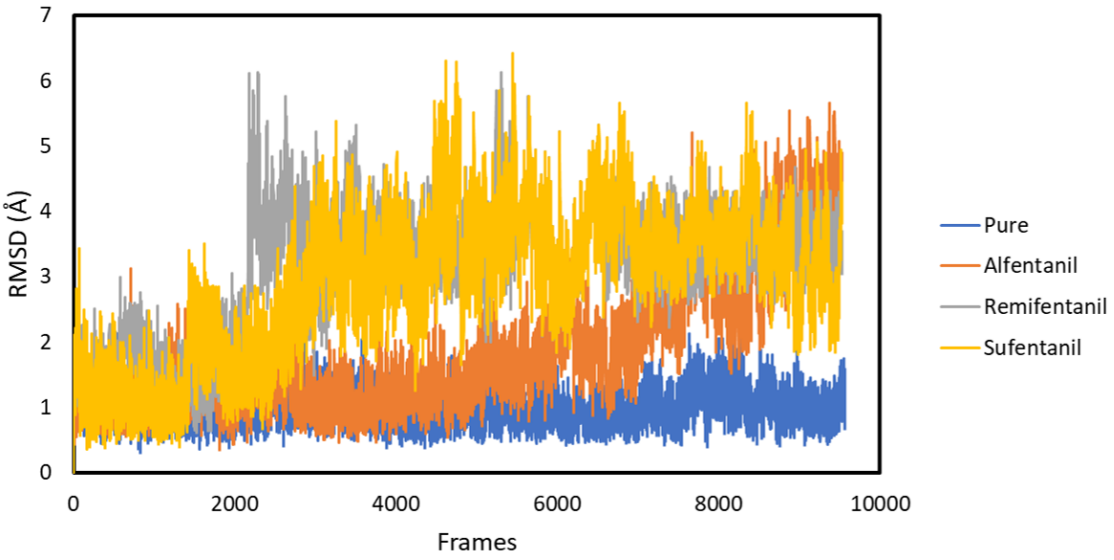

FIGURE 5.9: Root mean squared deviations of loop C in the drug bound systems compared to the pure GLIC system

Uncertainties still remain over the role loop C plays in the gating of pLGICs with some thinking it plays a major role,[268] or just has mild effects,[269] and some believe it has no purpose in the gating activation pathway.[270,271]

The binding free energies were calculated using the MM-PBSA method and are shown in Table 5.2.

Drug	Binding free energy (kcal/mol)
Alfentanil	-16.24
Remifentanil	-19.67
Sufentanil	-15.15
Fentanyl	-27.35

TABLE 5.2: Binding free energies for fentanyl analogues compared to fentanyl

Remifentanil binds the strongest in this site which is likely why it has the longest residence time of around 740 ns in this site compared to the other analogues. When compared to fentanyl in its site, these binding free energies are significantly lower. The reason for this is likely due to the higher involvement of loop C in the fentanyl site. Loop C forms the top of the binding site for fentanyl, whereas only one or two residues from it interact at the analogue site. This highlights the possible importance of loop C not in terms of a direct contributor to the gating mechanism, but in the stability it provides ligands which bind near the orthosteric site.

To see whether or not the binding of the drug molecules in this site altered the function of the GLIC protein, the number of pore water molecules were computed using a custom python script which utilises the MDAnalysis python toolkit.[190] Pore water molecules were classified as those which occupied the M2 pore from the 245-Asn residues at the top of each M2 alpha helix to 222-Glu residues at the bottom of the M2 alpha helices. The pore was found to be full solvated during the full course of the pure GLIC systems. In the drug bound systems, pore de-wetting was observed in the hydrophobic gate region from 240-Ile to 233-Ile (Figure 5.10). The remaining water molecules within the pore are located above (245-Asn to 240-Ile) and below (233-Ile to 222-Glu) the hydrophobic gating region. The full hydrophobic gate region was also observed to be dehydrated by visual inspection in VMD.[133] This methodology in which pore water molecules are tracked along the course of the simulation trajectory has been used previously to identify hydrophobic gate formation in other channel proteins.[191,272,273] The analysis conducted on the pure system confirmed that the channel was in the open state and remained that way over the full length of the simulations. Form visual inspection, the formation of the hydrophobic gate was due to the presence of the 233 and 240 Ile residues blocking the pore causing the dehydrations. This observation is consistent with GLIC hydrophobic gate formation from previous studies.[2,166,192]

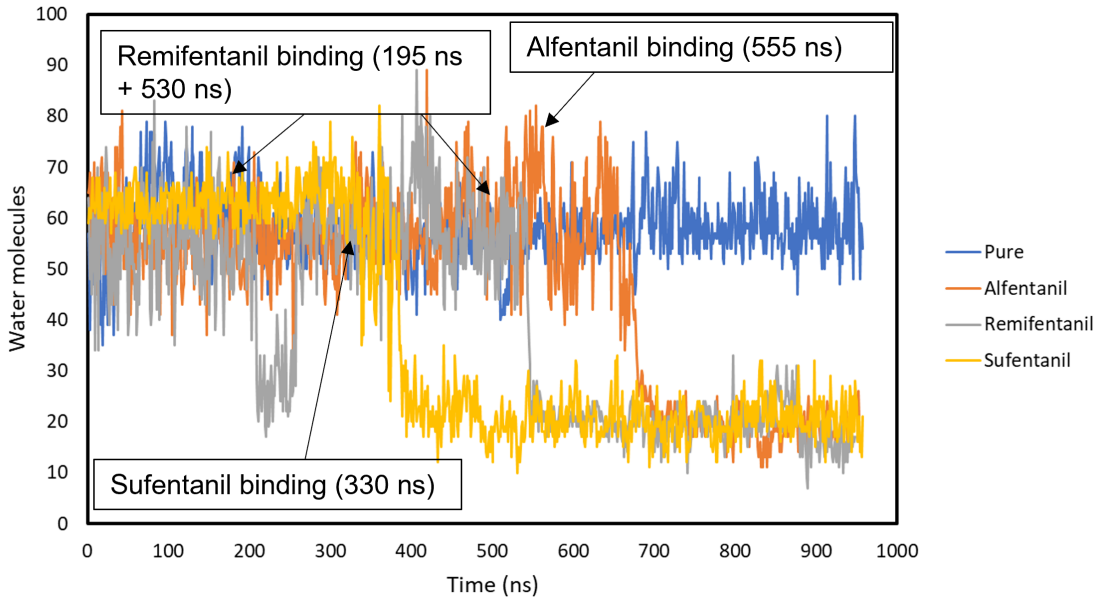

FIGURE 5.10: Plot highlighting the change in the number of pore water molecules within the M2 channel pore when the fentanyl analogues are bound

The pore water calculations show that channel dehydration occurs after binding of each drug molecule in the β-sandwich site. This dehydration of the pore suggests that the channel transitions from an open active state to a closed inactive state in which ion conduction from the extracellular region to intracellular region would not be possible.

It is relatively well accepted that the the conformational change that occurs within the M2 helices associated with pLGIC gating is an "iris-like" contraction in the upper region of the helices. To analyse how the binding of the drug molecules alter the geometry and structure of M2 helices, the TRAJELIX module[197] which is part of the Simulaid analysis package[198] and the Bendix plugin[199] for VMD. These tools were used to investigate a wide variety of properties, such as; global helix x, y and z tilt angles; turn angle per residue; local helix tilt; helix rotation and angle of curvature for each helix over the course of the 1 μs trajectories.

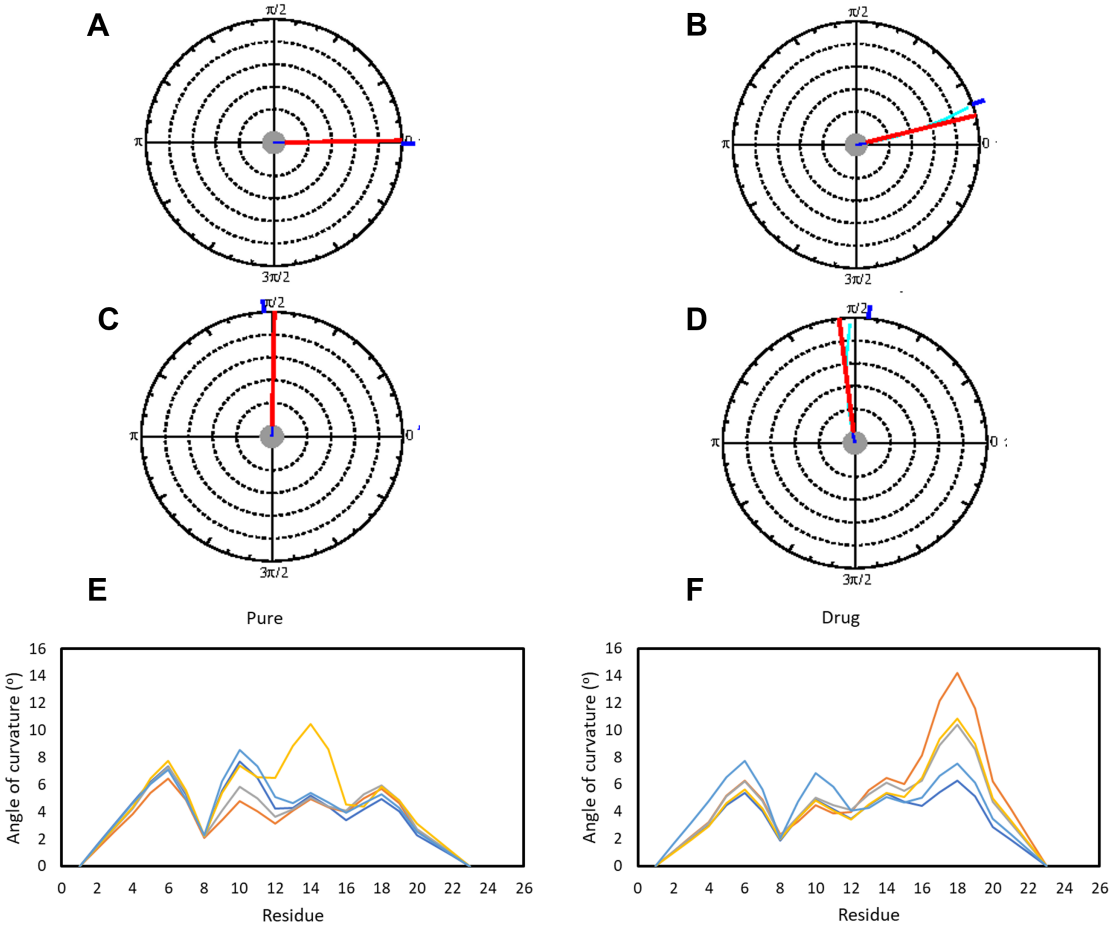

FIGURE 5.11: (A) Helix rotation for pure GLIC system. (B) Helix rotation for drug-bound GLIC systems. (C) Helix tilt for pure GLIC system. (D) Helix tilt for drug-bound GLIC systems. (E) Angle of curvature for each M2 helix for pure GLIC system, each line represents one helix. (F) Angle of curvature for each M2 helix for drug-bound GLIC systems, each line represents one helix

Figure 5.11 shows that helix rotation of $\sim$ 10 degrees is present in the drug-bound system which will rotate Ile residues into the center of the pore which forms the hydrophobic gate, like was observed for fentanyl.[2] Helix tilting was also observed which has previously been shown to occur when other anesthetic molecules bind to this channel and cause a constriction in the conducting pore. Curvature analysis shows that unlike fentanyl, the analogues binding in the β-sandwich site cause an increase in the curvature of the lower part of the channel. The binding of the analogues increased the RMSD of the M2 helices compared to the pure system (Figure 5.12).

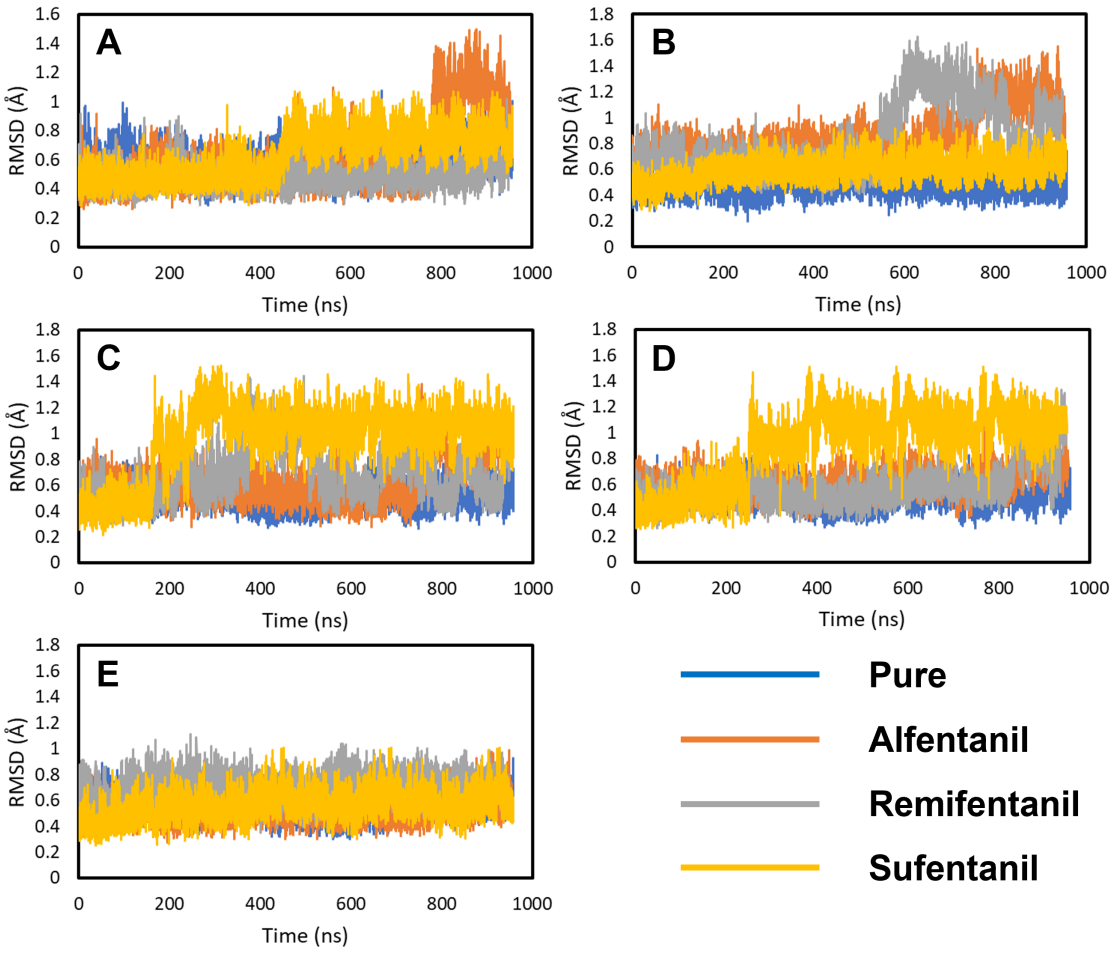

FIGURE 5.12: RMSD values for the helices corresponding to S1 (A) S2 (B) S3 (C) S4 (D) and S5 (E) in the drug-bound and pure GLIC systems. First 50 ns are excluded.

The average RMSD of the M2 helices was 0.55 ± 0.8 Å, which shows how stable the open channel remains in the pure system over the course of the simulation and maintains the water column within the pore (Figure 5.10). The RMSD values for the helices show significant fluctuations when the drug molecules are bound. The most noticeable fluctuations are seen for the sufentanil and remifentanil bound systems in which the RMSD values show considerable fluctuations in S3-S4 and S2-S3 respectively, up to 0.96 ± 0.27 Å for sufentanil in S3. These subunits are the ones in which the drug molecules bind in between. This observation suggests that there is a clear connection between the binding of the drug molecules in the intersubunit site and the motions of the pore forming M2 helices. A clear activation

pathway for pLGICs has yet to be found, but many examples have been shown in which molecules bind to the extracellular domain and cause a change in state of the channel. This suggests the possibility of a common activation pathway based on what site is being occupied, not necessarily the molecule which is bound to the specific site. These findings shows that the difference in binding site can cause different strucutral changes in the transmembrane domain, which results in the same outcome in which the channel moves from an open state to a closed state.

Possible ways to begin looking for potential activation pathways is to overlap the structure of the pure GLIC system with a structure of a drug-bound GLIC system, or an open and closed system which the pure and drug-bound represent respectively (Figure 5.13).

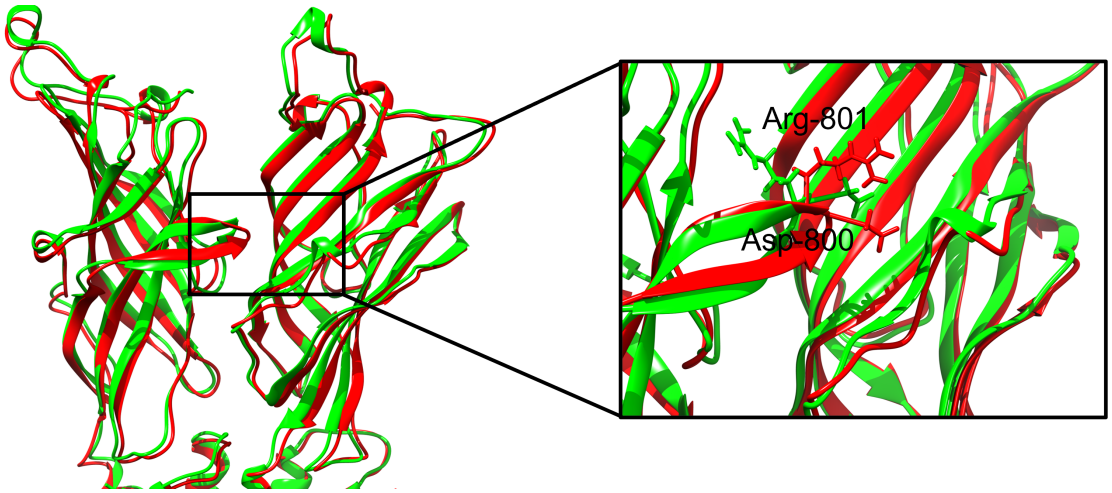

FIGURE 5.13: Extracellular domains of two adjacent subunits of the open GLIC structure (green) and the closed, drug-bound GLIC system (red). Asp-800 and Arg-801 residues are represented as sticks in the zoomed image. Drug molecule binding not shown for clarity.

When these structures are overlapped, differences in the structures can be clearly seen. Loop C plays a role in the binding of many drug molecules at this channel directly, and by forming the cavity in which drugs can bind. In the simulations which the fentanyl analogues bound within the β-sandwich region, loop C is shown to be destabilised and the movement caused can be seen in the overlapped structure

where there has been an outward bending of the loop. This bending can be explained by the interaction of residues 800 and 801 with the drug molecules when they are bound. As described earlier, the function of loop C in the activation mechanism of pLGICs is still highly uncertain. The rest of the extracellular domain remains consistent with the pure structure.

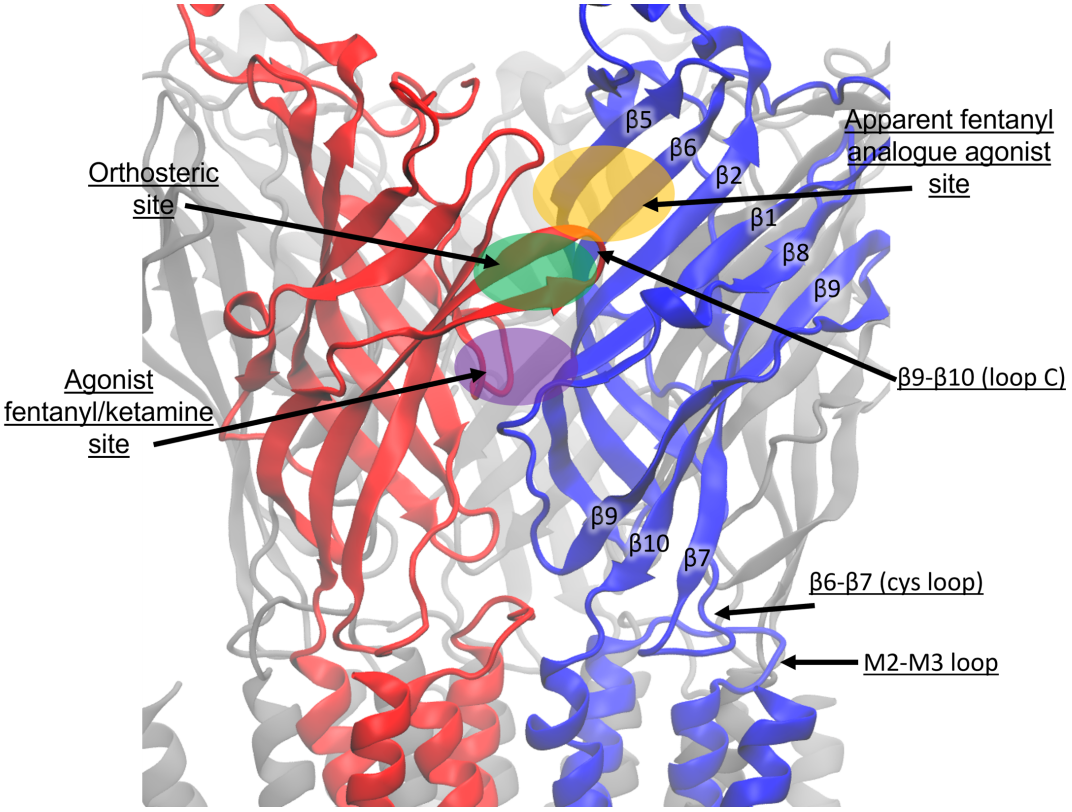

FIGURE 5.14: Fentanyl analogue binding site with reference to the orthosteric and fentanyl/ketamine binding sites

5.5 Conclusion

A novel binding site for three fentanyl based opioid analgesics/anesthetics which is the first evidence of these drug molecules interacting with the GLIC channel which is a target for general anesthetics. This binding site is located in an intersubunit site above both the fentanyl/ketamine site and the orthosteric agonist binding site

but still interacts with loop C which is important in the binding of fentanyl/ketamine and an orthosteric agonist. Molecular dynamics simulations show that the binding of these three fentanyl analogues causes the ion channel to move from an active, ion conducting state to an inactive, non-conducting state. This closure is achieved by conformational changes of the M2 helices within the transmembrane domain which form the channel pore. Conformational analysis conducted using the TRAJELIX module of the simulaid package showed rotation and tilting of the M2 helices when the drug molecules were bound, noticeable curvature of the helices was also observed in the lower part of the helices. These conformational changes formed a hydrophobic gate within the pore which caused rapid dehydration of the channel and blocked the flow of water and ions from the extracellular domain to the intracellular domain. The discovery of the fentanyl analogue binding site is an important step in revealing the molecular mechanisms of opioid anesthesia and future design of opioid-based drugs.

Chapter 6

Conclusions and outlook

General anesthesia has been a revolutionary advance in the field of medicine and general surgery, yet the molecular mechanisms behind this phenomenon remain uncertain despite the technique being routinely used for many decades. Discovering and understanding the mechanisms behind general anesthesia will lead to advances in the design of new anesthetic drugs, which can be used more efficiently and increase patient safety and reduce recovery times. The discovery of these mechanisms could also play a very important role in understanding consciousness, which remains the biggest mystery of our time. Experimental work has shown that general anesthetics can interact with, and alter the physical and mechanical properties of lipid membranes, bind to ion channels resulting in changes to the activation state of the channel, and interact with lipid membranes in ways which could indirectly modulate the effect of ion channel proteins. These findings suggest that general anesthetic molecules act at multiple targets as opposed to one specific membrane protein, for example. One thing that is clear from previous studies is that often only one drug is studied, which is rarely the case in surgical procedures as often there are multiple drugs used in combination during the procedure, the most interesting of which is opioids. Opioids, such as fentanyl and its analogues possess anesthetic properties and are extensively used in general anesthesia so understanding how these opioids exert their anesthetic properties is also fundamental in understanding the molecular mechanisms of general anesthesia.

In this work the interactions between two anesthetic drugs, the intravenous general anesthetic propofol and the opioid anesthetic/analgesic fentanyl , and two different phospholipid bilayers, 1,2-dioleoyl-sn-glycero-3-phosphocholine (DOPC) and 1,2-dipalmitoyl-sn-glycero-3-phosphocholine (DPPC) were investigated using molecular dynamics simulations, which allows the simulations of the drug molecules with a fully hydrated lipid membrane at atomistic resolution. Simulations of single molecules of each drug were initially carried out to study specific interactions with the membrane, then simulations at clinical concentrations were carried out to ascertain if the presence of the drug molecules significantly altered the membranes physical, mechanical and dynamic properties. The main findings from these simulations may be summarised as follows:

- Both propofol and fentanyl prefer to reside within the hydrophobic region of the membranes. Propofol forms hydrogen bonds with the carbonyl oxygens in the upper acyl region and fentanyl orientates itself parallel to the head groups at the interface where it forms hydrogen bonds with water molecules.
- Hydrogen bonding and radial distribution function analysis show an increase in the presence of water molecules within the head group region when the drug molecules were present, this was more noticeable in the fentanyl systems.
- Both drug molecules caused increases in the area per lipid and isothermal area compressibility modulus at clinical concentrations.
- At these concentrations, both drug molecules caused an increase in lipid head group hydration, stiffening of the acyl chains, and hence a decrease in membrane fluidity.
- The results show that there is a large similarity between both drug molecules in the effects that they have on the lipid bilayers.

- Both drug molecules caused significant strucutral perturbations of the membrane structure, largely independent of the bilayer tail structure. Perturbations of this magnitude could possibly cause disruption in the function of other membrane components.

Moving on from these findings, the interactions between fentanyl and a pLGIC were investigated. Anesthetics have been shown to bind at these ion channels and induce conformational changes which render the channel non-functional. The *Gloeobacter violaceus* ion channel was chosen as the target ion channel due to high resolution crystal structures being available for the open form of the channel allowing possible gating to be investigated. Various anesthetics have also been shown to modulate the function of this ion channel experimentally and computationally. The anesthetic action of fentanyl has received very little attention, as most anesthesia related research has mainly focused on hypnotic agents, such as propofol. Fentanyl can, and often is used as the main general anesthetic component so it is important that this is investigated. This study utilises molecular dynamics simulations and end-state free energy calculations to study the interactions between fentanyl and the *Gloeobacter violaceus* ion channel, the main findings can be summarised as follows:

- Fentanyl was found to bind within an extracellular intersubunit site in which ketamine has been shown to bind. This site is located approximately 10 Å below the orthosteric agonist-binding site. Fentanyl remains stable in this binding site for over 400 ns.

- MM-PBSA calculations showed that the binding strength of fentanyl was similar to other drug molecules which bind to pLGICs and modulate their function.

- Analysis of the pore water molecules show a rapid dehydration of the M2 helix pore after fentanyl binding. Visual analysis showed the formation of a hydrophobic gate region formed by the 233-Ile and 240-Ile residues.

- Conformational analysis of the transmembrane M2 helices which form the ion conducting pore showed that helix rotation and helix curvature, with minimal tilting occurred upon fentanyl binding which cause the ion channel to move to an inactive state.

- The similarity between fentanyl and ketamine clinically and in this binding site suggest that this site is relevant in the general anesthesia process.

- This study shows that fentanyl can act at this channel which is a target for general anesthetics, this should hopefully show that fentanyl is worth while studying in the context of anesthesia.

- Understanding where fentanyl binds and interacts is important for the future development of "opioid-like" drugs.

The discovery of fentanyl modulating the function of GLIC is consistent with the intravenous anesthetic propofol which also binds to and modulates this channel, albeit in a transmembrane, intrasubunit site. Propofol and fentanyl are routinely used in general surgery to perform total intravenous anesthesia (TIVA) which has several advantages over traditional volatile techniques, namely; reduction of post-operative nausea, rapid recovery, greater haemodynamic stability and less atmospheric pollution. As these drugs are used together, there is a possibility that there are interactions between them both, and the GLIC structure. In this study, flooding style simulations were used alongside gaussian accelerated molecular dynamics to look for signs of interaction between these drugs and GLIC. The main findings can be summarised as follows:

- The gaussian accelerated MD simulations revealed a detailed pathway for the pore blocking mechanism by propofol, which had not been previously observed with conventional MD simulations.

- Propofol was also shown to be able to hop between transmembrane intrasubunit binding sites by diffusing a tunnel formed by helices of the occupied and adjacent subunit.

- Fentanyl was shown to stabilise propofol molecules in several binding sites. Multiple propofol molecules interacted with one fentanyl molecule in the aqueous phase and then diffused towards the protein where the fentanyl molecule remained with one propofol molecule in an extracellular binding site.

- Density calculations show that fentanyl and propofol share many sites, mostly located in the extracellular domain.

- The stabilisation by fentanyl was shown to occur close to the orthosteric agonist-binding site.

- The results of this study present a case for the allosteric action of anesthetics and opioids at pLGIC sites.

So far the results have shown that fentanyl acts in similar ways to the general anesthetic propofol in lipid bilayers and at the *Gloeobacter violaceus* ion channel. Although fentanyl is a vital component in general anesthesia, various analogues have been developed which have different clinical effects, such as higher potency, decreased onset time, reduced duration of action, and greater metabolism rates. The lipid membrane is though to play an important role in opioid anesthesia, so understanding how these drugs behave in these environments is important. One of the most important properties to understand is the membrane permeability which can be predicted from molecular simulations. Multiple simple bilayer models were used to show how crucial lipid choice is in membrane permeability prediction. In this study, extensive umbrella sampling simulations were used to predict the membrane permeability of fentanyl and three of its analogues (alfentanil, remifentanil and sufentanil) and the results were compared to the available experimental data. The main findings can be summarised as follows:

- The simulations showed that for all four drug molecules, the main resistance to permeation was at the lipid head group interface due to it being partially charged and polar, whereas the drug molecules were all hydrophobic in nature.

- The simulations were able to identify the DMPC lipid bilayer as the most reliable lipid to use for these drug molecules.
- The DMPC system gave the best comparisons to the literature values from PAMPA and Caco-2 methods which are extensively used in pharmaceutical research.
- Biophysical data on the free energy of permeation, local resistance and diffusion can be obtained from these simulations, as well as the permeability coefficients.
- The results from the umbrella sampling simulations showed that accurate predictions of the membrane permeability coefficients can be made using simple membrane models and adequate sampling.
- The results for each model showed how important the testing for suitable lipid systems is when performing membrane permeability coefficient calculations using the umbrella sampling methodology.

To further investigate the differences between fentanyl and its analogues, the interactions between them and the *Gloeobacter violaceus* ion channel were investigated using molecular dynamics and end-state free energy calculations. Fentanyl was shown to bind within an extracellular intersubunit binding site which can also be occupied by the anesthetic drug ketamine. Ascertaining whether the analogues interact with the channel in the same, or similar way to fentanyl and other general anesthetics will be important for understanding the anesthetic properties of these drugs, and for future drug design. The main findings can be summarised as follows.

- All three fentanyl analogues were found to bind within an extracellular intersubunit site above the fentanyl/ketamine site.
- This binding site shared residues located on loop C which also form part of the fentanyl/ketamine site.

- Pore dehydration was observed when the drug molecules were bound within this site, suggesting that the channel moved to an inactive state when these drug molecules were bound.
- Conformational analysis of the M2 helices which form the ion conducting pore suggest that there is rotation and tilting of these helices which cause the channel to close.
- This is consistent with what has previously been observed for other anesthetic molecules, but this binding site has not previously been identified.
- A clear activation pathway has yet to be found for pLGICs, but many examples of molecules which bind in the extracellular domain and cause conformational changes in the transmembrane domain. This suggests the possibility of a common activation pathway based on a site being occupied, not necessarily the molecule that is bound.
- These findings show that a difference in binding site can cause different strucutral changes which result in the same outcome.

In the past decades, research into general anesthesia has progressed significantly along with huge progress in computational hardware and software which has opened up new possibilities in the study of the interactions between anesthetic drugs and biological systems. As highlighted in this thesis, advances in experimental structure determination techniques, such as x-ray crystallography and cryo-electron microscopy have allowed structures to be determined which show anesthetics binding to ion channel proteins. These structures allow the interactions with the bound drug, and other possible ligands to be probed at atomistic detail with molecular simulations. However, an important step which has to be overcome will be the applicability of these observations to complex mammalian systems, and to put these results into the overall context of a cell, and then the brain as a whole. The work presented in this thesis will also hopefully show that the focus of anesthesia research should be broadened to include other molecules with anesthetic properties, such as opioids, which will add more pieces to the

puzzle. With current advances in receptor discovery, electrophysiology, structure prediction and computational power, I am hopeful that the mysteries of general anesthesia, and human consciousness will begin to be revealed, which will allow the development of safer and more effective drugs, as well as an understanding of the greatest mystery in the universe.

Bibliography

[1] Miao, Y.; Feher, V. A.; McCammon, J. A. Gaussian accelerated molecular dynamics: Unconstrained enhanced sampling and free energy calculation. *Journal of chemical theory and computation* **2015**, *11*, 3584–3595.

[2] Faulkner, C.; Plant, D. F.; de Leeuw, N. H. Modulation of the Gloeobacter violaceus Ion Channel by Fentanyl: A Molecular Dynamics Study. *Biochemistry* **2019**, *58*, 4804–4808.

[3] Wormald, P. J.; Van Renen, G.; Perks, J.; Jones, J. A.; Langton-Hewer, C. D. The effect of the total intravenous anesthesia compared with inhalational anesthesia on the surgical field during endoscopic sinus surgery. *American journal of rhinology* **2005**, *19*, 514–520.

[4] Miller, T. E.; Gan, T. J. Total intravenous anesthesia and anesthetic outcomes. *Journal of cardiothoracic and vascular anesthesia* **2015**, *29*, S11–S15.

[5] Bajwa, S. J. S.; Bajwa, S. K.; Kaur, J. Comparison of two drug combinations in total intravenous anesthesia: Propofol–ketamine and propofol–fentanyl. *Saudi journal of anaesthesia* **2010**, *4*, 72.

[6] Thomas, B. Remifentanil versus fentanyl in total intravenous anesthesia for lumbar spine surgery: a retrospective cohort study. *Journal of clinical anesthesia* **2015**, *27*, 391–395.

[7] Kannabiran, N.; Bidkar, P. U. Total intravenous anesthesia in neurosurgery. *Journal of Neuroanaesthesiology and Critical Care* **2018**, *5*, 141–149.

[8] Meyer, H. Zur theorie der alkoholnarkose. *Naunyn-Schmiedeberg's Archives of Pharmacology* **1899**, *42*, 109–118.

[9] Overton, C. E. *Studien über die Narkose zugleich ein Beitrag zur allgemeinen Pharmakologie*; Fischer, 1901.

[10] Meyer, K. H. Contributions to the theory of narcosis. *Transactions of the Faraday Society* **1937**, *33*, 1062–1064.

[11] Miller, K.; Paton, W.; Smith, R.; Smith, E. The pressure reversal of general anesthesia and the critical volume hypothesis. *Molecular pharmacology* **1973**, *9*, 131–143.

[12] Janoff, A.; Miller, K. A CRITICAL-ASSESSMENT OF THE LIPID THEORIES OF GENERAL ANESTHETIC ACTION. *Biological membranes* **1982**, *4*, 417–476.

[13] Miller, K. W. *International review of neurobiology*; Elsevier, 1985; Vol. 27; pp 1–61.

[14] Chin, J.; Goldstein, D. Effects of low concentrations of ethanol on the fluidity of spin-labeled erythrocyte and brain membranes. *Molecular Pharmacology* **1977**, *13*, 435–441.

[15] Chin, J.; Goldstein, D. Electron paramagnetic resonance studies of ethanol on membrane fluidity. *Advances in experimental medicine and biology* **1977**, *85*, 111–122.

[16] Schroeder, F.; Morrison, W. J.; Gorka, C.; Wood, W. G. Transbilayer effects of ethanol on fluidity of brain membrane leaflets. *Biochimica et Biophysica Acta (BBA)-Biomembranes* **1988**, *946*, 85–94.

[17] Franks, N.; Lieb, W. Molecular mechanisms of general anaesthesia. *Nature* **1982**, *300*, 487.

[18] Koblin, D. D.; Chortkoff, B. S.; Laster, M. J.; Halsey, M.; Ionescu, P., et al. Polyhalogenated and perfluorinated compounds that disobey the Meyer-Overton hypothesis. *Anesthesia and analgesia* **1994**, *79*, 1043–1048.

[19] Taheri, S.; Laster, M. J.; Liu, J.; Halsey, M.; Koblin, D., et al. Anesthesia by n-alkanes not consistent with the Meyer-Overton hypothesis: determinations of the solubilities of alkanes in saline and various lipids. *Anesthesia and analgesia* **1993**, *77*, 7–11.

[20] Weir, C. J. The molecular mechanisms of general anaesthesia: dissecting the GABAA receptor. *Continuing Education in Anaesthesia, Critical Care and Pain* **2006**, *6*, 49–53.

[21] Cantor, R. S. The lateral pressure profile in membranes: a physical mechanism of general anesthesia. *Biochemistry* **1997**, *36*, 2339–2344.

[22] Cantor, R. S. Lateral pressures in cell membranes: a mechanism for modulation of protein function. *The Journal of Physical Chemistry B* **1997**, *101*, 1723–1725.

[23] Cantor, R. S. The influence of membrane lateral pressures on simple geometric models of protein conformational equilibria. *Chemistry and physics of lipids* **1999**, *101*, 45–56.

[24] Lerner, R. A. A hypothesis about the endogenous analogue of general anesthesia. *Proceedings of the National Academy of Sciences* **1997**, *94*, 13375–13377.

[25] Pavel, M. A.; Petersen, E. N.; Wang, H.; Lerner, R. A.; Hansen, S. B. Studies on the mechanism of membrane mediated general anesthesia. *BioRxiv* **2019**, 313973.

[26] Overington, J. P.; Al-Lazikani, B.; Hopkins, A. L. How many drug targets are there? *Nature reviews Drug discovery* **2006**, *5*, 993.

[27] Franks, N.; Lieb, W. Do general anaesthetics act by competitive binding to specific receptors? *Nature* **1984**, *310*, 599.

[28] Franks, N.; Jenkins, A.; Conti, E.; Lieb, W.; Brick, P. Structural basis for the inhibition of firefly luciferase by a general anesthetic. *Biophysical journal* **1998**, *75*, 2205–2211.

[29] Conti, E.; Franks, N. P.; Brick, P. Crystal structure of firefly luciferase throws light on a superfamily of adenylate-forming enzymes. *Structure* **1996**, *4*, 287–298.

[30] Franks, N.; Lieb, W. Mapping of general anaesthetic target sites provides a molecular basis for cutoff effects. *Nature* **1985**, *316*, 349.

[31] Gomez, R. S.; Guatimosim, C.; Gomez, M. V. Mechanism of action of volatile anesthetics: role of protein kinase C. *Cellular and molecular neurobiology* **2003**, *23*, 877–885.

[32] Pennisi, E. Working the (gene count) numbers: finally, a firm answer? *Science* **2007**, *316*, 1113–1113.

[33] Hemmings Jr, H. C.; Akabas, M. H.; Goldstein, P. A.; Trudell, J. R.; Orser, B. A.; Harrison, N. L. Emerging molecular mechanisms of general anesthetic action. *Trends in pharmacological sciences* **2005**, *26*, 503–510.

[34] Lugli, A. K.; Yost, C. S.; Kindler, C. H. Anaesthetic mechanisms: update on the challenge of unravelling the mystery of anaesthesia. *European journal of anaesthesiology* **2009**, *26*, 807.

[35] Oakes, V.; Domene, C. Capturing the Molecular Mechanism of Anesthetic Action by Simulation Methods. *Chemical Reviews* **2018**, *119*, 5998–6014.

[36] Nelson, D. L.; Lehninger, A. L.; Cox, M. M. *Lehninger principles of biochemistry*; Macmillan, 2008.

[37] van Meer, G.; de Kroon, A. I. Lipid map of the mammalian cell. *Journal of cell science* **2011**, *124*, 5–8.

[38] Harayama, T.; Riezman, H. Understanding the diversity of membrane lipid composition. *Nature reviews Molecular cell biology* **2018**, *19*, 281–296.

[39] Virtanen, J. A.; Cheng, K. H.; Somerharju, P. Phospholipid composition of the mammalian red cell membrane can be rationalized by a superlattice model. *Proceedings of the National Academy of Sciences* **1998**, *95*, 4964–4969.

[40] Symons, J. L.; Cho, K.-J.; Chang, J. T.; Du, G.; Waxham, M. N.; Hancock, J. F.; Levental, I.; Levental, K. R. Lipidomic atlas of mammalian cell membranes reveals hierarchical variation induced by culture conditions, subcellular membranes, and cell lineages. *Soft Matter* **2021**, *17*, 288–297.

[41] Cocucci, E.; Kim, J.; Bai, Y.; Pabla, N. Role of Passive diffusion, Transporters, and membrane trafficking-mediated processes in cellular drug transport. *Clinical Pharmacology & Therapeutics* **2017**, *101*, 121–129.

[42] Dodson, B. A.; Moss, J. Molecular mechanisms of action of general anesthetics. *Molecular and cellular biochemistry* **1984**, *64*, 97–103.

[43] Hubatsch, I.; Ragnarsson, E. G.; Artursson, P. Determination of drug permeability and prediction of drug absorption in Caco-2 monolayers. *Nature protocols* **2007**, *2*, 2111–2119.

[44] Pickholz, M.; Giupponi, G. Coarse grained simulations of local anesthetics encapsulated into a liposome. *The Journal of Physical Chemistry B* **2010**, *114*, 7009–7015.

[45] Kawamoto, S.; Klein, M. L.; Shinoda, W. Coarse-grained molecular dynamics study of membrane fusion: Curvature effects on free energy barriers along the stalk mechanism. *The Journal of Chemical Physics* **2015**, *143*, 243112.

[46] Huang, P.; Bertaccini, E.; Loew, G. H. Molecular dynamics simulation of anesthetic-phospholipid bilayer interactions. *Journal of Biomolecular Structure and Dynamics* **1995**, *12*, 725–754.

[47] Pohorille, A.; Cieplak, P.; Wilson, M. A. Interactions of anesthetics with the membrane-water interface. *Chemical physics* **1996**, *204*, 337–345.

[48] Pohorille, A.; Wilson, M. A.; New, M. H.; Chipot, C. Concentrations of anesthetics across the water–membrane interface; the Meyer–Overton hypothesis revisited. *Toxicology letters* **1998**, *100*, 421–430.

[49] Tu, K.; Tarek, M.; Klein, M. L.; Scharf, D. Effects of anesthetics on the structure of a phospholipid bilayer: molecular dynamics investigation of halothane in the hydrated liquid crystal phase of dipalmitoylphosphatidylcholine. *Biophysical journal* **1998**, *75*, 2123–2134.

[50] Baber, J.; Ellena, J. F.; Cafiso, D. S. Distribution of general anesthetics in phospholipid bilayers determined using 2H NMR and 1H-1H NOE spectroscopy. *Biochemistry* **1995**, *34*, 6533–6539.

[51] Koubi, L.; Tarek, M.; Klein, M. L.; Scharf, D. Distribution of halothane in a dipalmitoylphosphatidylcholine bilayer from molecular dynamics calculations. *Biophysical journal* **2000**, *78*, 800–811.

[52] Chen, J.; Chen, L.; Wang, Y.; Wang, X.; Zeng, S. Exploring the effects on lipid bilayer induced by noble gases via molecular dynamics simulations. *Scientific reports* **2015**, *5*, 1–6.

[53] Gurtovenko, A. A.; Anwar, J. Interaction of ethanol with biological membranes: the formation of non-bilayer structures within the membrane interior and their significance. *The journal of physical chemistry B* **2009**, *113*, 1983–1992.

[54] Fábián, B.; Darvas, M.; Picaud, S.; Sega, M.; Jedlovszky, P. The effect of anaesthetics on the properties of a lipid membrane in the biologically relevant phase: a computer simulation study. *Physical Chemistry Chemical Physics* **2015**, *17*, 14750–14760.

[55] Johnson, F. H.; Flagler, E. A. Hydrostatic pressure reversal of narcosis in tadpoles. *Science* **1950**, *112*, 91–92.

[56] Miller, K. W.; Wilson, M. W. The pressure reversal of a variety of anesthetic agents in mice. *Anesthesiology* **1978**, *48*, 104–110.

[57] Braganza, L. F.; Worcester, D. L. Hydrostatic pressure induces hydrocarbon chain interdigitation in single-component phospholipid bilayers. *Biochemistry* **1986**, *25*, 2591–2596.

[58] Girard, E.; Marchal, S.; Perez, J.; Finet, S.; Kahn, R.; Fourme, R.; Marassio, G.; Dhaussy, A.-C.; Prangé, T.; Giffard, M., et al. Structure-function perturbation and dissociation of tetrameric urate oxidase by high hydrostatic pressure. *Biophysical journal* **2010**, *98*, 2365–2373.

[59] Boonyaratanakornkit, B. B.; Park, C. B.; Clark, D. S. Pressure effects on intra-and intermolecular interactions within proteins. *Biochimica et Biophysica Acta (BBA)-Protein Structure and Molecular Enzymology* **2002**, *1595*, 235–249.

[60] Chau, P.-L.; Jedlovszky, P.; Hoang, P.; Picaud, S. Pressure reversal of general anaesthetics: a possible mechanism from molecular dynamics simulations. *Journal of Molecular Liquids* **2009**, *147*, 128–134.

[61] Wieteska, J.; Welche, P.; Tu, K.-M.; ElGamacy, M.; Csanyi, G.; Payne, M.; Chau, P.-L. Isoflurane does not aggregate inside POPC bilayers at high pressure: Implications for pressure reversal of general anaesthesia. *Chemical Physics Letters* **2015**, *638*, 116–121.

[62] Yamakura, T.; Bertaccini, E.; Trudell, J. R.; Harris, R. A. Anesthetics and ion channels: molecular models and sites of action. *Annual review of pharmacology and toxicology* **2001**, *41*, 23–51.

[63] Hilf, R. J.; Dutzler, R. Structure of a potentially open state of a proton-activated pentameric ligand-gated ion channel. *Nature* **2009**, *457*, 115–118.

[64] Bocquet, N.; Nury, H.; Baaden, M.; Le Poupon, C.; Changeux, J.-P.; Delarue, M.; Corringer, P.-J. X-ray structure of a pentameric ligand-gated ion channel in an apparently open conformation. *Nature* **2009**, *457*, 111–114.

[65] Pan, J.; Chen, Q.; Willenbring, D.; Yoshida, K.; Tillman, T.; Kashlan, O. B.; Cohen, A.; Kong, X.-P.; Xu, Y.; Tang, P. Structure of the pentameric ligand-gated ion channel ELIC cocrystallized with its competitive antagonist acetylcholine. *Nature communications* **2012**, *3*, 1–8.

[66] Weng, Y.; Yang, L.; Corringer, P.-J.; Sonner, J. M. Anesthetic sensitivity of the Gloeobacter violaceus proton-gated ion channel. *Anesthesia and analgesia* **2010**, *110*, 59.

[67] Cheng, M. H.; Coalson, R. D.; Cascio, M. Molecular dynamics simulations of ethanol binding to the transmembrane domain of the glycine receptor: implications for the channel potentiation mechanism. *Proteins: Structure, Function, and Bioinformatics* **2008**, *71*, 972–981.

[68] Liu, L. T.; Haddadian, E. J.; Willenbring, D.; Xu, Y.; Tang, P. Higher susceptibility to halothane modulation in open-than in closed-channel $\alpha4\beta2$ nAChR revealed by molecular dynamics simulations. *The Journal of Physical Chemistry B* **2010**, *114*, 626–632.

[69] Woll, K. A.; Murlidaran, S.; Pinch, B. J.; Hénin, J.; Wang, X.; Salari, R.; Covarrubias, M.; Dailey, W. P.; Brannigan, G.; Garcia, B. A., et al. A novel bifunctional alkylphenol anesthetic allows characterization of γ-aminobutyric acid, type A (GABAA), receptor subunit binding selectivity in synaptosomes. *Journal of Biological Chemistry* **2016**, *291*, 20473–20486.

[70] Yoluk, Ö.; Brömstrup, T.; Bertaccini, E. J.; Trudell, J. R.; Lindahl, E. Stabilization of the GluCl ligand-gated ion channel in the presence and absence of ivermectin. *Biophysical journal* **2013**, *105*, 640–647.

[71] Brannigan, G.; LeBard, D. N.; Hénin, J.; Eckenhoff, R. G.; Klein, M. L. Multiple binding sites for the general anesthetic isoflurane identified in the nicotinic acetylcholine receptor transmembrane domain. *Proceedings of the National Academy of Sciences* **2010**, *107*, 14122–14127.

[72] Nury, H.; Van Renterghem, C.; Weng, Y.; Tran, A.; Baaden, M.; Dufresne, V.; Changeux, J.-P.; Sonner, J. M.; Delarue, M.; Corringer, P.-J. X-ray structures of general anaesthetics bound to a pentameric ligand-gated ion channel. *Nature* **2011**, *469*, 428–431.

[73] Willenbring, D.; Liu, L. T.; Mowrey, D.; Xu, Y.; Tang, P. Isoflurane alters the structure and dynamics of GLIC. *Biophysical journal* **2011**, *101*, 1905–1912.

[74] Chen, Q.; Cheng, M. H.; Xu, Y.; Tang, P. Anesthetic binding in a pentameric ligand-gated ion channel: GLIC. *Biophysical journal* **2010**, *99*, 1801–1809.

[75] Cheng, M. H.; Coalson, R. D.; Tang, P. Molecular dynamics and brownian dynamics investigation of ion permeation and anesthetic halothane effects on a proton-gated ion channel. *Journal of the American Chemical Society* **2010**, *132*, 16442–16449.

[76] Lee, W. Y.; Sine, S. M. Principal pathway coupling agonist binding to channel gating in nicotinic receptors. *Nature* **2005**, *438*, 243–247.

[77] LeBard, D. N.; Hénin, J.; Eckenhoff, R. G.; Klein, M. L.; Brannigan, G. General anesthetics predicted to block the GLIC pore with micromolar affinity. *PLoS computational biology* **2012**, *8*.

[78] Pan, J.; Chen, Q.; Willenbring, D.; Mowrey, D.; Kong, X.-P.; Cohen, A.; Divito, C. B.; Xu, Y.; Tang, P. Structure of the pentameric ligand-gated ion channel GLIC bound with anesthetic ketamine. *Structure* **2012**, *20*, 1463–1469.

[79] Ion, B. F.; Wells, M. M.; Chen, Q.; Xu, Y.; Tang, P. Ketamine Inhibition of the Pentameric Ligand-Gated Ion Channel GLIC. *Biophysical journal* **2017**, *113*, 605–612.

[80] JA Craddock, T.; R Hameroff, S.; T Ayoub, A.; Klobukowski, M.; A Tuszynski, J. Anesthetics act in quantum channels in brain microtubules to prevent consciousness. *Current topics in medicinal chemistry* **2015**, *15*, 523–533.

[81] Hameroff, S. R.; Watt, R. C.; Borel, J. D.; Carlson, G. General anesthetics directly inhibit electron mobility: dipole dispersion theory of anesthetic action. *Physiological chemistry and physics* **1982**, *14*, 183–187.

[82] Hameroff, S. Anesthesia, consciousness and hydrophobic pockets—A unitary quantum hypothesis of anesthetic action. *Toxicology letters* **1998**, *100*, 31–39.

[83] Hameroff, S. R. The entwined mysteries of anesthesia and consciousness: is there a common underlying mechanism? *The Journal of the American Society of Anesthesiologists* **2006**, *105*, 400–412.

[84] Hameroff, S.; Nip, A.; Porter, M.; Tuszynski, J. Conduction pathways in microtubules, biological quantum computation, and consciousness. *Biosystems* **2002**, *64*, 149–168.

[85] Turin, L.; Skoulakis, E. M.; Horsfield, A. P. Electron spin changes during general anesthesia in Drosophila. *Proceedings of the National Academy of Sciences* **2014**, *111*, E3524–E3533.

[86] Stuart, H. Quantum computation in brain microtubules? The Penrose–Hameroff 'Orch OR 'model of consciousness. *Philosophical Transactions of the Royal Society of London. Series A: Mathematical, Physical and Engineering Sciences* **1998**, *356*, 1869–1896.

[87] Pan, J. Z.; Xi, J.; Eckenhoff, M. F.; Eckenhoff, R. G. Inhaled anesthetics elicit region-specific changes in protein expression in mammalian brain. *Proteomics* **2008**, *8*, 2983–2992.

[88] Dixit, R.; Ross, J. L.; Goldman, Y. E.; Holzbaur, E. L. Differential regulation of dynein and kinesin motor proteins by tau. *Science* **2008**, *319*, 1086–1089.

[89] Kobayashi, N.; Mundel, P. A role of microtubules during the formation of cell processes in neuronal and non-neuronal cells. *Cell and tissue research* **1998**, *291*, 163–174.

[90] Craddock, T. J.; St. George, M.; Freedman, H.; Barakat, K. H.; Damaraju, S.; Hameroff, S.; Tuszynski, J. A. Computational predictions of volatile anesthetic interactions with the microtubule cytoskeleton: Implications for side effects of general anesthesia. *PLoS One* **2012**, *7*, e37251.

[91] Weiser, B. P.; Woll, K. A.; Dailey, W. P.; Eckenhoff, R. G. Mechanisms revealed through general anesthetic photolabeling. *Current anesthesiology reports* **2014**, *4*, 57–66.

[92] Emerson, D. J.; Weiser, B. P.; Psonis, J.; Liao, Z.; Taratula, O.; Fiamengo, A.; Wang, X.; Sugasawa, K.; Smith III, A. B.; Eckenhoff, R. G., et al. Direct modulation of microtubule stability contributes to anthracene general anesthesia. *Journal of the American Chemical Society* **2013**, *135*, 5389–5398.

[93] Portet, S.; Tuszyński, J.; Hogue, C.; Dixon, J. Elastic vibrations in seamless microtubules. *European Biophysics Journal* **2005**, *34*, 912–920.

[94] Conrad, M. Amplification of superpositional effects through electronic-conformational interactions. *Chaos, Solitons & Fractals* **1994**, *4*, 423–438.

[95] Matsuno, K. The internalist enterprise on constructing cell motility in a bottom-up manner. *BioSystems* **2001**, *61*, 115–124.

[96] Sahu, S.; Ghosh, S.; Hirata, K.; Fujita, D.; Bandyopadhyay, A. Multi-level memory-switching properties of a single brain microtubule. *Applied Physics Letters* **2013**, *102*, 123701.

[97] Lambert, N.; Chen, Y.-N.; Cheng, Y.-C.; Li, C.-M.; Chen, G.-Y.; Nori, F. Quantum biology. *Nature Physics* **2013**, *9*, 10–18.

[98] Fleming, G. R.; Scholes, G. D.; Cheng, Y.-C. Quantum effects in biology. *Procedia Chemistry* **2011**, *3*, 38–57.

[99] Ohmura, I.; Morimoto, G.; Ohno, Y.; Hasegawa, A.; Taiji, M. MDGRAPE-4: a special-purpose computer system for molecular dynamics simulations. *Philosophical Transactions of the Royal Society A: Mathematical, Physical and Engineering Sciences* **2014**, *372*, 20130387.

[100] Shaw, D. E.; Grossman, J.; Bank, J. A.; Batson, B.; Butts, J. A.; Chao, J. C.; Deneroff, M. M.; Dror, R. O.; Even, A.; Fenton, C. H., et al. Anton 2: raising the bar for performance and programmability in a special-purpose molecular dynamics supercomputer. Proceedings of the international conference for high performance computing, networking, storage and analysis. 2014; pp 41–53.

[101] Hall, G. G. The molecular orbital theory of chemical valency VIII. A method of calculating ionization potentials. *Proceedings of the Royal Society of London. Series A. Mathematical and Physical Sciences* **1951**, *205*, 541–552.

[102] Leach, A. R.; Leach, A. R. *Molecular modelling: principles and applications*; Pearson education, 2001.

[103] Ochsenfeld, C.; White, C. A.; Head-Gordon, M. Linear and sublinear scaling formation of Hartree–Fock-type exchange matrices. *The Journal of chemical physics* **1998**, *109*, 1663–1669.

[104] Case, D. A.; Cheatham III, T. E.; Darden, T.; Gohlke, H.; Luo, R.; Merz Jr, K. M.; Onufriev, A.; Simmerling, C.; Wang, B.; Woods, R. J. The Amber biomolecular simulation programs. *Journal of computational chemistry* **2005**, *26*, 1668–1688.

[105] Evans, M. Simulation and symmetry in molecular diffusion and spectroscopy. *Adv. Chem. Phys* **1992**, *81*, 361.

[106] Forester, T. R.; Smith, W. SHAKE, rattle, and roll: efficient constraint algorithms for linked rigid bodies. *Journal of computational chemistry* **1998**, *19*, 102–111.

[107] Mark, P.; Nilsson, L. Structure and dynamics of the TIP3P, SPC, and SPC/E water models at 298 K. *The Journal of Physical Chemistry A* **2001**, *105*, 9954–9960.

[108] Maier, J. A.; Martinez, C.; Kasavajhala, K.; Wickstrom, L.; Hauser, K. E.; Simmerling, C. ff14SB: improving the accuracy of protein side chain and backbone parameters from ff99SB. *Journal of chemical theory and computation* **2015**, *11*, 3696–3713.

[109] Dickson, C. J.; Madej, B. D.; Skjevik, Å. A.; Betz, R. M.; Teigen, K.; Gould, I. R.; Walker, R. C. Lipid14: the amber lipid force field. *Journal of chemical theory and computation* **2014**, *10*, 865–879.

[110] Wang, J.; Wolf, R. M.; Caldwell, J. W.; Kollman, P. A.; Case, D. A. Development and testing of a general amber force field. *Journal of computational chemistry* **2004**, *25*, 1157–1174.

[111] Rosso, L.; Gould, I. R. Structure and dynamics of phospholipid bilayers using recently developed general all-atom force fields. *Journal of computational chemistry* **2008**, *29*, 24–37.

[112] Shirts, M. R. Simple quantitative tests to validate sampling from thermodynamic ensembles. *Journal of chemical theory and computation* **2013**, *9*, 909–926.

[113] Anézo, C.; de Vries, A. H.; Höltje, H.-D.; Tieleman, D. P.; Marrink, S.-J. Methodological issues in lipid bilayer simulations. *The Journal of Physical Chemistry B* **2003**, *107*, 9424–9433.

[114] Poger, D.; Mark, A. E. Lipid bilayers: The effect of force field on ordering and dynamics. *Journal of chemical theory and computation* **2012**, *8*, 4807–4817.

[115] Ponder, J. W.; Wu, C.; Ren, P.; Pande, V. S.; Chodera, J. D.; Schnieders, M. J.; Haque, I.; Mobley, D. L.; Lambrecht, D. S.; DiStasio Jr, R. A., et al. Current status of the AMOEBA polarizable force field. *The journal of physical chemistry B* **2010**, *114*, 2549–2564.

[116] Jaap Vuyk, M. Pharmacokinetic and pharmacodynamic interactions between opioids and propofol. *Journal of clinical anesthesia* **1997**, *9*, 23S–26S.

[117] Robinson, B.; Ebert, T.; O'brien, T.; Colinco, M.; Muzi, M. Mechanisms whereby Propofol Mediates Peripheral Vasolidation in HumansSympathoinhibition or Direct Vascular Relaxation? *Anesthesiology: The Journal of the American Society of Anesthesiologists* **1997**, *86*, 64–72.

[118] Langley, M. S.; Heel, R. C. Propofol. *Drugs* **1988**, *35*, 334–372.

[119] Trapani, G.; Altomare, C.; Sanna, E.; Biggio, G.; Liso, G. Propofol in anesthesia. Mechanism of action, structure-activity relationships, and drug delivery. *Current medicinal chemistry* **2000**, *7*, 249–271.

[120] Lin, L.; Chen, L.; Zirrolli, J.; Harris, R. General anesthetics potentiate gamma-aminobutyric acid actions on gamma-aminobutyric acidA receptors expressed by Xenopus oocytes: lack of involvement of intracellular calcium. *Journal of Pharmacology and Experimental Therapeutics* **1992**, *263*, 569–578.

[121] Nagase, Y.; Kaibara, M.; Uezono, Y.; Izumi, F.; Sumikawa, K.; Taniyama, K. Propofol inhibits muscarinic acetylcholine receptor-mediated signal transduction in Xenopus oocytes expressing the rat M1 receptor. *The Japanese Journal of Pharmacology* **1999**, *79*, 319–325.

[122] Stanley, T. H. The fentanyl story. *The Journal of Pain* **2014**, *15*, 1215–1226.

[123] Phillips, A.; McMurray, T.; Mirakhur, R.; Gibson, F.; Elliott, P. Propofol-fentanyl anesthesia: a comparison with isoflurane-fentanyl anesthesia in coronary artery bypass grafting and valve replacement surgery. *Journal of cardiothoracic and vascular anesthesia* **1994**, *8*, 289–296.

[124] Petersen, K. D.; Landsfeldt, U.; Cold, G. E.; Petersen, C. B.; Mau, S.; Hauerberg, J.; Holst, P.; Olsen, K. S. Intracranial Pressure and Cerebral Hemodynamic in Patients with Cerebral TumorsA Randomized Prospective Study of Patients Subjected to Craniotomy in Propofol-Fentanyl, Isoflurane-Fentanyl, or Sevoflurane-Fentanyl Anesthesia. *Anesthesiology: The Journal of the American Society of Anesthesiologists* **2003**, *98*, 329–336.

[125] Chen, J.-C.; Smith, E. R.; Cahill, M.; Cohen, R.; Fishman, J. B. The opioid receptor binding of dezocine, morphine, fentanyl, butorphanol and nalbuphine. *Life sciences* **1993**, *52*, 389–396.

[126] Jo, S.; Kim, T.; Iyer, V. G.; Im, W. CHARMM-GUI: a web-based graphical user interface for CHARMM. *Journal of computational chemistry* **2008**, *29*, 1859–1865.

[127] Case, D.; Betz, R.; Cerutti, D.; Cheatham, T.; Darden, T.; Duke, R.; Giese, T.; Gohlke, H.; Goetz, A.; Homeyer, N., et al. AMBER16, 2016. *San Francisco*

[128] Salomon-Ferrer, R.; Götz, A. W.; Poole, D.; Le Grand, S.; Walker, R. C. Routine microsecond molecular dynamics simulations with AMBER on GPUs. 2. Explicit solvent particle mesh Ewald. *Journal of chemical theory and computation* **2013**, *9*, 3878–3888.

[129] Pastor, R. W.; Brooks, B. R.; Szabo, A. An analysis of the accuracy of Langevin and molecular dynamics algorithms. *Molecular Physics* **1988**, *65*, 1409–1419.

[130] Berendsen, H. J.; Postma, J. v.; van Gunsteren, W. F.; DiNola, A.; Haak, J. R. Molecular dynamics with coupling to an external bath. *The Journal of chemical physics* **1984**, *81*, 3684–3690.

[131] Ryckaert, J.-P.; Ciccotti, G.; Berendsen, H. J. Numerical integration of the cartesian equations of motion of a system with constraints: molecular dynamics of n-alkanes. *Journal of computational physics* **1977**, *23*, 327–341.

[132] Roe, D. R.; Cheatham III, T. E. PTRAJ and CPPTRAJ: software for processing and analysis of molecular dynamics trajectory data. *Journal of chemical theory and computation* **2013**, *9*, 3084–3095.

[133] Humphrey, W.; Dalke, A.; Schulten, K., et al. VMD: visual molecular dynamics. *Journal of molecular graphics* **1996**, *14*, 33–38.

[134] Skjevik, Å. A.; Madej, B. D.; Walker, R. C.; Teigen, K. LIPID11: a modular framework for lipid simulations using amber. *The Journal of Physical Chemistry B* **2012**, *116*, 11124–11136.

[135] Kučerka, N.; Nagle, J. F.; Sachs, J. N.; Feller, S. E.; Pencer, J.; Jackson, A.; Katsaras, J. Lipid bilayer structure determined by the simultaneous analysis of neutron and X-ray scattering data. *Biophys. J.* **2008**, *95*, 2356–2367.

[136] Evans, E.; Rawicz, W.; Smith, B. Concluding remarks back to the future: mechanics and thermodynamics of lipid biomembranes. *Faraday Discuss.* **2013**, *161*, 591–611.

[137] Filippov, A.; Orädd, G.; Lindblom, G. Influence of cholesterol and water content on phospholipid lateral diffusion in bilayers. *Langmuir* **2003**, *19*, 6397–6400.

[138] Kučerka, N.; Tristram-Nagle, S.; Nagle, J. F. Closer look at structure of fully hydrated fluid phase DPPC bilayers. *Biophys. J.* **2006**, *90*, L83–L85.

[139] Nagle, J. F.; Tristram-Nagle, S. Structure of lipid bilayers. *Biochim. Biophys. Acta, Rev. Biomembr.* **2000**, *1469*, 159–195.

[140] Scheidt, H. A.; Huster, D.; Gawrisch, K. Diffusion of cholesterol and its precursors in lipid membranes studied by 1H pulsed field gradient magic angle spinning NMR. *Biophys. J.* **2005**, *89*, 2504–2512.

[141] Guixà-González, R.; Rodriguez-Espigares, I.; Ramírez-Anguita, J. M.; Carrió-Gaspar, P.; Martinez-Seara, H.; Giorgino, T.; Selent, J. MEMBPLUGIN: studying membrane complexity in VMD. *Bioinformatics* **2014**, *30*, 1478–1480.

[142] Venable, R. M.; Zhang, Y.; Hardy, B. J.; Pastor, R. W. Molecular dynamics simulations of a lipid bilayer and of hexadecane: an investigation of membrane fluidity. *Science* **1993**, *262*, 223–226.

[143] Nademi, Y.; Iranagh, S. A.; Yousefpour, A.; Mousavi, S. Z.; Modarress, H. Molecular dynamics simulations and free energy profile of Paracetamol in DPPC and DMPC lipid bilayers. *J. Chem. Sci.* **2014**, *126*, 637–647.

[144] Yousefpour, A.; Amjad Iranagh, S.; Nademi, Y.; Modarress, H. Molecular dynamics simulation of nonsteroidal antiinflammatory drugs, naproxen and relafen, in a lipid bilayer membrane. *Int. J. Quantum Chem.* **2013**, *113*, 1919–1930.

[145] Warschawski, D. E.; Devaux, P. F. Order parameters of unsaturated phospholipids in membranes and the effect of cholesterol: a 1 H–13 C solid-state NMR study at natural abundance. *Eur. Biophys. J.* **2005**, *34*, 987–996.

[146] Petrache, H. I.; Dodd, S. W.; Brown, M. F. Area per lipid and acyl length distributions in fluid phosphatidylcholines determined by 2H NMR spectroscopy. *Biophys. J.* **2000**, *79*, 3172–3192.

[147] Douliez, J.-P.; Leonard, A.; Dufourc, E. J. Restatement of order parameters in biomembranes: calculation of CC bond order parameters from CD quadrupolar splittings. *Biophys. J.* **1995**, *68*, 1727–1739.

[148] Mojumdar, E. H.; Lyubartsev, A. P. Molecular dynamics simulations of local anesthetic articaine in a lipid bilayer. *Biophys. Chem.* **2010**, *153*, 27–35.

[149] Luzar, A. Resolving the hydrogen bond dynamics conundrum. *J. Chem. Phys.* **2000**, *113*, 10663–10675.

[150] Sall, J. W.; Stratmann, G.; Leong, J.; Woodward, E.; Bickler, P. E. Propofol at clinically relevant concentrations increases neuronal differentiation but is not toxic to hippocampal neural precursor cells in vitro. *Anesthesiology* **2012**, *117*, 1080.

[151] Park, K.-E.; Sohn, J.-T.; Jeong, Y. S.; Sung, H.-J.; Shin, I.-W.; Lee, H.-K.; Chung, Y.-K. Inhibitory effect of fentanyl on phenylephrine-induced contraction of the rat aorta. *Yonsei medical journal* **2009**, *50*, 414–421.

[152] Dickson, C. In silico modelling of membranes and drug membrane interactions. *Imperial College London* **2014**,

[153] Teo, R. D.; Tieleman, D. P. Modulation of phospholipid bilayer properties by simvastatin. *The Journal of Physical Chemistry B* **2021**, *125*, 8406–8418.

[154] Alberts, B.; Johnson, A.; Lewis, J.; Raff, M.; Roberts, K.; Walter, P. *Molecular Biology of the Cell. 4th edition*; Garland Science, 2002.

[155] Patra, M.; Salonen, E.; Terama, E.; Vattulainen, I.; Faller, R.; Lee, B. W.; Holopainen, J.; Karttunen, M. Under the influence of alcohol: the effect of ethanol and methanol on lipid bilayers. *Biophys. J.* **2006**, *90*, 1121–1135.

[156] Porasso, R. D.; Drew Bennett, W.; Oliveira-Costa, S.; Lopez Cascales, J. Study of the benzocaine transfer from aqueous solution to the interior of a biological membrane. *J. Phys. Chem. B* **2009**, *113*, 9988–9994.

[157] Koubi, L.; Saiz, L.; Tarek, M.; Scharf, D.; Klein, M. L. Influence of anesthetic and nonimmobilizer molecules on the physical properties of a polyunsaturated lipid bilayer. *J. Phys. Chem. B* **2003**, *107*, 14500–14508.

[158] Wohlert, J.; Edholm, O. The range and shielding of dipole-dipole interactions in phospholipid bilayers. *Biophys. J.* **2004**, *87*, 2433–2445.

[159] Högberg, C.-J.; Maliniak, A.; Lyubartsev, A. P. Dynamical and structural properties of charged and uncharged lidocaine in a lipid bilayer. *Biophys. Chem.* **2007**, *125*, 416–424.

[160] Mi, W.; Sakai, T.; Singh, H.; Kudo, T.; Kudo, M.; Matsuki, A. Hypnotic endpoints vs. the bispectral index, 95% spectral edge frequency and median frequency during propofol infusion with or without fentanyl. *European journal of anaesthesiology* **1999**, *16*, 47–52.

[161] Wynands, J. E.; Townsend, G. E.; Wong, P.; Whalley, D. G.; Srikant, C. B.; Patel, Y. C. Blood pressure response and plasma fentanyl concentrations during high-and very high-dose fentanyl anesthesia for coronary artery surgery. *Anesthesia and analgesia* **1983**, *62*, 661–665.

[162] Unwin, N. Neurotransmitter action: opening of ligand-gated ion channels. *Cell* **1993**, *72*, 31–41.

[163] Campagna, J. A.; Miller, K. W.; Forman, S. A. Mechanisms of actions of inhaled anesthetics. *New England Journal of Medicine* **2003**, *348*, 2110–2124.

[164] Krasowski, M.; Harrison, N. General anaesthetic actions on ligand-gated ion channels. *Cellular and Molecular Life Sciences CMLS* **1999**, *55*, 1278–1303.

[165] Sauguet, L.; Poitevin, F.; Murail, S.; Van Renterghem, C.; Moraga-Cid, G.; Malherbe, L.; Thompson, A. W.; Koehl, P.; Corringer, P.-J.; Baaden, M., et al. Structural basis for ion permeation mechanism in pentameric ligand-gated ion channels. *The EMBO journal* **2013**, *32*, 728–741.

[166] Arcario, M. J.; Mayne, C. G.; Tajkhorshid, E. A membrane-embedded pathway delivers general anesthetics to two interacting binding sites in the Gloeobacter violaceus ion channel. *Journal of Biological Chemistry* **2017**, *292*, 9480–9492.

[167] Chiara, D. C.; Gill, J. F.; Chen, Q.; Tillman, T.; Dailey, W. P.; Eckenhoff, R. G.; Xu, Y.; Tang, P.; Cohen, J. B. Photoaffinity labeling the propofol binding site in GLIC. *Biochemistry* **2014**, *53*, 135–142.

[168] Mowrey, D.; Cheng, M. H.; Liu, L. T.; Willenbring, D.; Lu, X.; Wymore, T.; Xu, Y.; Tang, P. Asymmetric ligand binding facilitates conformational transitions in pentameric ligand-gated ion channels. *Journal of the American Chemical Society* **2013**, *135*, 2172–2180.

[169] Hollenbeck, P. J.; Bamburg, J. R. *Neurons: methods and applications for the cell biologist*; Gulf Professional Publishing, 2003; Vol. 71.

[170] Klesse, G.; Tucker, S. J.; Sansom, M. S. Electric field induced wetting of a hydrophobic gate in a model nanopore based on the 5-HT3 receptor channel. *ACS nano* **2020**, *14*, 10480–10491.

[171] Kiss, L.; Bennett, P. B.; Uebele, V. N.; Koblan, K. S.; Kane, S. A.; Neagle, B.; Schroeder, K. High throughput ion-channel pharmacology: planar-array-based voltage clamp. *Assay and Drug Development Technologies* **2003**, *1*, 127–135.

[172] Cerdan, A. H.; Cecchini, M. On the functional annotation of open-channel structures in the glycine receptor. *Structure* **2020**, *28*, 690–693.

[173] Delemotte, L.; Dehez, F.; Treptow, W.; Tarek, M. Modeling membranes under a transmembrane potential. *The Journal of Physical Chemistry B* **2008**, *112*, 5547–5550.

[174] Miranda, W. E.; DeMarco, K. R.; Guo, J.; Duff, H. J.; Vorobyov, I.; Clancy, C. E.; Noskov, S. Y. Selectivity filter modalities and rapid inactivation of the hERG1 channel. *Proceedings of the National Academy of Sciences* **2020**, *117*, 2795–2804.

[175] Zwanzig, R. W. High-temperature equation of state by a perturbation method. I. Nonpolar gases. *The Journal of Chemical Physics* **1954**, *22*, 1420–1426.

[176] Straatsma, T.; Berendsen, H. Free energy of ionic hydration: Analysis of a thermodynamic integration technique to evaluate free energy differences by molecular dynamics simulations. *The Journal of chemical physics* **1988**, *89*, 5876–5886.

[177] Genheden, S.; Ryde, U. The MM/PBSA and MM/GBSA methods to estimate ligand-binding affinities. *Expert opinion on drug discovery* **2015**, *10*, 449–461.

[178] Kuhn, B.; Gerber, P.; Schulz-Gasch, T.; Stahl, M. Validation and use of the MM-PBSA approach for drug discovery. *Journal of medicinal chemistry* **2005**, *48*, 4040–4048.

[179] Mikulskis, P.; Genheden, S.; Ryde, U. Effect of explicit water molecules on ligand-binding affinities calculated with the MM/GBSA approach. *Journal of molecular modeling* **2014**, *20*, 2273.

[180] Pearlman, D. A. Evaluating the molecular mechanics Poisson- Boltzmann surface area free energy method using a congeneric series of ligands to p38 MAP kinase. *Journal of medicinal chemistry* **2005**, *48*, 7796–7807.

[181] Miller III, B. R.; McGee Jr, T. D.; Swails, J. M.; Homeyer, N.; Gohlke, H.; Roitberg, A. E. MMPBSA. py: an efficient program for end-state free energy calculations. *Journal of chemical theory and computation* **2012**, *8*, 3314–3321.

[182] Comitani, F.; Cohen, N.; Ashby, J.; Botten, D.; Lummis, S. C.; Molteni, C. Insights into the binding of GABA to the insect RDL receptor from atomistic simulations: a comparison of models. *Journal of computer-aided molecular design* **2014**, *28*, 35–48.

[183] Ladefoged, L. K.; Munro, L.; Pedersen, A. J.; Lummis, S. C.; Bang-Andersen, B.; Balle, T.; Schiøtt, B.; Kristensen, A. S. Modeling and mutational analysis of the binding mode for the multimodal antidepressant drug vortioxetine to the human 5-HT3A receptor. *Molecular pharmacology* **2018**, *94*, 1421–1434.

[184] Brömstrup, T.; Howard, R. J.; Trudell, J. R.; Harris, R. A.; Lindahl, E. Inhibition versus potentiation of ligand-gated ion channels can be altered by a single mutation that moves ligands between intra-and intersubunit sites. *Structure* **2013**, *21*, 1307–1316.

[185] Xie, H.-B.; Sha, Y.; Wang, J.; Cheng, M.-S. Some insights into the binding mechanism of the gaba a receptor: a combined docking and mm-gbsa study. *Journal of molecular modeling* **2013**, *19*, 5489–5500.

[186] Eken, Y.; Almeida, N.; Wang, C.; Wilson, A. K. SAMPL7: Host–guest binding prediction by molecular dynamics and quantum mechanics. *Journal of Computer-Aided Molecular Design* **2021**, *35*, 63–77.

[187] Maffucci, I.; Contini, A. *Frontiers in Computational Chemistry*; Elsevier, 2015; pp 82–120.

[188] Aggarwal, A.; Naskar, S.; Maroli, N.; Gorai, B.; Dixit, N. M.; Maiti, P. K. Mechanistic insights into the effects of key mutations on SARS-CoV-2 RBD–ACE2 binding. *Physical Chemistry Chemical Physics* **2021**, *23*, 26451–26458.

[189] Singh, N.; Warshel, A. Absolute binding free energy calculations: on the accuracy of computational scoring of protein–ligand interactions. *Proteins: Structure, Function, and Bioinformatics* **2010**, *78*, 1705–1723.

[190] Michaud-Agrawal, N.; Denning, E. J.; Woolf, T. B.; Beckstein, O. MDAnalysis: a toolkit for the analysis of molecular dynamics simulations. *Journal of computational chemistry* **2011**, *32*, 2319–2327.

[191] Jia, Z.; Yazdani, M.; Zhang, G.; Cui, J.; Chen, J. Hydrophobic gating in BK channels. *Nature communications* **2018**, *9*, 1–8.

[192] Zhu, F.; Hummer, G. Pore opening and closing of a pentameric ligand-gated ion channel. *Proceedings of the National Academy of Sciences* **2010**, *107*, 19814–19819.

[193] Corrie, J.; Baenziger, J. E. Gating of pentameric ligand-gated ion channels: structural insights and ambiguities. *Structure* **2013**, *21*, 1271–1283.

[194] Miyazawa, A.; Fujiyoshi, Y.; Unwin, N. Structure and gating mechanism of the acetylcholine receptor pore. *Nature* **2003**, *423*, 949–955.

[195] Imoto, K.; Busch, C.; Sakmann, B.; Mishina, M.; Konno, T.; Nakai, J.; Bujo, H.; Mori, Y.; Fukuda, K.; Numa, S. Rings of negatively charged amino acids determine the acetylcholine receptor channel conductance. *Nature* **1988**, *335*, 645–648.

[196] Zhu, F.; Hummer, G. Drying transition in the hydrophobic gate of the GLIC channel blocks ion conduction. *Biophysical journal* **2012**, *103*, 219–227.

[197] Mezei, M.; Filizola, M. TRAJELIX: a computational tool for the geometric characterization of protein helices during molecular dynamics simulations. *Journal of computer-aided molecular design* **2006**, *20*, 97–107.

[198] Mezei, M. Simulaid: a simulation facilitator and analysis program. *Journal of computational chemistry* **2010**, *31*, 2658–2668.

[199] Dahl, A. C. E.; Chavent, M.; Sansom, M. S. Bendix: intuitive helix geometry analysis and abstraction. *Bioinformatics* **2012**, *28*, 2193–2194.

[200] Law, R. J.; Lightstone, F. C. Modeling neuronal nicotinic and GABA receptors: important interface salt-links and protein dynamics. *Biophysical journal* **2009**, *97*, 1586–1594.

[201] Venkatachalan, S. P.; Czajkowski, C. A conserved salt bridge critical for GABAA receptor function and loop C dynamics. *Proceedings of the National Academy of Sciences* **2008**, *105*, 13604–13609.

[202] Spurny, R.; Billen, B.; Howard, R. J.; Brams, M.; Debaveye, S.; Price, K. L.; Weston, D. A.; Strelkov, S. V.; Tytgat, J.; Bertrand, S., et al. Multisite binding of a general anesthetic to the prokaryotic pentameric Erwinia chrysanthemi ligand-gated ion channel (ELIC). *Journal of Biological Chemistry* **2013**, *288*, 8355–8364.

[203] Fourati, Z.; Howard, R. J.; Heusser, S. A.; Hu, H.; Ruza, R. R.; Sauguet, L.; Lindahl, E.; Delarue, M. Structural basis for a bimodal allosteric mechanism of general anesthetic modulation in pentameric ligand-gated ion channels. *Cell reports* **2018**, *23*, 993–1004.

[204] Bondarenko, V.; Mowrey, D.; Liu, L. T.; Xu, Y.; Tang, P. NMR resolved multiple anesthetic binding sites in the TM domains of the $\alpha 4\beta 2$ nAChR. *Biochimica et Biophysica Acta (BBA)-Biomembranes* **2013**, *1828*, 398–404.

[205] Tyler, M. W.; Yourish, H. B.; Ionescu, D. F.; Haggarty, S. J. Classics in chemical neuroscience: ketamine. *ACS chemical neuroscience* **2017**, *8*, 1122–1134.

[206] Yamakura, T.; Chavez-Noriega, L. E.; Harris, R. A. Subunit-dependent inhibition of human neuronal nicotinic acetylcholine receptors and other ligand-gated ion channels by dissociative anesthetics ketamine and dizocilpine. *Anesthesiology: The Journal of the American Society of Anesthesiologists* **2000**, *92*, 1144–1153.

[207] Lichtenbelt, B.-J.; Mertens, M.; Vuyk, J. Strategies to optimise propofol-opioid anaesthesia. *Clinical pharmacokinetics* **2004**, *43*, 577–593.

[208] Smith, C.; McEwan, A. I.; Jhaveri, R.; Wilkinson, M.; Goodman, D.; Smith, L. R.; Canada, A. T.; Glass, P. S. The interaction of fentanyl on the Cp50 of propofol for loss of consciousness and skin incision. *The Journal of the American Society of Anesthesiologists* **1994**, *81*, 820–828.

[209] Faulkner, C.; de Leeuw, N. H. In silico studies of the interactions between propofol and fentanyl using Gaussian accelerated molecular dynamics. *Journal of Biomolecular Structure and Dynamics* **2020**, 1–13.

[210] Jorgensen, W. L.; Chandrasekhar, J.; Madura, J. D.; Impey, R. W.; Klein, M. L. Comparison of simple potential functions for simulating liquid water. *The Journal of chemical physics* **1983**, *79*, 926–935.

[211] Lomize, M. A.; Pogozheva, I. D.; Joo, H.; Mosberg, H. I.; Lomize, A. L. OPM database and PPM web server: resources for positioning of proteins in membranes. *Nucleic acids research* **2012**, *40*, D370–D376.

[212] Pettersen, E. F.; Goddard, T. D.; Huang, C. C.; Couch, G. S.; Greenblatt, D. M.; Meng, E. C.; Ferrin, T. E. UCSF Chimera—a visualization system for exploratory research and analysis. *Journal of computational chemistry* **2004**, *25*, 1605–1612.

[213] Van Der Spoel, D.; Lindahl, E.; Hess, B.; Groenhof, G.; Mark, A. E.; Berendsen, H. J. GROMACS: fast, flexible, and free. *Journal of computational chemistry* **2005**, *26*, 1701–1718.

[214] Raju, S.; Barber, A. F.; LeBard, D. N.; Klein, M. L.; Carnevale, V. Exploring volatile general anesthetic binding to a closed membrane-bound bacterial voltage-gated sodium channel via computation. *PLoS Comput Biol* **2013**, *9*, e1003090.

[215] Miao, Y.; McCammon, J. A. *Annual reports in computational chemistry*; Elsevier, 2017; Vol. 13; pp 231–278.

[216] Palermo, G.; Miao, Y.; Walker, R. C.; Jinek, M.; McCammon, J. A. CRISPR-Cas9 conformational activation as elucidated from enhanced molecular simulations. *Proceedings of the National Academy of Sciences* **2017**, *114*, 7260–7265.

[217] Eckenhoff, M. F.; Chan, K.; Eckenhoff, R. G. Multiple specific binding targets for inhaled anesthetics in the mammalian brain. *Journal of Pharmacology and Experimental Therapeutics* **2002**, *300*, 172–179.

[218] of Molecular Neuropharmacology, C. S. L.; Harrison, N. L. Ion channels take center stage: twin spotlights on two anesthetic targets. *The Journal of the American Society of Anesthesiologists* **2000**, *92*, 936–936.

[219] Herold, K. F.; Hemmings Jr, H. C. Sodium channels as targets for volatile anesthetics. *Frontiers in pharmacology* **2012**, *3*, 50.

[220] Miao, Y.; Sinko, W.; Pierce, L.; Bucher, D.; Walker, R. C.; McCammon, J. A. Improved reweighting of accelerated molecular dynamics simulations for free energy calculation. *Journal of Chemical Theory and Computation* **2014**, *10*, 2677–2689.

[221] Faulkner, C.; Santos-Carballal, D.; Plant, D. F.; de Leeuw, N. H. Atomistic molecular dynamics simulations of propofol and fentanyl in phosphatidylcholine lipid bilayers. *ACS omega* **2020**, *5*, 14340–14353.

[222] Xiu, X.; Hanek, A. P.; Wang, J.; Lester, H. A.; Dougherty, D. A. A unified view of the role of electrostatic interactions in modulating the gating of Cys loop receptors. *Journal of Biological Chemistry* **2005**, *280*, 41655–41666.

[223] Cederholm, J. M.; Schofield, P. R.; Lewis, T. M. Gating mechanisms in Cys-loop receptors. *European biophysics journal* **2009**, *39*, 37–49.

[224] Nys, M.; Kesters, D.; Ulens, C. Structural insights into Cys-loop receptor function and ligand recognition. *Biochemical pharmacology* **2013**, *86*, 1042–1053.

[225] Schofield, C. M.; Jenkins, A.; Harrison, N. L. A highly conserved aspartic acid residue in the signature disulfide loop of the α1 subunit is a determinant of gating in the glycine receptor. *Journal of Biological Chemistry* **2003**, *278*, 34079–34083.

[226] Booker, R. D.; Sum, A. K. Biophysical changes induced by xenon on phospholipid bilayers. *Biochimica et Biophysica Acta (BBA)-Biomembranes* **2013**, *1828*, 1347–1356.

[227] Stone, D. J.; DiFazio, C. A. Anesthetic action of opiates: correlations of lipid solubility and spectral edge. *Anesthesia and analgesia* **1988**, *67*, 663–666.

[228] Kelly, E.; Sutcliffe, K.; Cavallo, D.; Ramos-Gonzalez, N.; Alhosan, N.; Henderson, G. The anomalous pharmacology of fentanyl. *British Journal of Pharmacology* **2021**,

[229] Sutcliffe, K. J.; Corey, R. A.; Charlton, S. J.; Sessions, R. B.; Henderson, G.; Kelly, E. Fentanyl binds to the mu-opioid receptor via the lipid membrane and transmembrane helices. *bioRxiv* **2021**,

[230] Di, L.; Kerns, E. H.; Fan, K.; McConnell, O. J.; Carter, G. T. High throughput artificial membrane permeability assay for blood–brain barrier. *European journal of medicinal chemistry* **2003**, *38*, 223–232.

[231] Artursson, P.; Palm, K.; Luthman, K. Caco-2 monolayers in experimental and theoretical predictions of drug transport. *Advanced drug delivery reviews* **2012**, *64*, 280–289.

[232] Lee, C. T.; Comer, J.; Herndon, C.; Leung, N.; Pavlova, A.; Swift, R. V.; Tung, C.; Rowley, C. N.; Amaro, R. E.; Chipot, C., et al. Simulation-based approaches for determining membrane permeability of small compounds. *J. Chem. Inf. Model.* **2016**, *56*, 721–733.

[233] Moss, G. P.; Dearden, J. C.; Patel, H.; Cronin, M. T. Quantitative structure–permeability relationships (QSPRs) for percutaneous absorption. *Toxicology in vitro* **2002**, *16*, 299–317.

[234] Mitragotri, S.; Anissimov, Y. G.; Bunge, A. L.; Frasch, H. F.; Guy, R. H.; Hadgraft, J.; Kasting, G. B.; Lane, M. E.; Roberts, M. S. Mathematical models of skin permeability: an overview. *International journal of pharmaceutics* **2011**, *418*, 115–129.

[235] Swift, R. V.; Amaro, R. E. Back to the future: can physical models of passive membrane permeability help reduce drug candidate attrition and move us beyond QSPR? *Chemical biology & drug design* **2013**, *81*, 61–71.

[236] Torrie, G. M.; Valleau, J. P. Nonphysical sampling distributions in Monte Carlo free-energy estimation: Umbrella sampling. *Journal of Computational Physics* **1977**, *23*, 187–199.

[237] Torrie, G. M.; Valleau, J. P. Monte Carlo free energy estimates using non-Boltzmann sampling: Application to the sub-critical Lennard-Jones fluid. *Chemical Physics Letters* **1974**, *28*, 578–581.

[238] Marrink, S.-J.; Berendsen, H. J. Simulation of water transport through a lipid membrane. *The Journal of Physical Chemistry* **1994**, *98*, 4155–4168.

[239] Marrink, S. J.; Berendsen, H. J. Permeation process of small molecules across lipid membranes studied by molecular dynamics simulations. *The Journal of Physical Chemistry* **1996**, *100*, 16729–16738.

[240] Martin, L. J.; Chao, R.; Corry, B. Molecular dynamics simulation of the partitioning of benzocaine and phenytoin into a lipid bilayer. *Biophysical chemistry* **2014**, *185*, 98–107.

[241] Carpenter, T. S.; Kirshner, D. A.; Lau, E. Y.; Wong, S. E.; Nilmeier, J. P.; Lightstone, F. C. A method to predict blood-brain barrier permeability of drug-like compounds using molecular dynamics simulations. *Biophysical journal* **2014**, *107*, 630–641.

[242] Campbell, S. D.; Regina, K. J.; Kharasch, E. D. Significance of lipid composition in a blood-brain barrier–mimetic PAMPA assay. *Journal of biomolecular screening* **2014**, *19*, 437–444.

[243] Bernards, C. M.; Hill, H. F. Physical and chemical properties of drug molecules governing their diffusion through the spinal meninges. The Journal of the American Society of Anesthesiologists. 1992; pp 750–756.

[244] Kalyanaraman, C.; Jacobson, M. P. An atomistic model of passive membrane permeability: application to a series of FDA approved drugs. *Journal of computer-aided molecular design* **2007**, *21*, 675–679.

[245] Avdeef, A. *Absorption and drug development: solubility, permeability, and charge state*; John Wiley & Sons, 2012.

[246] Vizserálek, G.; Balogh, T.; Takács-Novák, K.; Sinkó, B. PAMPA study of the temperature effect on permeability. *European Journal of Pharmaceutical Sciences* **2014**, *53*, 45–49.

[247] Johnson, M. E.; Blankschtein, D.; Langer, R. Evaluation of solute permeation through the stratum corneum: lateral bilayer diffusion as the primary transport mechanism. *Journal of pharmaceutical sciences* **1997**, *86*, 1162–1172.

[248] Tsinman, O.; Tsinman, K.; Sun, N.; Avdeef, A. Physicochemical selectivity of the BBB microenvironment governing passive diffusion—matching with a porcine brain lipid extract artificial membrane permeability model. *Pharmaceutical research* **2011**, *28*, 337–363.

[249] Abraham, M. H.; Martins, F. Human skin permeation and partition: General linear free-energy relationship analyses. *Journal of pharmaceutical sciences* **2004**, *93*, 1508–1523.

[250] Zhao, R.; Kalvass, J. C.; Pollack, G. M. Assessment of blood–brain barrier permeability using the in situ mouse brain perfusion technique. *Pharmaceutical research* **2009**, *26*, 1657–1664.

[251] Neale, C.; Pomès, R. Sampling errors in free energy simulations of small molecules in lipid bilayers. *Biochimica et Biophysica Acta (BBA)-Biomembranes* **2016**, *1858*, 2539–2548.

[252] Gupta, R.; Sridhar, D.; Rai, B. Molecular dynamics simulation study of permeation of molecules through skin lipid bilayer. *The Journal of Physical Chemistry B* **2016**, *120*, 8987–8996.

[253] Subczynski, W. K.; Wisniewska, A.; Yin, J.-J.; Hyde, J. S.; Kusumi, A. Hydrophobic barriers of lipid bilayer membranes formed by reduction of water penetration by alkyl chain unsaturation and cholesterol. *Biochemistry* **1994**, *33*, 7670–7681.

[254] Khajeh, A.; Modarress, H. The influence of cholesterol on interactions and dynamics of ibuprofen in a lipid bilayer. *Biochimica et Biophysica Acta (BBA)-Biomembranes* **2014**, *1838*, 2431–2438.

[255] Retamal, J. S.; Ramírez-García, P. D.; Shenoy, P. A.; Poole, D. P.; Veldhuis, N. A. Internalized GPCRs as potential therapeutic targets for the management of pain. *Frontiers in molecular neuroscience* **2019**, *12*, 273.

[256] Haeseler, G.; Foadi, N.; Ahrens, J.; Dengler, R.; Hecker, H.; Leuwer, M. Tramadol, fentanyl and sufentanil but not morphine block voltage-operated sodium channels. *Pain* **2006**, *126*, 234–244.

[257] Mahmoud, S.; Thorsell, A.; Sommer, W. H.; Heilig, M.; Holgate, J. K.; Bartlett, S. E.; Ruiz-Velasco, V. Pharmacological consequence of the A118G μ opioid receptor polymorphism on morphine-and fentanyl-mediated modulation of Ca2+ channels in humanized mouse sensory neurons. *The Journal of the American Society of Anesthesiologists* **2011**, *115*, 1054–1062.

[258] Tschirhart, J. N.; Li, W.; Guo, J.; Zhang, S. Blockade of the Human Ether A-Go-Go–Related Gene (hERG) Potassium Channel by Fentanyl. *Molecular Pharmacology* **2019**, *95*, 386–397.

[259] Ringuette, A. E.; Spock, M.; Lindsley, C. W.; Bender, A. M. DARK classics in chemical neuroscience: carfentanil. *ACS Chemical Neuroscience* **2020**, *11*, 3955–3967.

[260] Scholz, J.; Steinfath, M.; Schulz, M. Clinical pharmacokinetics of alfentanil, fentanyl and sufentanil. *Clinical pharmacokinetics* **1996**, *31*, 275–292.

[261] Heard, C. M.; Fletcher, J. E. In *Pediatric Critical Care (Fourth Edition)*, fourth edition ed.; Fuhrman, B. P., Zimmerman, J. J., Eds.; Mosby: Saint Louis, 2011; pp 1654–1681.

[262] Vuckovic, S.; Prostran, M.; Ivanovic, M.; Dosen-Micovic, L.; Todorovic, Z.; Nesic, Z.; Stojanovic, R.; Divac, N.; Mikovic, Z. Fentanyl analogs: structure-activity-relationship study. *Current medicinal chemistry* **2009**, *16*, 2468–2474.

[263] Koyyalagunta, D. In *Pain Management*; Waldman, S. D., Bloch, J. I., Eds.; W.B. Saunders: Philadelphia, 2007; pp 939–964.

[264] Scott, L. J.; Perry, C. M. Remifentanil. *Drugs* **2005**, *65*, 1793–1823.

[265] Dolinsky, T. J.; Czodrowski, P.; Li, H.; Nielsen, J. E.; Jensen, J. H.; Klebe, G.; Baker, N. A. PDB2PQR: expanding and upgrading automated preparation of biomolecular structures for molecular simulations. *Nucleic acids research* **2007**, *35*, W522–W525.

[266] Søndergaard, C. R.; Olsson, M. H.; Rostkowski, M.; Jensen, J. H. Improved treatment of ligands and coupling effects in empirical calculation and rationalization of p K a values. *Journal of chemical theory and computation* **2011**, *7*, 2284–2295.

[267] Faulkner, C.; de Leeuw, N. H. Predicting the Membrane Permeability of Fentanyl and Its Analogues by Molecular Dynamics Simulations. *The Journal of Physical Chemistry B* **2021**, *125*, 8443–8449.

[268] Mukhtasimova, N.; Lee, W. Y.; Wang, H.-L.; Sine, S. M. Detection and trapping of intermediate states priming nicotinic receptor channel opening. *Nature* **2009**, *459*, 451–454.

[269] Gonzalez-Gutierrez, G.; Cuello, L. G.; Nair, S. K.; Grosman, C. Gating of the proton-gated ion channel from Gloeobacter violaceus at pH 4 as revealed by X-ray crystallography. *Proceedings of the National Academy of Sciences* **2013**, *110*, 18716–18721.

[270] Hu, H.; Ataka, K.; Menny, A.; Fourati, Z.; Sauguet, L.; Corringer, P.-J.; Koehl, P.; Heberle, J.; Delarue, M. Electrostatics, proton sensor, and networks governing the gating transition in GLIC, a proton-gated pentameric ion channel. *Proceedings of the National Academy of Sciences* **2018**, *115*, E12172–E12181.

[271] Bertozzi, C.; Zimmermann, I.; Engeler, S.; Hilf, R. J.; Dutzler, R. Signal transduction at the domain interface of prokaryotic pentameric ligand-gated ion channels. *PLoS biology* **2016**, *14*, e1002393.

[272] Chamberlin, A.; Qiu, F.; Rebolledo, S.; Wang, Y.; Noskov, S. Y.; Larsson, H. P. Hydrophobic plug functions as a gate in voltage-gated proton channels. *Proceedings of the National Academy of Sciences* **2014**, *111*, E273–E282.

[273] Jia, Z.; Chen, J. Specific PIP 2 binding promotes calcium activation of TMEM16A chloride channels. *Communications biology* **2021**, *4*, 1–10.

Copyright permissions

Copyright Figure 4.9

Dear Christopher Faulkner,

Thank you for contacting ACS Publications Support.

Your permission requested is granted and there is no fee for this reuse. In your planned reuse, you must cite the ACS article as the source, add this direct link https://pubs.acs.org/doi/full/10.1021/acs.jctc.5b00436, and include a notice to readers that further permissions related to the material excerpted should be directed to the ACS.

If you need further assistance, please let me know.

Best regards,
Ranjith Alexander
ACS Publications Support
Customer Services and Information
Website: https://acs.service-now.com/acs
Email: support@services.acs.org
Phone: 800-227-9919 | 202-872-(HELP) 4357